UNIVERSITÀ DI PARMA

UNIVERSITÀ DEGLI STUDI DI PARMA

DOTTORATO DI RICERCA IN

“Ingegneria Industriale"

CICLO XXXIII

Fabrication and characterization of bio-based and biodegradable cellulosic composites in polyhydroxyalkanoate matrix

Coordinatore:
Chiar.mo Prof. Gianni Royer Carfagni

Tutore:
Chiar.ma Prof.ssa Federica Bondioli

Co-tutore:
Chiar.mo Prof. Daniel Milanese

Dottorando: *Alberto Giubilini*

Anni Accademici 2017/2018 – 2019/2020

Firma Coordinatore

Firma Tutore

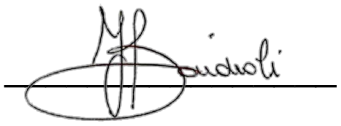

Firma Co-tutore

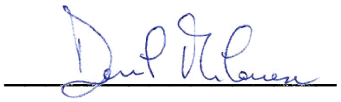

Abstract

Environmental concerns are increasingly important in modern society, and the development of innovative and sustainable materials, which can substitute the oil-based polymers, is one of the main achievements for science and industry. This PhD thesis deals with the fabrication of bio-based and biodegradable composites, obtained melt compounding a poly(3-hydroxybutyrate-*co*-3-hydroxyhexanoate) matrix with different cellulose agents. Here, a dual approach to the topic was investigated, first cellulose industrial by-product was used as inert filler to replace the biopolymer matrix and hence valorizing an agro-food waste. Secondly, chemically modified cellulose nanocrystals were used to obtain improved and tunable final properties of the composites. Furthermore, 3D-printability of these biocomposites was proved by developing structures of complex designs with a Fused Deposition Modeling 3D printer. The applicability of these innovative materials in biomedical field gave some promising results, and hence a deeper investigation was dedicated to biological characterization and use in tissue engineering. Findings from this research study can serve as an important step forward toward the development of ecofriendly materials for 3D-printing complex architectures with tailored mechanical properties and functionalities.

Acknowledgments

First of all, I would like to thank my tutor Professor Federica Bondioli for the expert guide demonstrated in the three years of my doctorate, and for revealing continuous and precious support and trust in my research.

I would also like to sincerely thank Professor Massimo Messori for co-tutoring my thesis and for having always shown interest and willingness to assist me and my research project. Thanks are also due to Dr Corrado Sciancalepore and Professor Daniel Milanese for the big help, the precious advice and encouragements showed to me.

Besides, I would like to thank all people who have warmly welcomed me in UNIMORE and who have given me a strong support: Dr Gabriele Taormina, Rachele Sergi, Vittorio Vezzali, Dr Alessandro Nanni, Dr Rosa Taurino, and particularly Dr Francesca Bisi for introducing me to the world of the laboratory.

I cannot forget to thank Dr Gilberto Siqueira and Dr Gustav Nyström, for the trust, the opportunity to visit the wonderful “Cellulose & Wood Materials” laboratory in Empa and for sharing with me their high scientific expertise. Moreover, I would like to express all my gratitude and friendship to the fellows who shared a portion of their path with me and who made me feel at home in Switzerland: Electra, Michael, Débora, Tingting, Silvia, Luca, Sefora, Nico, Alexandre, Xavier, Kevin, Zhihui, Rani, Yannick, Luana, Alessia, Silvia, Maddalena, Marta and Camilla.

Special gratitude goes to my family and my lifelong friends who have always encouraged me to give the best of myself.

Table of content

Table of figures

Table of tables

1. Introduction

In the last few decades, due to the growing relevance of environmental issues, such as depletion of fossil resources and waste management, interest in sustainable materials has exponentially increased. In fact, at least 5 of the 17 global goals set by the United Nations in 2015 (with the name of “Transforming our World: the 2030 Agenda for Sustainable Development”) are related to this topic. The scientific community is investing a lot of energy to investigate innovative materials and manufacturing processes that could contribute to reduce the industrial production footprint, lowering the amount of energy and chemical treatments required.

Bioplastics are receiving increasing interest in different application fields, e.g. packaging, agriculture, electronics, automotive and biomedical. In fact, biopolymers offer several additional advantages if compared to traditional petroleum-based plastics, such as a reduced carbon footprint and a greener waste management. Polyhydroxyalkanoates (PHAs) are a new broad class of biobased and biodegradable aliphatic polyesters that assumed great prominence in recent years, first of all, for their origin from renewable resources and their sustainable end-of-life.

Natural fibers drew attention of researchers due to their characteristics of renewability and biodegradability, and hence the possibility to be an optimal reinforcing agent or filler for biopolymer-based composites. Particularly, cellulose and nanocellulose have attracted significant interest, most prevalently due to exceptional mechanical properties and the possibility to undergo chemical functionalization.

One of the greatest issues about compounding cellulose and polymers is obtaining a well-dispersed and distributed filler phase, without aggregations, and a good adhesion between the hydrophobic matrix and the hydrophilic filler. To achieve this goal, many studies have been carried out and many different cellulose chemical functionalizations have been experimented, like silanization, grafting “onto”, grafting “from”, esterification or acetylation.

The research work presented in this doctoral thesis is aimed to explore the fabrication and optimization processes of bio-based and biodegradable polymer composites, evaluating also innovative application in biomedical field, thanks to the connection with additive manufacturing (AM) technique.

The dissertation of this thesis focuses in particular on the design, production and characterization of poly(3-hydroxybutyrate-*co*-3-hydroxyhexanoate) (PHBH)-based materials compounded with different cellulose-based particles, in order to reach tailored final properties, to be used in the emergent field of biomedical engineering, 3D printing custom-personalized devices. The most versatile and the best-known AM technology, Fused Deposition Modeling (FDM), was considered and investigated.

Additive manufacturing found a significant application in the biomedical engineering due to the high degree of customization and freedom in design that is possible to reach, compared to traditional techniques. In fact, AM can support the production of medical devices, which not only could offer a suitable biocompatibility, but which could also mimic the natural structure of the patient injured part.

In this research work, two distinct final effects of cellulose agents were investigated, i.e. cellulose used as filler or as reinforcing phase, along with two distinct cellulose modifications, i.e. silanization and acetylation. For the former application, a by-product of agro-food industry was used to pursue waste valorization and replacement of part of the biopolymer matrix in order to decrease the cost of the final item. For the latter effect, cellulose nanocrystals (CNCs) were used to tune the final thermo-mechanical properties, the superficial roughening, the water affinity and the disintegration rate.

All composites were produced with melt-compounding approach, to minimize the amount of harmful solvents needed and to suggest a procedure easier to ramp up to an industrial scale. Different characterization tests were carried out to validate each fabrication passage and to quantify the final results obtained.

1.1. Biopolymers

The term “biopolymer” is nowadays very common and widely spread in different fields of application. However, it is sometimes improperly used, due to the fact that there is not a brief and comprehensive definition of this word. To clarify the meaning of “biopolymer”, it is important to define the concepts of “bio-based” and “biodegradable”, and if the former is strictly connected with the origin of the material, at the opposite, the latter is related to its end-of-life.

A bio-based material can be so defined if it derives in whole or in part from biomass resources, i.e. organic materials that are renewable. [1] The normative also describes a quantitative method to evaluate the “bio-based carbon content”. A radiocarbon analysis is used to reveal the presence of ^{14}C as an indication of the natural source of the material, differently from petroleum-based polymers that no longer have any amount of ^{14}C, totally disappeared due to radioactive decay.

A material can be properly defined biodegradable if it can be used as a carbon source by microorganisms and converted safely into CO_2, biomass and water. [2] Besides, if the material undergoes a biodegradation and a physical disintegration level of at least 90 %, in less than 6 months, then, it can also be defined as “compostable”. [3]

Hence, the family of biopolymers can be divided into three main groups and in Figure 1 it is shown a graphical representation of this arrangement:

1 biopolymers coming from renewable resources but not biodegradable (e.g. bio-PET, bio-PP, bio-PE);
2 biopolymers coming from not renewable resources but biodegradable (e.g. PBAT);
3 biopolymers coming from renewable resources and biodegradable (e.g. PHA, PLA, PBS).

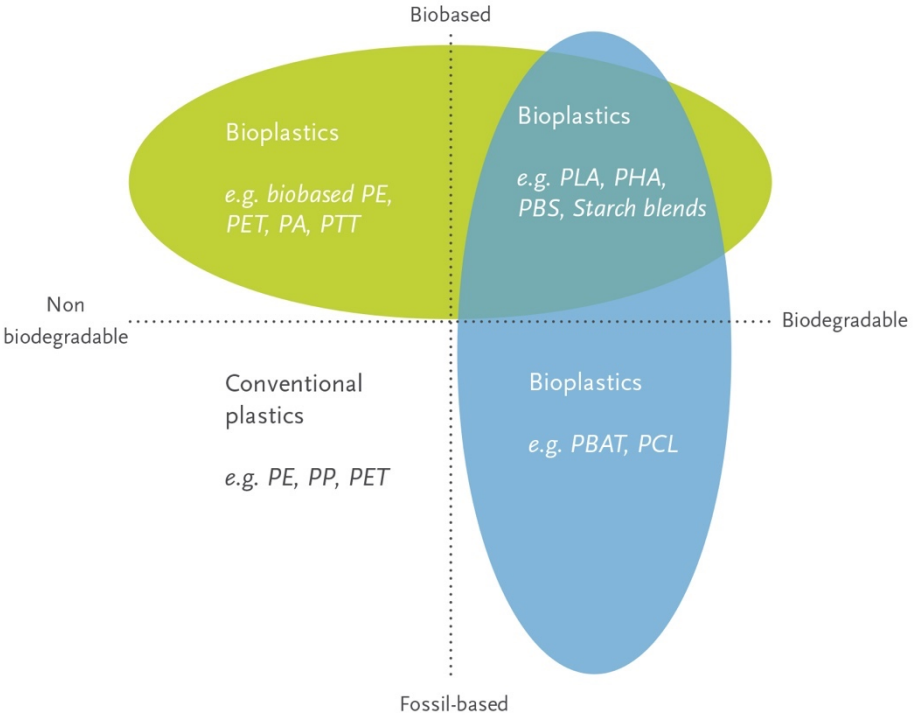

Figure 1 - Graphical classification of bioplastics according to European Bioplastic (reproduced from [4])

Due to the global awareness of the environmental impact of fossil-based polymers, [5] the main goal of plastic industry and government institutions is nowadays to tackle plastic pollution and its sociopolitical and economic challenges by developing new materials that can combine the advantages of traditional plastic with a sustainable production and disposal. In this research field, biopolymers can play a central role due to their great benefits, such as: carbon footprint reduction, fossil resources saving and landfill decrease. [6]

Despite the fact that in 2019 only 1% of the world's annual plastics production was accounted for by the bioplastics sector, the growth rate of this new and promising polymer class bodes well. In fact, according to the latest market data compiled by European Bioplastics with nova-Institute, global bioplastics production capacity is set to increase from around 2.11 million tons in 2019 to approximately 2.43 million tons in 2024. [4]

From an environmental and eco-friendly point of view, the bio-based and biodegradable polymers are undoubtedly the most attractive and

challenging category among all. This is reflected not only in a higher production capacity (55.5 % of the global bioplastics production), but also on a higher growth rate prediction over the next five years. The most interesting example concerns polyhydroxyalkanoates (PHAs) that have the highest relative growth rate among all bio-based and biodegradable polymers, with an estimation of a tripled production volume by 2024. [4]

1.1.1. Polyhydroxyalkanoates (PHAs)

PHA is a large family of thermoplastic aliphatic polyesters, whose general chemical structure is reported in Figure 2, where m can be equal or greater than one and R can be a hydrogen atom or an alkyl substituent, depending on the type of PHA.

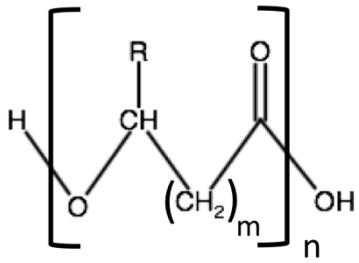

Figure 2 - General chemical structure of Polyhydroxyalkanoates (PHAs). “m” varies from 1 to 4 and “n” ranges from 100 to 30,000. R denotes an hydrogen atom or an alkyl side chain.

In 1926, a French microbiologist called Maurice Lemoigne was the first researcher who identified the synthesis of PHA from bacteria using a culture of *Bacillus megaterium* to isolate poly(3-hydroxybutyrate) (PHB). [7] PHAs are mainly produced by prokaryotic organisms, such as bacteria and archaea, under conditions of nutrient depletion and in the presence of an excess of carbon source. [8] Although, it is interesting to cite that, even if only at a preliminary research level, the production of PHAs was achieved also from plants. [9] PHAs bio-based origin derives from bacterial and archaeal fermentation, and specifically some microorganisms, when they are subjected to an environmental stress, such as a depletion of essential nutrients, they can start a conversion of the carbon sources in

hydroxyalkanoate units, as carbon and energy reserve, which are further polymerized into PHA granules through a biosynthetic pathway and stored in the bacterial cell cytoplasm. [10] The average size of the PHA granules is approximately 0.2 – 0.5 μm. [11,12] In Figure 3 a transmission electron micrograph of *Echerichia coli* cells containing PHA granules is reported.

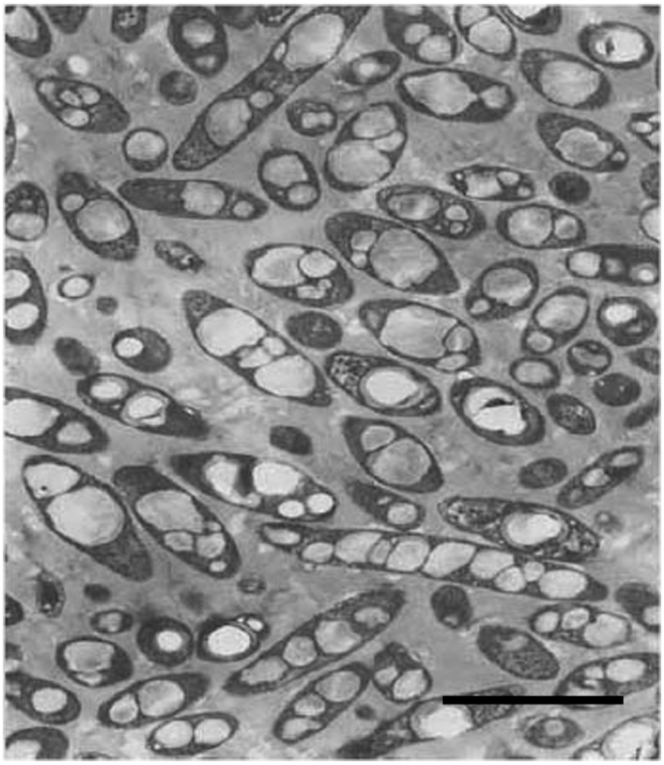

Figure 3 - TEM image of Escherichia coli accumulating PHB, appearing as whitish and luminous bodies (scale bar = 1 μm; reproduced from [13]).

Synthesis and extraction

The biosynthetic pathway of PHB consists of three enzymatic reactions catalyzed by three different enzymes: phbA, phbB and phbC. The first reaction is a condensation of two acetyl coenzyme A (acetyl-CoA) molecules into acetoacetyl-CoA by β-ketoacyl-CoA thiolase (encoded by phbA). The second reaction is the reduction of acetoacetyl-CoA to (R)-3-hydroxybutyryl-CoA by a NADPH-dependent acetoacetyl-CoA dehydrogenase (encoded by phbB). Lastly, the (R)-3-hydroxybutyryl-CoA monomers are polymerized into PHB by PHB polymerase (encoded by

phbC). [14,15] The scheme in Figure 4 synthesizes the fundamental enzymatic biosynthetic pathway.

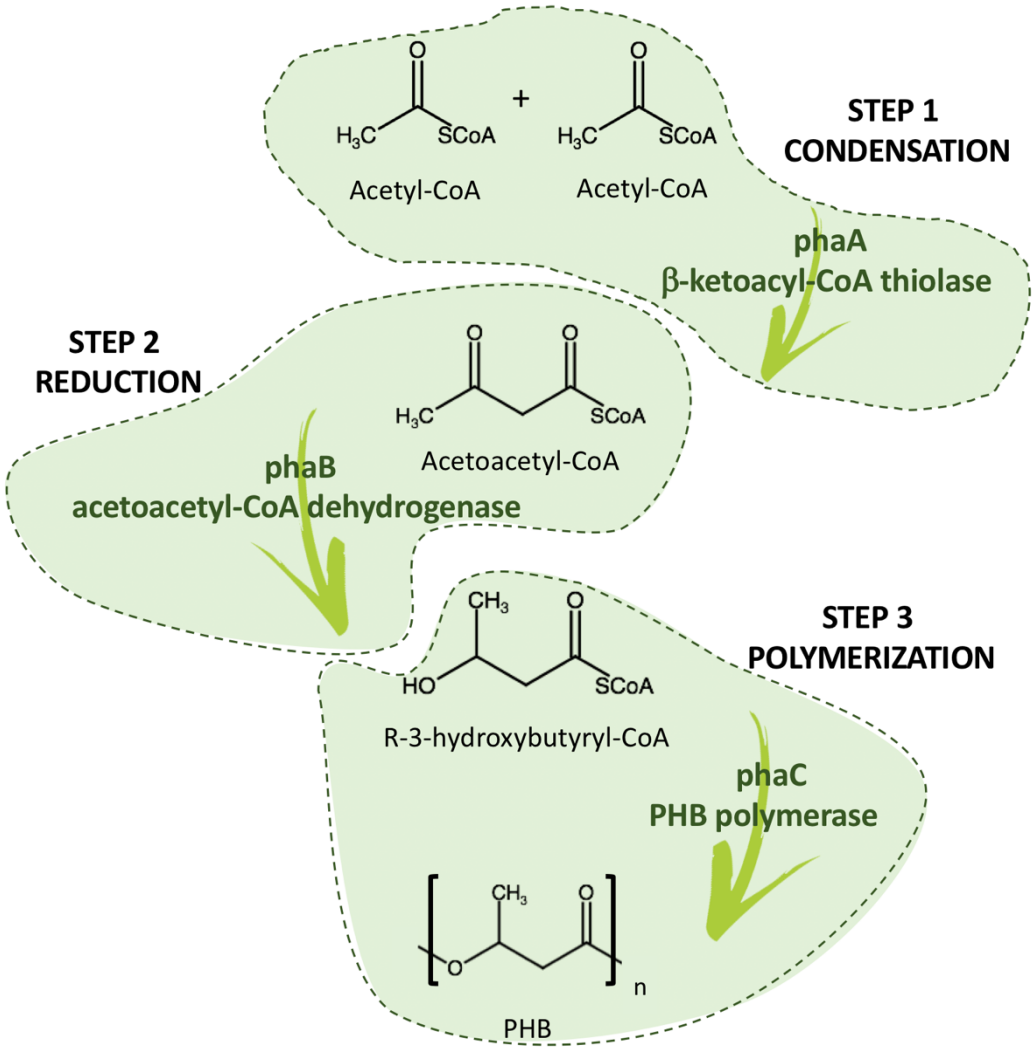

Figure 4 - Biosynthetic pathway of PHB production within the bacterial cytoplasm. PHB is synthesized by the successive action of three enzymes: β-ketoacyl-CoA thiolase (phbA), acetoacetyl-CoA dehydrogenase (phbB) and PHB polymerase (phbC) in a three-step pathway.

Carbon is at the basis of organic chemistry and it the fundamental element for all biomasses, therefore, there are different possible carbon sources that can be used to feed the microorganisms during PHA production, and they can be distinguished in three different substrates: carbohydrates (e.g. sucrose, lactose, starch or lignocellulose), [16–18] triacylglycerols (e.g. animal fats or plant oils) [19,20] and hydrocarbons. The last group is not economically significant since only few species of bacteria are capable to

synthetize PHAs from this source and the process tends to have a low efficiency. [21] Apart from the carbon, other chemical compounds are required such as nitrogen sources, and some of the most used are $(NH_4)_2SO_4$, NH_4Cl or NH_4NO_3. [10] Variation on carbon to nitrogen ratios showed different rates of PHA concentration in bacterial cells, [22] and most of the studies showed that limiting nitrogen concentration while increasing carbon substrates has a positive effect on the PHA production rate. [23,24]

Since the biosynthesis process ends with the storage of PHA granules into the cell cytoplasm, other two crucial steps are requested and they are first the extraction of the PHAs granules from the cell and secondly their purification. They are two important steps because they can affect the extraction yield as well as the quality grade of the final product, and moreover, the chosen recovery method may highly influence the sustainability and the economical applicability of the overall synthesis. [25] The choice of the most suitable recovery method depends on several factors such as the microbial strain, the type of PHA and the required purity grade of the final product. The approaches for biopolymer recovery can be different and they are here synthesized:

- Solvent dissolution: the extraction is performed on pre-treated cells, where PHA granules were made accessible by rupture of the cell membrane, and halogenated solvents are then used to dissolve the granules and then precipitate them in a non-solvent solution. [26] The biggest limitation of this method is the need of a high amount of harmful solvents, which hinders the environmental benefits of PHA biosynthesis. [27] In order to overcome this drawback, the use of non-halogenated solvents or supercritical CO_2 are being investigated as alternatives. [28]
- Enzymatic digestion: this method consists in a digestion of the cell membrane by action of enzymes followed by filtration, floatation or centrifugation recover of the PHA granules. [29]
- Chemical digestion: the procedure consists, as in the previous procedure, in a digestion of the cell membrane by the chemical action of sodium hypochlorite at high pH values, which makes most of the cellular

components soluble in water, due to oxidation, and then be removed. [30]

- Mechanical disruption: the microbial cells are mechanically disintegrated by high-pressure homogenization or ultrasonication, thus making PHA granules recuperable. [31]
- Osmophilic disruption: the rupture of the cell is caused by the high internal pressure in hypotonic media due to osmotic absorption, which causes the release of the intracellular content. [32]
- Biological extraction: this ecological procedure consists in the use of some insects such as mealworm that can be fed on lyophilized cells of *Cupriavidus necator*, with intracellular PHB granules. Once the feeding is complete, PHB can be extracted from the fecal pellets of the black soldier fly larvae. [33]

Classification

Nowadays, the number of bacteria that are able to produce PHA is remarkable, more than eighty different genera. [34] The most commonly used bacteria species belong to the genera of *Alcaligenes*, *Azotobacter*, *Bacillus*, *Cupriavidus*, *Chromobacterium*, *Delftia*, *Pseudomonas*, *Ralstonia* and *Staphylococcus*. [35] Different microorganisms own different polymerase enzymes and this leads to the fact that every single microorganism is capable of producing small differences in the final biopolymer. [36] Hence, the PHAs family has a rather wide array of constituent monomers and their respective compositions, therefore a classification was introduced depending on the chain-length monomeric composition, according to the number of carbon atoms per monomer: [37]

- short-chain-length PHA (scl-PHA) has 3 to 5 carbon atoms;
- medium-chain-length PHA (mcl-PHA) has 6 to 14 carbon atoms;
- long-chain-length PHA (lcl-PHA) has more than 14 carbon atoms.

Generally, scl-PHAs, containing mainly 3-hydroxybutyrate (3HB) or 3-hydroxyvalerate (3HV) units, and they have a higher crystalline degree, a higher glass transition temperature and a higher molecular mass compared

to mcl-PHAs, [38–40] containing 3-hydroxyvalerate (3HV), 3-hydroxyhexanoate (3HH), 3-hydroxyoctanoate (3HO), 3-hydroxydecanoate (3HD) or 3-hydroxydodecanoate (3HHD) monomers.

Another possible distinction can be made between homopolymer, of which the most famous and widespread example is PHB, and copolymer, such as poly(3-hydroxybutyrate-*co*-3-hydroxyvalerate) (PHBV), poly(3-hydroxybutyrate-*co*-4-hydroxybutyrate) (PHB4HB) or poly(3-hydroxybutyrate-*co*-3-hydroxyhexanoate) (PHBH). The physical blending or the chemical copolymerization allow to obtain a final material with tuned properties, which directly depend on the structures of the single constituent monomers. [8] For example, PHB has a high crystallinity and brittleness, which can be reduced introducing a new monomer unit, as 3-hydroxyvalerate (3HV) or 3-hydroxyhexanoate (3HH). [41] The molar composition ratio of the copolymers is a key factor to tune the final properties, such as elongation at break and degree of crystallinity, which increase with the increase of 3-hydroxyvalerate (3HV) [42] or 3-hydroxyhexanoate (3HH) [43] molar content in the structure. Figure 5 shows a schematic representation and categorization of the PHA family according to the chain-length and the composition of the structural units.

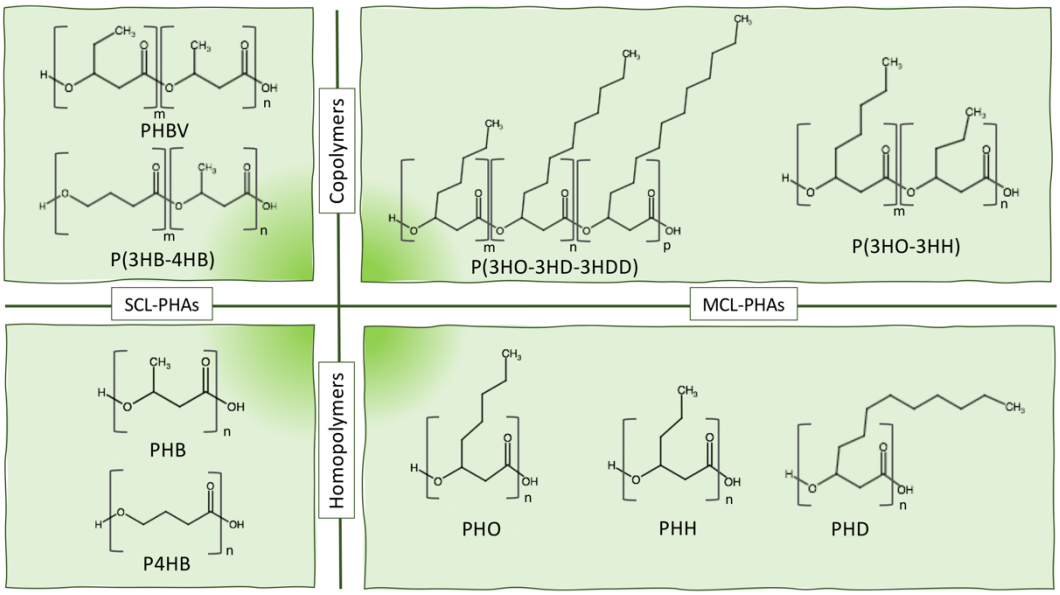

Figure 5 - PHAs classification depending on the chain length and the chemical structure of the monomers.

Besides the impressive number of microorganisms, also the variety of substrates has to be considered, as well as the fact that not all bacteria can grow and produce PHAs on every substrate. Thereby, the combination of all these factors leads to a broad range of polymers and copolymers containing various functional groups, depending on the type of the strain and substrate the bacteria are grown on. Also the PHA production yield can vary significantly from 0.25 g/L, using terephthalic acid as carbon source for *Pseudomonas putida* GO16, to 51.2 g/L, using commercial glycerol as carbon source for *Cupriavidus necator* DSM 545. [8] For this reason, when the PHA production yield is evaluated, it is important to consider both the bacterial strain and the substrate used. From this point of view, it is noteworthy the fact that if the *Cupriavidus* bacterial genus is the one that gave the highest production yield, *Pseudomonas* bacterial genus was reported as the most versatile accumulator of PHAs. [34]

Properties

The great variety of microorganisms, combined with a large variability of substrates and biosynthesis conditions are reflected in a wide spectrum of physical and mechanical properties of PHAs, varying from a more stiff behavior, comparable to polystyrene for PHB, to a more flexible behavior with elongation at break values of PHBV similar to those of PP or even LDPE. [44,45] Generally, PHAs are characterized by low glass transition temperature, between -50 °C and 0 °C, and a melting temperature lower than 200 °C. [46] They are not hydrophilic, but largely soluble in chlorinated hydrocarbons, such as chloroform or dichloromethane.

But probably the most attractive property of PHAs is their biodegradability, which can occur both in aerobic [47] and anaerobic [48] environments, without developing toxic products. The biodegradation of PHAs evolves in three main stages:

1) Biodeterioration, which consists in the colonization of the surface, or the bulk of the material, by microorganisms which modify the physical properties of the polymer.

2) Biodepolymerization, which is the conversion of polymers into oligomers and monomers induced by enzymes (i.e., PHA depolymerase or lipase), secreted by microorganisms such as bacteria or fungi, which hydrolyze the ester bond of the PHAs.
3) Assimilation, which is the final step where the low molecular weight molecules are metabolized as carbon and energy sources by microorganisms and they convert the carbon of PHAs into CO_2, water and biomass. [49,50]

The factors that influence the degradation rate of PHA are different and they can be substantially distinguished between environmental factors and intrinsic PHA properties. Generally, PHA degrades faster in areas with abundance of bacteria, due to an easy colonization of the biopolymer surface by these microorganisms. [51] However, also PHA chemical structure has to be considered, for example not all microorganisms can decompose PHA with aromatic side chains. [52] It was found that an increase in anaerobic condition, [53] temperature [54] and humidity [55] can increment the degradation rate of the PHA. On the contrary, an inverse correlation was found between the degradation rate and some properties of the PHA such as the side chain length, [56] the molecular weight and the degree of crystallinity. [57] Therefore, a useful aspect of this biopolymer family is the possibility of foreseeing a tunable degradation of the final device, according to the particular application. In Table 1 the main correlations between affecting factors and degradation rate are summarized.

Table 1 - Main correlations between the degradation rate and affecting factor of degradation. The ↑ symbol indicates an increase; the symbol ↓ indicates a decrease.

	Factor	Degradation rate	Reference
Environmental factor	↑ microbial population	↑	[51]
	↑ anaerobic condition	↑	[53]
	↑ temperature	↑	[54]
	↑ humidity	↑	[55]
PHA properties	↑ side chain length	↓	[56]
	↑ degree of crystallinity	↓	[57]
	↑ molecular weight	↓	[57]

Field of applications

Considering the similarity in mechanical, thermal and barrier properties of PHAs with commodity polymers along with their bio-based origin and biodegradability, this leads to a great curiosity of PHAs as possible replacements of conventional polymers in different industrial applications, [10] such as household or agricultural items manufacturing [58] and packaging. [59,60] And it is precisely this last sector that holds the primacy over the production capacity and use of bioplastics, as shown in Figure 6.

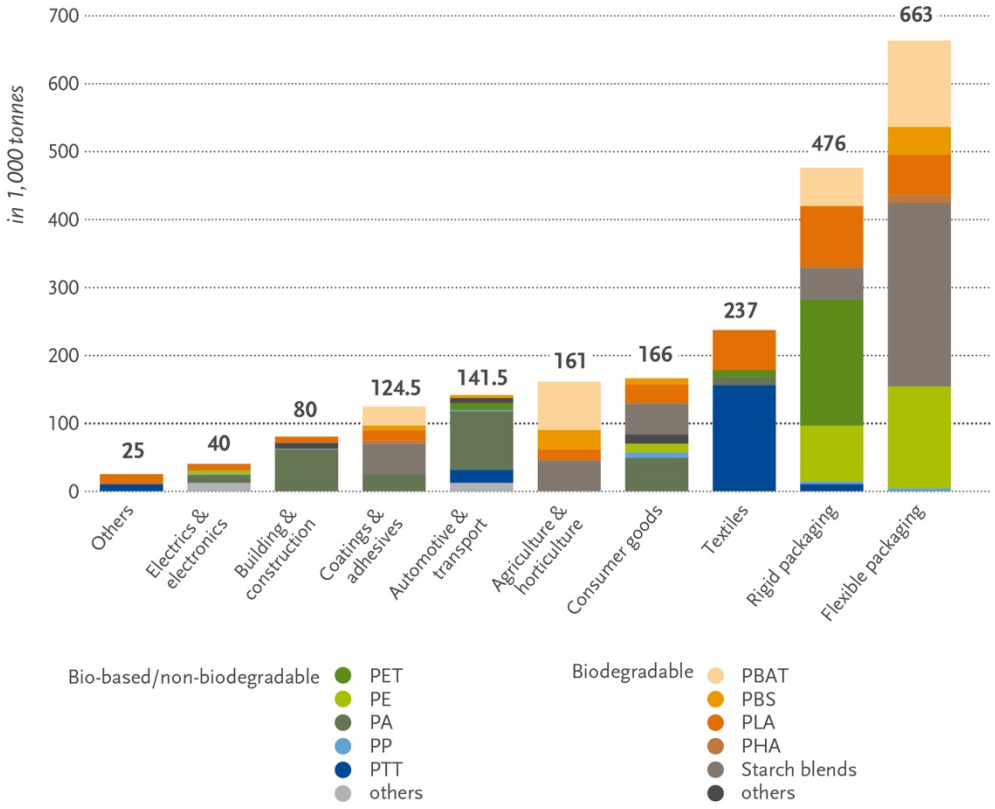

Figure 6 - Global production capacities of bioplastic by market segment 2019 (reproduced from [4]).

Considering the huge production volumes of plastic in packaging industry and the serious ecological problems of their disposal, PHAs can find a really revolutionary and promising future in this application field. In fact, PHAs have similar mechanical and barrier properties to those of traditional packages, but their bio-based origin can help saving precious petroleum resources and their biodegradability can reduce the volumes of landfills or the numbers of packaging discharged into marine waters.

Another application field where PHAs found success was biomedicine, because of two other key properties of PHAs: biocompatibility and biodegradability in physiological environments. These peculiarities along with the processing versatility of PHA for different fabrication techniques enabled a fast-growing and promising emergence of these biopolymers for the production of resorbable biomedical devices, which support cellular adhesion, proliferation and differentiation. [61] Since the beginning of the

twenty-first century, an increasing number of scientific studies and clinical trials have been published about PHA medical devices for different final applications, such as tissue engineering, drug release or vascular stent. [62] A great advantage of PHA compared to other polymers clinically used (e.g., PLGA, PCL, PGA or PLA) is their wide variety of mechanical properties depending on the chemical structure of the monomers. In fact, PLA and PGA have a high Young's modulus (i.e., 3 and 6 GPa respectively) and a limited elongation at break (i.e., around 2%); differently, PCL has an inferior Young's modulus (i.e., 0.35 GPa), but a much higher elongation at break (i.e., 4,000%). These materials are optimal for specific biomedical application, according to their own properties. However, PHAs can be customized, via compounding or copolymerization, in order to obtain a final material with tuned properties suitable for the final application. [63] Moreover, compared to the abovementioned polymers, PHA has a better interaction with the immune system, due to the unchanged local pH value during its degradation, without toxic or inflammatory reactions. [57] As the other properties, also degradation times for PHAs depend on the chemical structure of the bioresorbable polymers. Nevertheless, a previous research study for bioresorbable cardiovascular scaffolds showed that P4HB has a degradation time ranging between two and twelve months. Differently, PGA has an approximate degradation time starting from 6 months; PLLA and PCL degradation takes longer than 2 years. [64]

Current market and future challenges

To date, the higher prices of PHAs make them noncompetitive compared to the fossil-based polymers. In fact, whilst common polyolefins like polyethylene and polypropylene nowadays cost less than 1 €/kg, [65] PHAs can range from 2 €/kg to 5 €/kg depending on the grade. [66] Their higher prices are mainly due to the cost of carbon sources, substrates and to the low extraction yield at industrial scale. [67] Therefore, some important parameters to push PHAs towards commercially competitive production include substrate choice, water and wastewater, oxygen utilization, energy consumption, process complexity and substrate-to-PHA conversion

efficiency. [68] Thus, PHAs producers are trying different ways to reduce the cost of PHAs production by combining the optimization of the biosynthesis and extraction process of PHA pellets and the valorization of agro-industrial wastes with high carbon content, used as raw material to feed microorganisms. [69] Different agro-industry byproducts were investigated as innovative and sustainable feedstocks to encourage waste valorization and decrease the production costs of PHAs. The most interesting results were obtained with whey, a byproduct of dairy and cheese industry; molasses, a byproduct of sugar industry; residual cooking oil or other lipid waste; and glycerol, a byproduct of soap manufacturing. [70] Recently, an increasing number of regulations are limiting or forbidding the production, sale and use of disposable plastic objects such as plastic bags, plastic tableware, delivery packaging and microplastic in cosmetics. [71,72] Hence, the situation promotes the development of PHAs industrialization almost all over the world, as an indication, in Table 2 some PHA commercial companies are listed. Besides, in June 2019 a global organization called GO!PHA has been established to coordinate the promotion of PHAs as a carbon-neutral green bioplastic to address the global plastic pollution issue. Under these circumstances, the global production of PHAs can be expected to expand steadily to meet the growing market demand.

Table 2 – PHA commercial companies (adapted from [68])

Company	PHA type	Scale [ton/year]
PhaBuilder, China	All types	1000-10,000
Medpha, China	P(3HB-4HB)	100
COFCO, China	PHB	1000
Bluepha, China	PHBH	1000
TianAn Biopolymer, China	PHBV	2000
GreenBio, Tianjin, China	P(3HB-4HB)	10,000
Ecomann, Shenzhen, China	P(3HB-4HB)	10,000
RWDC, Singapore, USA	PHBH	Unknown
Danimer Scientific, USA	PHBH	10,000
Newlight, USA	PHB	Unknown
Metabolix, USA	P(3HB-4HB)	5000
Genecis, Canada	PHBV	Unknown
TerraVerdae Bioworks, Canada	PHA	Unknown
Kaneka, japan	PHBH	5000
Nafigate	PHB	Unknown
CJ, Korea	P(3HB-4HB)	Unknown
Helian Polymers, The Netherlands	PHB/PHBV	Unknown
Biocycle, Brazil	PHB	100
Biomer, Germany	PHB	Unknown
Bioextrax, Sweden	PHA	Unknown
SABIO srl, Italy	PHA	Unknown

1.2. Cellulose and its hierarchical structure

Cellulose is the most abundant polymer on Earth, since it is one of the three crucial components of all vegetable cells wall. Cellulose acts as reinforcing element, providing rigidity an structural stability, in an amorphous matrix mostly composed of hemicellulose and lignin, which works as a natural barrier to microbial degradation. [73] However, cellulose is not only present in plants but it can also be found in algae, fungi, bacteria and even sea animal, such as tunicates. [74]

Although cellulose has been used for centuries by human society, it is only since 1838 that Anselme Payen established that the fibrous component of all plant cells has a unique chemical structure and he was the first to use the term “cellulose”. He discovered that when plant tissues are purified with an acid-ammonia treatment, followed by an extraction in water, a constant fibrous material is formed. It required 75 more years for the basic cellulose formula to be established by Willstätter and Zechmeister in 1913. [75] In Figure 7 it is shown the basic chemical structure of cellulose, which is composed of two β-1,4-linked D-glucopyranose rings, and it is called anhydroglucose (AGU) unit.

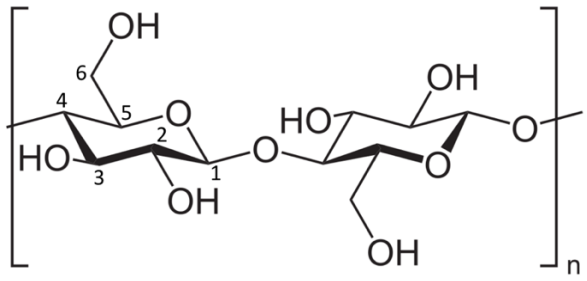

Figure 7 - Chemical structure of cellulose and numbering system for carbon atoms.

One important aspect of cellulose is that each of its monomers bears three functional hydroxyl groups, as a matter of fact most of the chemical properties of celluloses strictly depend on the presence of them. For example, cellulose is basically hydrophilic; however, its solubility in water

can be highly affected by the hydrogen bonds, which are created among different -OH groups. [76] Besides, these hydroxyl groups represent some perfect grafting sites to perform various functionalization reactions. [77]

The other fundamental aspect of cellulose is its bottom-up biologically controlled self-assembly. In fact, AGU units are naturally organized into fibers in different length scales, forming nano-, micro- and macro-fibers. [78] These cellulose microfibrils are composed as an alternation of amorphous and crystalline regions. In the former region, the cellulose chains have a disordered arrangement; whereas, in the crystalline domains, cellulose chains are tightly arranged in ordinated structures to form stiff crystal domains. [79] In Figure 8 there is a schematic representation of the multi-scale hierarchical cellulose organization.

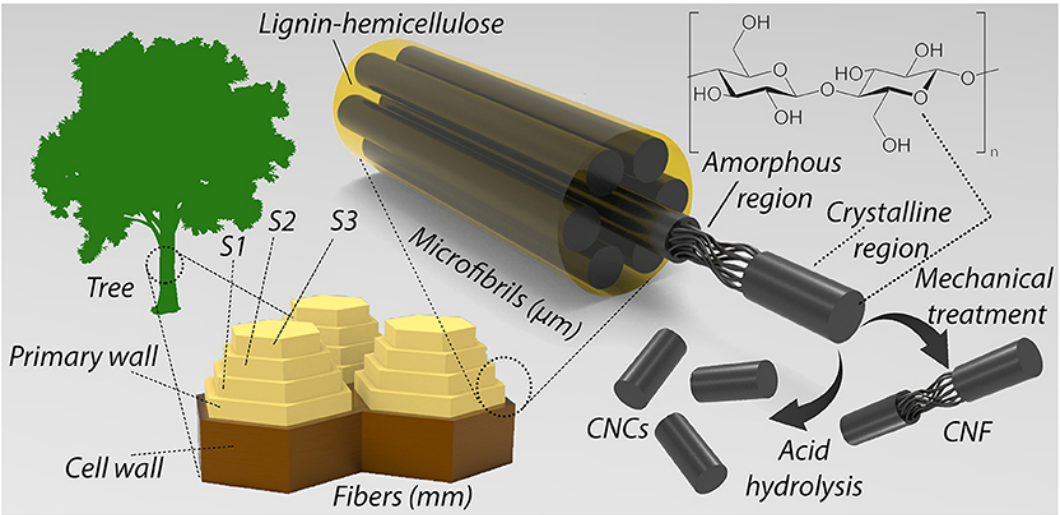

Figure 8 - schematic representation of the multi-scale hierarchical cellulose organization (reproduced from [80]).

Nowadays, the term “nanocellulose” is becoming increasingly common, and it can be used when we refer to a cellulosic treated material with structural dimensions at the nanoscale. Nanocellulose may be differentiated into: bacterial cellulose (BC), cellulose nanofibrils (CNFs), and cellulose nanocrystals (CNCs). BC differs from the other types for its origin, in fact, it is produced by bacteria as microbial extracellular polymer; whilst, CNFs and CNCs are mainly obtained from plants. According to the “deconstruction”

process that a cellulosic material undergoes to attain a nano-size, it is possible to obtain diverse final morphological structures. Specifically, a mechanical disintegration, such as homogenization or grinding, can transform cellulose fibers into CNFs; [81] differently, a chemical process, like acid hydrolysis, can be used to obtain CNCs. [82]

1.2.1. Bacterial cellulose (BC)

In 1886 A. J. Brown discovered that cellulose could also be synthesized as an extracellular product of vinegar bacteria in the form of a gelatinous pellicle (Figure 9); specifically, he obtained it from the *Acetobacter xylinum* bacterium during a vinegar fermentation. [83] Bacterial or microbial cellulose belongs to specific products of primary metabolism and it constitutes mainly a protective coating, for example, from drying or from ultraviolet light. Nowadays, BC can be synthetized by more than ten different bacteria genera, but from a commercial point of view, only the *Acetobacter* species produce enough cellulose. [84]

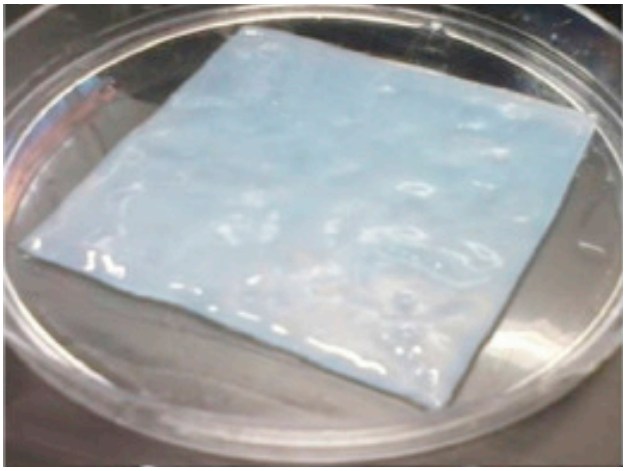

Figure 9 – Visual appearance of bacterial cellulose (reproduced from [85]).

One of the most important features of bacterial cellulose is its chemical purity, which distinguishes this cellulose from that of plants, usually associated with hemicelluloses and lignin. BC is a nanofibrillar material with a combination of properties such as high crystallinity (84% ÷ 89%) and polymerization degree, high aspect ratio of fibers, with diameter ranging

between 20 and 100 nm, high flexibility and tensile strength (i.e., Young's modulus of 15 ÷ 18 GPa) and high water-holding capacity (over 100 times of its own weight). [86] These interesting properties ensured many different industrial applications for the BC; for example, it is used in biomedicine, micro-electronics, cosmetic and textile manufacturing, water and waste treatment and also food industry. [87] Nevertheless, there are still some limitations for its extensive use, which are the lack of a large scale production capacity and its high price, roughly 100 times higher than plant cellulose. [84]

1.2.2. Cellulose Nanofibril (CNF)

The mechanical fibrillation process allows to destruct the cellulose fibers into smaller fibrils with a weblike structure (Figure 10), where crystalline and amorphous regions alternate along the fibril itself. According to the final sizes, it is possible to differentiate between the microfibrillated cellulose (MFC) and the cellulose nanofibrils (CNFs). Even if there is no univocal definitions of the two terms, and this can lead to ambiguities, both expressions indicate a cellulose fiber that underwent a mechanical fibrillation process, involving high shearing forces. However, as an indication of their difference, we can state that CNFs have a diameter of 5 ÷ 60 nm and a length of several micrometers; [88] while, MFC have a diameter of hundreds of nanometers and a length of tens of microns. [89]

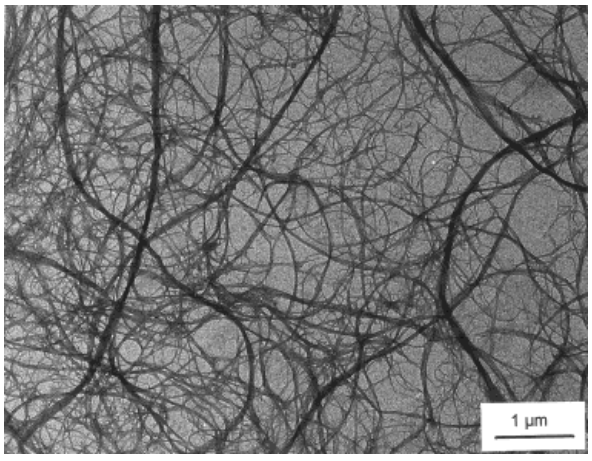

Figure 10 – TEM image showing cellulose nanofibrils after high-pressure mechanical treatment (reproduced from [90]).

Different top-down mechanically induced destructuring strategies have been investigated so far, but the most common are here summarized:

- High-pressure homogenization: first a suspension of pulp in water is prepared and then it passes through a thin fissure and hence it is subjected to a high pressure drop with impact force and cavitation effect. [91]
- Microfluidizer: the cellulose suspension is pumped at high velocities through z-shaped micro-channels, impacting on wear-resistant surfaces and thus obtaining high shear forces. [92]
- Ultra-fine friction grinding: the cellulose slurry first undergoes a massive compression and then a grinding by friction, caused by the cyclic crushing of the suspension between two discs, the upper fixed and the lower rotating. [81]
- Cryocrushing: the fibers are immersed in liquid nitrogen to freeze the water stuck inside, then, the pulp is crushed with a cast iron mortar and pestle. [93]
- Aqueous counter collision: the suspension is expelled by two nozzles, so that the two jets collide one against the other under high pressure, obtaining a wet pulverization and the formation of an aqueous dispersion of cellulose nanofibrils. [94]
- High-intensity ultrasonication: this is a laboratory-scale method that applies ultrasound to the sample. A high frequency (i.e., 20 ÷ 50 kHz) is transmitted to the sample via a metal probe that oscillates, generating a localized high-pressure region, which breaks down the cellulose fibers by effect of cavitation. [95]
- Ball milling: this technique works on the principle of impact and attrition; it is used a hollow cylindrical shell rotating around its axis, and filled with steel balls, which act as grinding media, and with the fiber suspension. [96]

All these procedures have one common limitation, in fact, they are largely energy consuming. Hence, in order to reduce the energy and the cost required to break down the cellulose fibers, some chemical pre-treatments

have been investigated to favorize the following defibrillation. These are some of the most frequently used: acid hydrolysis, TEMPO-oxidation, enzymatic pretreatment or carboxymethylation. [81]

NFC possess really attractive properties, like a high Young's modulus of about 100 GPa, [88] an aspect ratio varying from 100 to 150, [97] its biodegradability, its biocompatibility and it has a shear-thinning behavior. [76] These properties are the reason for the fortune that this material encountered primarily as reinforcing agent for different polymer matrices, [98–101] but also for electronic devices, [102] food products, [103] medical and tissue engineering, [104,105] cosmetic [106] and also automotive industry. [88]

1.2.3. Cellulose nanocrystal (CNC)

Cellulose nanocrystals are produced by dissolving the amorphous domains from the cellulose fibers and by isolating the crystalline regions. A strong chemical reaction, such as an acid hydrolysis, is required to isolate cellulose nanocrystals, which are needle-like particles (Figure 11).

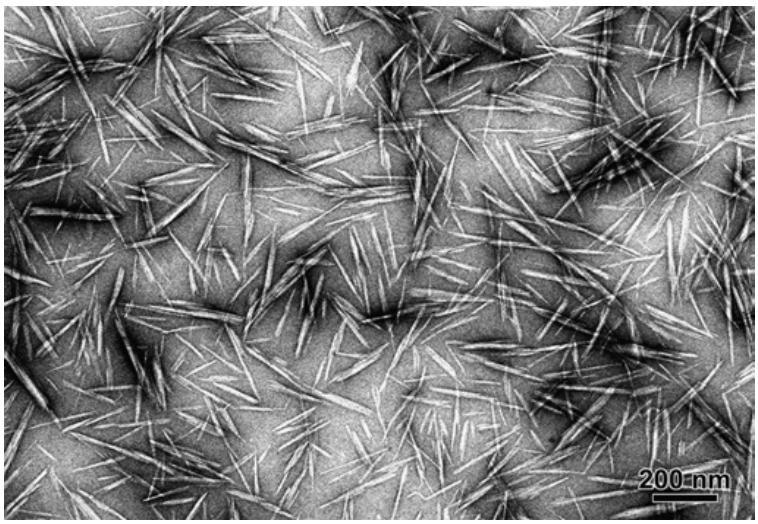

Figure 11 – TEM image of cellulose nanocrystals (reproduced from [107]).

Wood and cotton are the principal sources for CNC extraction, due to their natural abundance and high cellulose content, respectively. However, depending on the source of cellulose and the hydrolysis conditions, such as

time, temperature and acid concentration, the physical dimensions of the CNCs can vary, along with the degree of crystallinity and the yield. [82] As an indication of the order of magnitude, the diameter and the length of the CNC can be considered 2 ÷ 20 nm and 150 ÷ 300 nm, respectively. [108]

The chemical procedure to obtain CNCs starting from a natural fiber is represented in Figure 12 and here summarized: [82]

1. Purification: preliminary step to remove non-cellulosic constituents from the fibers.
    a. It starts with an alkali procedure, either with NaOH or KOH, to solubilize the hemicellulose.
    b. A bleaching step with acetate buffer and $NaClO_2$ is needed to remove lignin and to whiten the material.
2. Acid hydrolysis: consists in the penetration and diffusion of the acid, most frequently sulfuric acid, into the cellulose chains and promoting the hydrolytic cleavage of the glycosidic bonds in the amorphous domains, releasing individual crystals. The motivation for which the cleavage starts from amorphous regions, rather than crystalline ones, is ascribed to the faster hydrolysis kinetics of amorphous domains than the others.
3. Post-treatment: the suspension resulting from the acid hydrolysis is first cooled at room temperature and subsequently, filtered, diluted with water, and washed with successive centrifugations. In the end, dialysis against distilled water is performed to remove any free acid molecules from the dispersion.

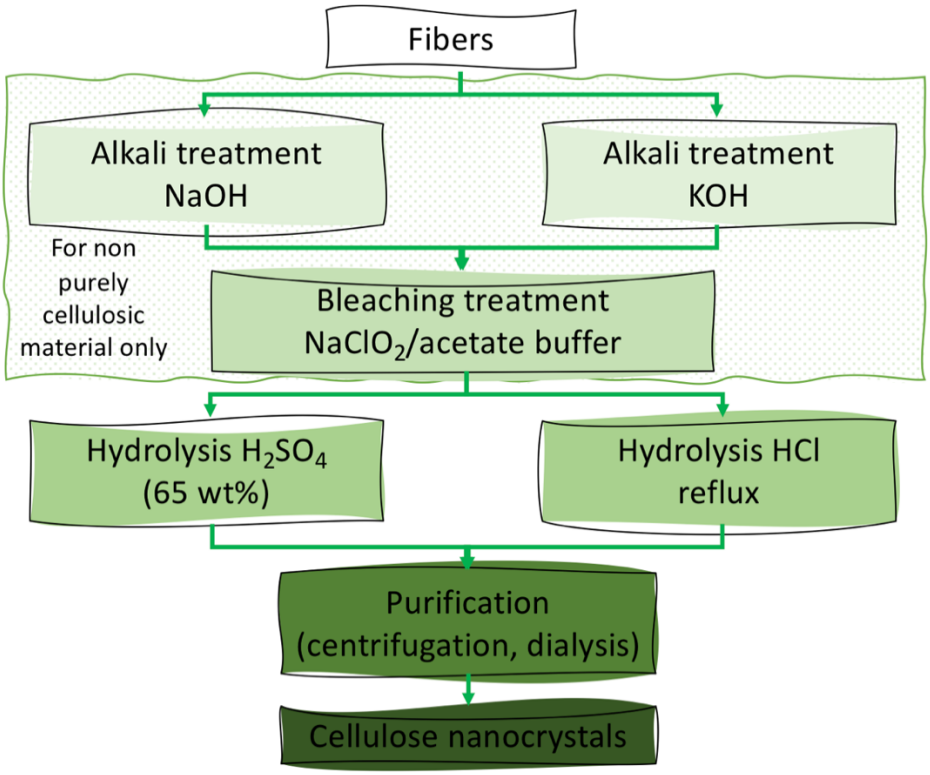

Figure 12 - General treatment to obtain CNC starting from natural fibers.

Even if CNCs and CNFs have similar properties, we consider for example the similar Young's modulus, i.e. around 140 GPa for CNCs, [109] the fact that also cellulose nanocrystals are biodegradable, biocompatible and they possess a shear-thinning behavior. But, one important morphological difference between CNC and CNF is that the former have a lower aspect ratio, ranging from 10 to 50, but a higher surface area. [110]

Due to the similarity with the CNFs properties, also the application fields are quite similar for the two materials: papermaking, [111] electronic, [80] food, [112,113] medicine and pharmaceutical industries; [114,115] moreover, CNCs found a great application as green reinforcing agent for composites material. [116–118]

1.2.4. Cellulose functionalization

Previous research investigating the reinforcing effect of nanocellulose indicates that a great challenge, when compounding hydrophilic nanocellulose with apolar polymer matrices, is obtaining an efficient

nanoparticle dispersion and a good nanofiller-matrix interfacial interaction. [119] In fact, it is expected that a fine adhesion between the matrix and the dispersed phase can enhance the stress transfer between the two phases and then improve the load-bearing capacity of the material. [120] Different approaches have been experimented to perform a chemical modification of the nanocellulose surface, including coupling hydrophobic small molecules, grafting polymers or oligomers, and adsorbing hydrophobic compounds to surface hydroxyl groups. These modifications besides improving the reinforcing effect of nanocellulose, are also used to tailor its properties, for example, by grafting on the surface specific molecules that can act as binding sites for active agents in drug delivery systems or for toxins in purifying and treatment applications.

According to its molecular structure, cellulose is an active chemical because of the presence of three hydroxyl groups, which are the main responsible for cellulose reactions. Each anhydroglucose unit has one primary -OH group at the carbon 6^{th} position, and two secondaries -OH groups at the 2^{nd} and 3^{rd} positions. An important parameter to characterize the efficiency of reaction of cellulose is the degree of substitution (DS). It indicates the average number of hydroxyl groups of AGU unit that are substituted after reaction. Therefore, the DS value ranges between 0 and 3 and the maximum value of 3 indicates that all three hydroxyl groups are substituted. Due to its more accessible position and to its higher distance from the glucopyranose ring, it was reported that the primary hydroxyl group can react ten times faster than the other -OH groups. [121]

Different studies have been conducted to investigate the possible routes to substitute the cellulose hydroxyl groups with hydrophobic tails and hence introduce new functionalities to nanocellulose. The most important functionalization procedures are hereby recapitulated:

- Esterification: is a reaction that introduces an ester functional group (-CO-O) on the surface of cellulose nanoparticles by condensation of a carboxylic acid group (-CO-OH) and an alcohol group (-OH) of cellulose. [99,122] The reaction is schematized in Figure 13.

Figure 13 - Scheme reaction of esterification procedure.

- Acetylation: is a particular method of esterification that introduces an acetyl functional group (-CO-CH_3) on the surface of cellulose nanoparticles. [123,124] The reaction is schematized in Figure 14.

Figure 14 – Scheme reaction of acetylation procedure.

- Silanization: consists in the introduction of silyl groups R_3Si on the surface of cellulose nanoparticles. Many organofunctional silanes have been examined as coupling agents and their general formula is $R_1R_2R_3SiX$. The bond between X and the Si in coupling agents is replaced by a bond between the cellulosic substrate and the Si atom. X is a hydrolysable group, typically methoxy or ethoxy, which gives methanol and ethanol as by-products during coupling reaction. [125,126] The modification is schematized in Figure 15.

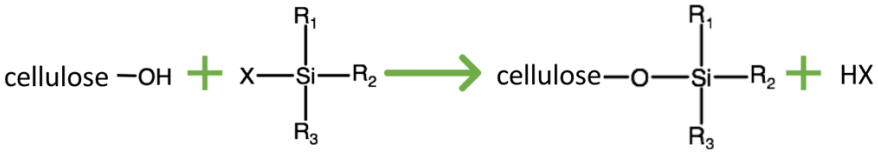

Figure 15 – Scheme reaction of silanization procedure.

- TEMPO-mediated oxidation: involves the use of 2,2,6,6-tetramethylpiperidine-1-oxyl (TEMPO) as catalytic oxidative reagent to transform the hydroxyl groups, from the surface of cellulose, first into aldehyde and then into carboxylate functional groups, under

aqueous and mild conditions. [101,127] The reaction is schematized in Figure 16.

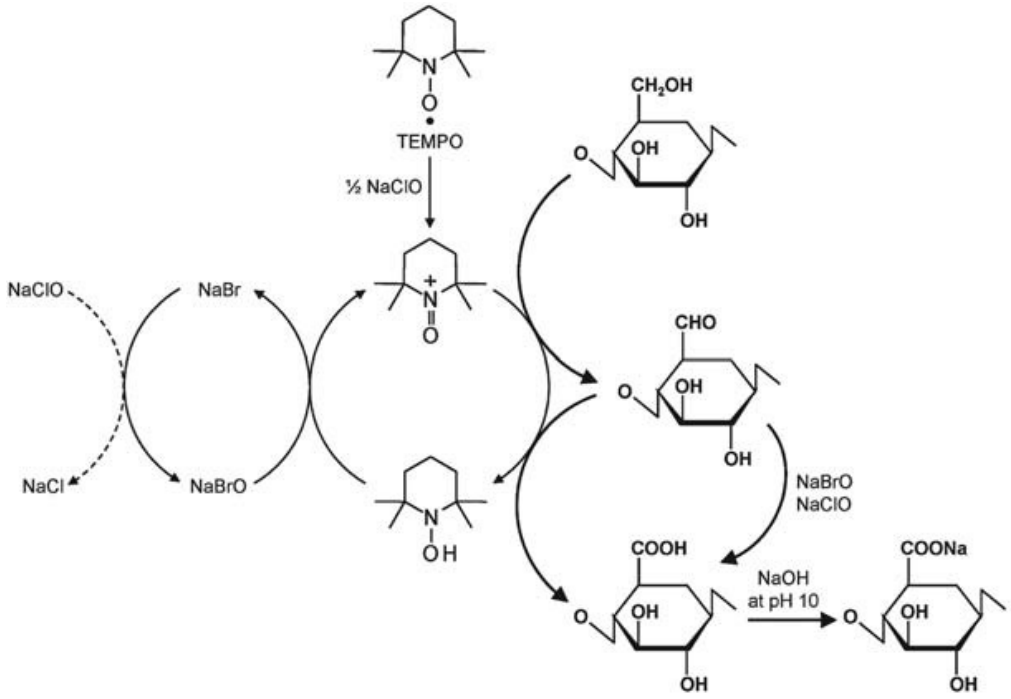

Figure 16 – Scheme reaction of TEMPO-mediated oxidation procedure (reproduced from [128]).

- Polymer grafting: consists in grafting agents bearing a reactive end group and a compatibilizer tail. Two main different approaches can be used to graft polymers on cellulose surface. These two strategies are schematized in Figure 17.
    - Grafting “onto”: this approach implies mixing the cellulosic nanoparticles with a polymer and a coupling agent to attach the polymer to the cellulose surface. [129]
    - Grafting “from”: this approach implies mixing the cellulosic nanoparticles with a monomer and an initiator agent to induce the polymerization of the monomer from the nanoparticle surface. [130]

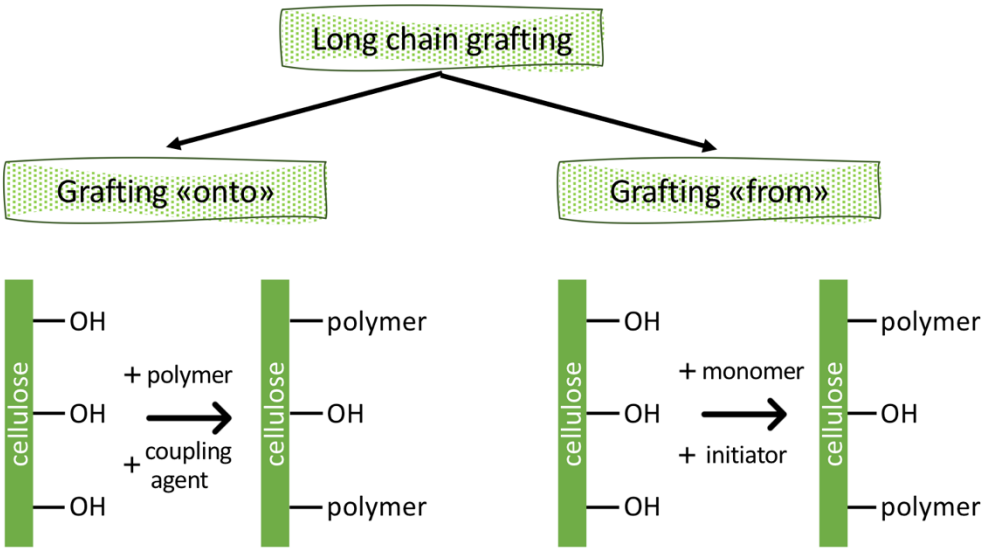

Figure 17 – Schematic representation of the grafting “onto” and grafting “from” approaches.

1.3. PHA-based green composites: state of the art

The fabrication of environmentally friendly PHA-based composites has a huge potential because it can combine sustainability and tunable properties, such as stiffness, strength, thermal stability, or gas-barrier functionality, in a single material. Previous research has focused on different reinforcing effects of some agents, such as glass fibers [43] for improving the stiffness and the strength or graphene oxide [131] for increasing the gas-barrier properties and decreasing the diffusivity. However, particular interest has been reserved for natural reinforcements, so that the overall sustainability of the product was not affected. Table 3 provides a schematic summary of the most relevant scientific studies on PHA-based green composites, together with the production methodology and results obtained.

Table 3 – Major scientific investigations on PHA-based green composites

PHA matrix	Natural agent	Production method	Results	REF.
PHB	Carnauba fibers	Solvent casting	Carnauba fibers were successfully compounded and they proved an alternative to plain PHB, with cost reduction and similar mechanical properties.	[132]

PHA matrix	Natural agent	Production method	Results	REF.
PHBV	CNF	Melt-compounding	Increased tensile modulus of the composites (nearly twofold), but faster thermal degradation of PHBV matrix. Increased storage modulus in the glassy state. Decreased CO_2 solubility in the composites and increased desorption diffusivity.	[133]
PHBH	Porous cellulose	Solvent casting	Good transparency, accelerated crystallization rate and decreased spherulite size of PHBH. Higher Young's modulus, strain at break and tensile strength for composites.	[134]
PHB	Coffee Wastes	Melt-compounding	Improved thermal stability of the composites, decreased degree of crystallinity, increased water absorption, tensile strength and Izod strength.	[135]

PHA matrix	Natural agent	Production method	Results	REF.
PHBH	Cellulose and wood flour	Melt-compounding	Wood flour enhanced crystallization effect on PHBH (5.6 mol % of 3HH): increased crystallization peak temperature, degree of crystallinity under nonisothermal conditions, and decreased crystallization half time under isothermal conditions.	[136]
PHBV	CNC and CNF	Melt-compounding	Improved thermal stability of composites, reduction in the crystalline size of PHBV spherulites. CNC led to higher tensile modulus of composites, compared to CNF.	[137]
PHBV	CNC	Solvent casting	Nucleating effect of cellulose nanoparticles, rougher surface for composites. Better barrier properties against water vapor and oxygen.	[138]

PHA matrix	Natural agent	Production method	Results	REF.
PHB/PHBV	Rice husk flour	Melt-compounding	Up to 20 wt% of biowaste used for green composite films with a high transparency, relatively low crystallinity, high thermal stability, improved mechanical ductility, and medium barrier performance to water vapor and aroma.	[139]
PHB	BC	Melt-compounding	Increased stiffness and strength. After a plasma treatment, the storage modulus and tensile strength of PHB increased. In addition, plasma treatment also inhibited the growth of *Staphylococcus aureus* and *Escherichia coli*.	[140]
PHBV	Waste wood sawdust	Melt-compounding	Sustainable option of valorization of wood-industry residues and lowering the production cost of PHBHV-based compounds without affecting the mechanical properties, improving the impact resistance and biodegradability rates in terrestrial environments.	[141]

PHA matrix	Natural agent	Production method	Results	REF.
PHBH	CNC	Solvent casting	Improved mechanical properties of PHBH, decreased surface contact angle and spherulite size of PHBH, whilst the nuclei density increased.	[142]
PHBH	CNC	Solvent casting	Improved thermal stability and mechanical properties, increased water-vapor permeability coefficient and decreased oxygen permeability coefficient.	[143]
PHBH	CNC	Solvent casting	Improved tensile strength, Young's modulus, water-vapor and oxygen barrier properties. Also an enhancement on thermal stability was reached.	[144]
PHBH	CNF	Melt-compounding	Thermal properties were not affected by CNF compounding, as well as mechanical properties remained almost unchanged. But for the first time, filaments, suitable for FDM, were prepared and 3D printed.	[145]

PHA matrix	Natural agent	Production method	Results	REF.
PHB	Wine wastes	Melt-compounding	Wine lees have a stiffening effect also at high temperatures and they promote biodegradation both in soil and in marine water environments.	[146]

As it is shown in Table 3, different green PHA composites have been explored at distinct reinforcing contents. However, only a limited exploration has been conducted to determine the effect of oat hull fibers (OHF) as filler for a polymer matrix. Here, the novelty of this research study is that a fully bio-based composite material was obtained starting from a PHBH matrix, which was chosen as only component rather than a blend of different synthetic and fossil-based polymers. [147,148] A limitation that was overcome in this research, compared to the previous ones, is that the OHF worked properly as a replacement for the polymer matrix, but the mechanical properties of the composite were not affected by this.

Moreover, it is worth noting that most of the prior studies were focused on the fundamental analysis of the fabrication of biocomposites, not considering neither the technological aspects of the process, nor exploring their possible final applications. For example, the importance of industrial scalability was underestimated and frequently laboratory-scale approaches, such as solvent casting, were chosen rather than solvent-free methodologies, like melt compounding. In this study, all aspects starting from chemical interaction between cellulose phase and biopolymer matrix, technological compounding features and proper characterizations were considered for the biocomposites production. Besides, the research was not limited to the fabrication of new biobased composites, but it was pushed toward possible applications in growing interest fields: additive manufacturing and biomedical engineering. In fact, nowadays, the new challenging frontier of FDM is the use of unconventional polymers with

original properties and different possible applications. Previous research investigating PHBH 3D-printability is still extremely limited, and there is only one research focused on FDM 3D-printing of PHBH and CNF. [145] Furthermore, the findings obtained in the previous study are referred to composites with low CNF content (up to 3 wt%), and the mechanical properties obtained are inferior to those of pristine PHBH, probably due to a low affinity between the matrix and CNF. In this doctoral research, biobased composites at high CNC content (5−20 wt %) were developed after a chemical modification of CNCs to improve the interaction of the nanocellulose and the matrix and, thus, obtaining an enhancement in mechanical and thermal properties of the final composite. This innovative material was then successfully 3D-printed to realize complex and fully biodegradable architectures, which were, for the first time, different from simple bars or mechanical test samples. In this way, the advantages of an ecofriendly material were mixed with the possibility of producing objects with customizable designs by additive manufacturing.

1.4. Additive Manufacturing (AM) technologies for polymers

Additive manufacturing (AM) is probably the most revolutionary novelty introduced in the technological and engineering landscape of the last decades. It totally revolutionized the manufacturing process and the main reason for its great success are different, including the possibility to fabricate complex geometries with an ultra-high customization, the saving of material, the reduction of production and assembly steps, the elimination of some tooling (e.g. the stainless steel molds), as well as the waste diminution. [149] AM has been initially known as rapid prototyping (RP) because of its use as a cheap and quick way to produce prototypes but, nowadays, the precision and the efficiency that these innovative techniques introduced allow to consider them as full-fledged production technologies. [150]

The freedom in the designing of AM relies on the fact that the process starts with a 3D Computer-Aided Design (CAD) model, which represents the final shape of the device that is wanted to be fabricated. Thereafter, the CAD model has to be converted into a STL file, i.e. a file format that AM machines software can process. This file can be manipulated through a software that is able to orient the model, to generate supports if needed, to tailor the infill and finally complete the slicing operation that transforms a 3D object into a stack of 2D layers to be printed one on the top of the other. The results of this process are gcode files, a programming language that contains the instructions for the printer how to reproduce the 3D model, layer by layer. Subsequently, the actual printing process takes place; and after that, the piece can be removed from the printer and it might undergo some post-processing steps, such as: washing, thermal or UV post-curing and surface finishing.

A first important distinction among polymer materials for additive manufacturing has to be made between thermoplastic and thermosetting polymers. In fact, for the former it is possible to exploit thermal energy to

soften them and deposit in different final forms. Differently, for thermosetting polymers a photopolymerization process is requested to obtain a cross-linked structure and hence a solid final item. According to the starting form of the polymer material, it is possible to group the 3D printing technologies. Figure 18 shows a scheme of the suggested classification. Some technologies start from powder materials and create an object by selectively depositing a liquid bonding agent to join powder materials (binder jetting) or by selectively sintering or melting them with the thermal energy of an electron beam or a laser (powder bed fusion). Other technologies use solid materials (usually filaments or pellets) that are melted to be selectively dispensed through a nozzle in consecutive layers (material extrusion). Finally, other technologies start from a liquid photopolymer material, which can be either locally deposited and cured (material jetting) or selectively cured by light-activated polymerization from a liquid vat (vat photopolymerization, or VP). [151]

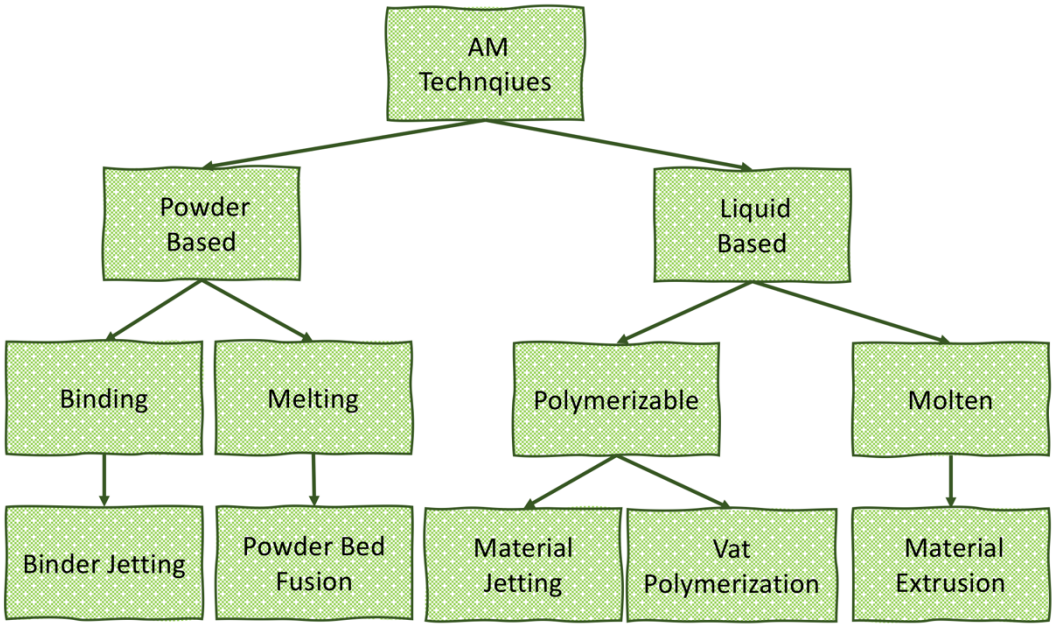

Figure 18 – Classification of the principal AM techniques for polymers (highlighted).

1.4.1. Fused Deposition Modeling (FDM)

FDM, also called Fused Filament Fabrication (FFF), is the most popular additive manufacturing technique, due to its straightforwardness, its design

freedom and low cost. It is a layer-by-layer melt-extrusion approach that consists in heating up a continuous filament of a thermoplastic material above its glass-transition temperature (T_g), and then force it to pass through a nozzle and deposit the extruded material still hot to ensure the adhesion with the underneath layer, already cooled down and hardened (Figure 19). The pressure needed to force the melt filament through the nozzle is given by a mechanical system, i.e. two opposite rolls, with knurls for a proper filament grip, are connected to an electric motor and can rotate to direct the filament through the nozzle. The final object is a fully solidified structure whose design accuracy is guaranteed by a computer control of movements of both printing platform and 3D printer extruder head. [152] Although FDM is capable of dealing with small overhangs, it has some restrictions on their slope, and it cannot produce unsupported shapes.

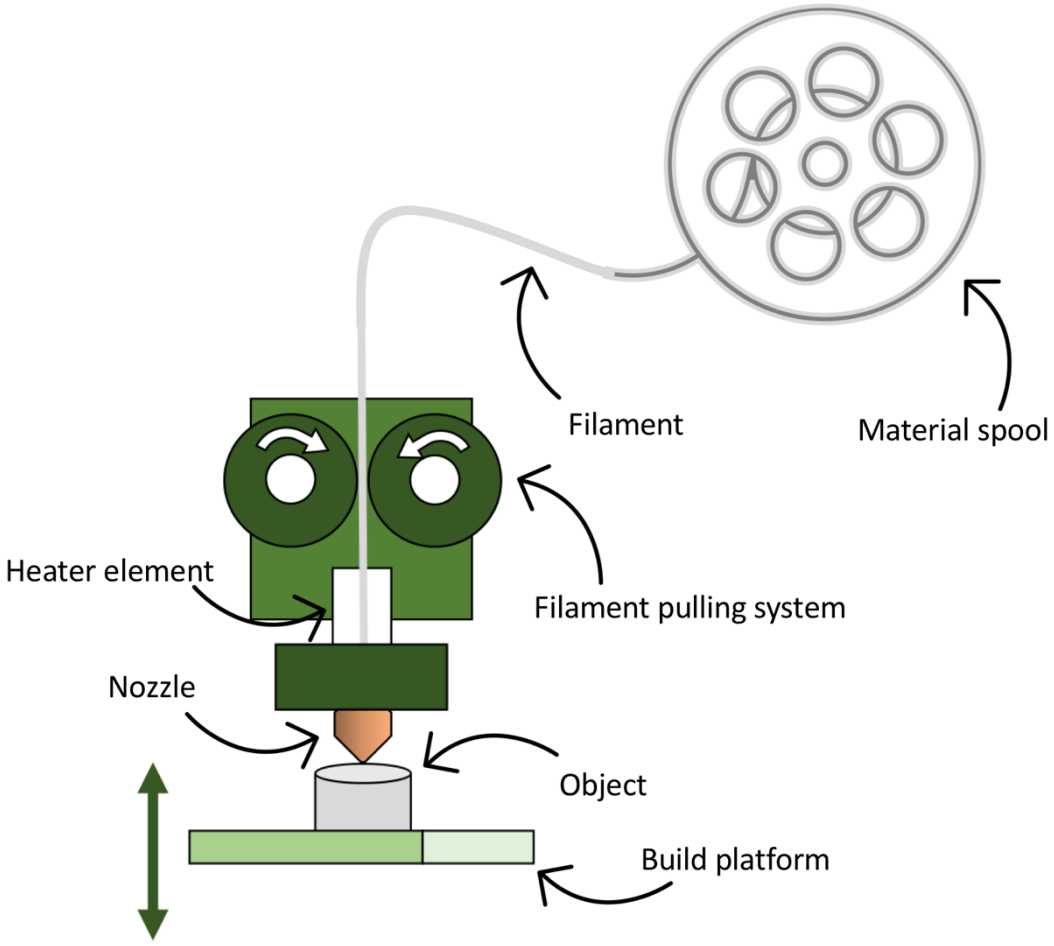

Figure 19 – Fused Deposition Modeling machine layout.

Polymers hold the absolute primacy in the field of FDM, whose great processing versatility is one of the key factors for the fortune that this technique found on the market. In fact, a wide variety of materials are nowadays commercially available for FDM, although the request for new materials with higher performance, or with innovative functionalities for specific applications, continues to grow. Some of the most commonly used polymers for FDM are: acrylonitrile-styrene-butadiene (ABS), polycarbonate (PC), polylactic acid (PLA), polystyrene (PS) and polyamide (PA). [153] One example of a high temperature and chemically resistant polymer that has been studied in the last years to be applied in FMD, is polyether ether ketone (PEEK). [154] However, the majority of the research interest is nowadays focused on the investigation of emerging composite and nanocomposite materials for FDM, which can enhance the thermal and mechanical properties of the polymer matrix, [155] decrease the cost of the final item, [156] or also introduce new functions to commercially-available polymers like electromagnetic interference shielding. [157]

The potential of FDM on personalization of products allowed this technique to find important scientific and industrial applications and here are listed the majors:

- Automotive industry: Light and high-end, specialized components are a prevailing trend in the automotive industry. And even if FDM cannot compare with the production volumes of traditional techniques, AM sector continues to increase. [158]
- Aerospatiale industry: The success in the aerospace industry is ascribable to the possibility of printing parts with complex designs, reducing the production costs and time. [159]
- Electronic fabrication: FDM is an innovative and valid alternative for the manufacture of micro-electronic components, where thermal management is required. [160,161]

A particular interest is reserved for bioengineering and biomedical applications of additive manufacturing. In fact, FDM technique allows for the fabrication of low-cost, rapid and customized solution for a diversity of

surgical and therapeutic scenarios. [162] First of all, the fabrication of scaffolds with complex shape and internal porous structure that contribute to the formation of new tissues. The precise control of scaffold structure, surface morphology and pore size is a challenge for current 3D printing methods. In order to facilitate tissue regeneration, scaffolds need to be designed to provide a suitable environment for cell growth, depending on the selection of materials, the geometrical features such as internal structures and pore size distribution and the mechanical properties of the scaffold, which have to match with those of the original tissue. [163] Besides, it is also possible to build with FDM external medical devices, such as a finger cast, [117] or also delivery drug systems. [164] Therefore, it is clear that there is still a huge potential for applying FDM printing in bioengineering.

2. Materials and methods

2.1. Materials

2.1.1. Poly(3-hydroxybutyrate-*co*-3-hydroxyhexanoate)

Poly(3-hydroxybutyrate-*co*-3-hydroxyhexanoate) (PHBH) is a bio-based and biodegradable copolymer belonging to the PHA family. It is constituted by two distinct monomers: 3-hydroxybutyrate (3HB) and 3-hydroxyhexanoate (3HH). In Figure 20 it is represented PHBH chemical structure.

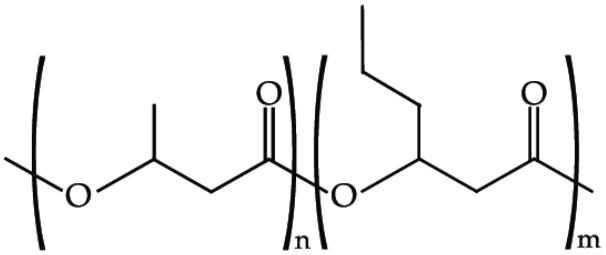

Figure 20 - PHBH chemical structure.

It is noteworthy that with the increase of 3HH/3HB molar ratio there is a decrease in the Young's modulus, melting temperature and in crystallinity but an increase in flexibility and elongation at break, due to the increased steric effect given by the side alkyl chain. In this research study, PHBH pellets were kindly provided by MAIP Group (MAIP SRL, Turin, Italy) with the trade name of B6H N15 and the composition ratio is 89 mol% of 3HB and 11 mol% of 3HH. This composition was chosen, because it represents the semi-rigid grade of PHBH and it has balanced values of ductility and elastic modulus, broadening the possible application fields. The main thermal and mechanical properties, according to datasheet provided by MAIP Group, are illustrated in Table 4.

Table 4 - Thermal and mechanical properties of PHBH (B6H N15) from MAIP datasheet

	PHBH (B6H N15)
Density [g cm^{-3}]	1.2
Melting temperature [°C]	135
Glass transition temperature [°C]	0
Tensile modulus [MPa]	1000
Tensile strength [MPa]	19
Strain at break [%]	24

2.1.2. Oat hull fiber

Oat hull fibers, OH, were provided by GEA Mechanical Equipment (Parma, Italy) as a powder. The fibers were obtained as a food waste from the oat processing, and their morphology is composed of fibrils many hundreds of microns long and several tens of microns thick; their aspect ratio is about 20. Figure 21 shows the morphology of the OHF.

Oat hull fibers were used in two different forms: as received, and also after a high-pressure homogenization process, in order to obtain microfibrillated cellulose (MFC) to be further used as cellulosic filler.

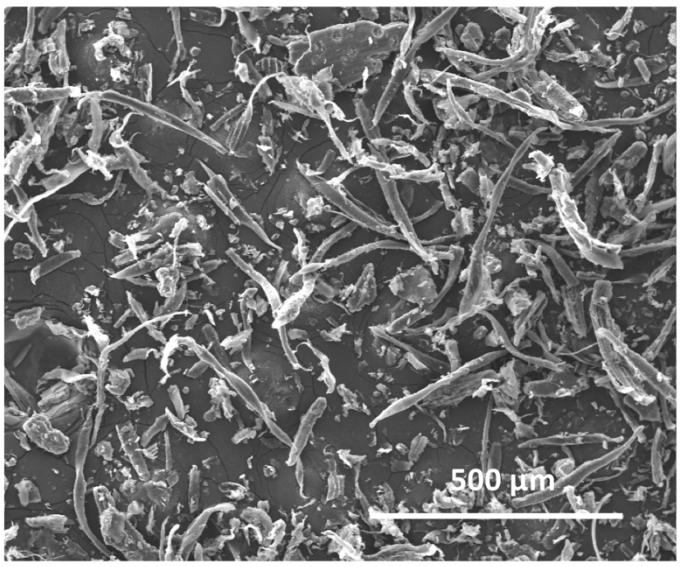

Figure 21 - SEM image of Oat hull fibers (scale bar = 500 µm).

2.1.3. Cellulose nanocrystals

Cellulose nanocrystals, CNCs, were purchased from CelluForce. According to the elaboration of the transmission electron microscopy images (Figure 22), nanocrystals have an average length (L) of 120 nm and an average diameter (d) of 6.5 nm, and they possess an aspect ratio (L/d) of about 18.

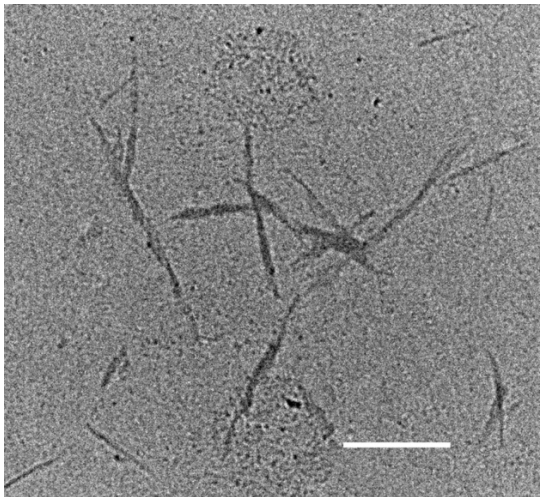

Figure 22 - TEM image of cellulose nanocrystals (scale bar = 150 nm).

2.2 Methods

2.2.1. Microfibrillated cellulose preparation

Trying to limit the use of chemical solvents and thinking of a closer industrial application, it was followed a purely mechanical process to obtain MFC from OHF. The oat hull fibers were dispersed in water with a concentration of 5 wt%, first by a mechanical mixer, and subsequently by a high-shear mixer (Ultra-Turrax) at 10,000 rpm. The suspension was then homogenized with a high-pressure process with a NS3006L homogenizer (GEA Mechanical Equipment) at 700 bar for 15 times. The obtained microfibrillated cellulose (MFC) suspension was stored at refrigerator temperature; in Figure 23 the morphology of the obtained MFC is shown.

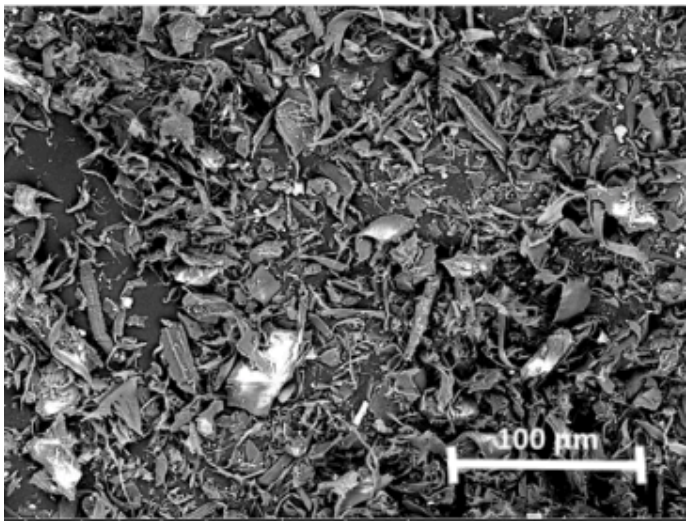

Figure 23 - SEM image of MFC (scael bar = 100 μm).

2.2.2. Cellulose functionalization

To improve the interfacial adhesion between the cellulose filler and PHBH matrix, two different cellulose functionalizations were carried out: a silanization and an acetylation. Hereafter, the chemical procedures are described.

2.2.2.1. Silanization

For the effective adhesion of MFC and PHBH, methyltriethoxysilane (MTES) was used as coupling agent, since it has both polar and nonpolar groups. In Figure 24, chemical modification mechanism of the cellulose silanization is schematically represented. The hydroxyl groups (-OH) of the cellulose react with an ethoxy group of MTES. With this condensation reaction, the silane coupling agent is chemically bonded to the external surface of cellulose.

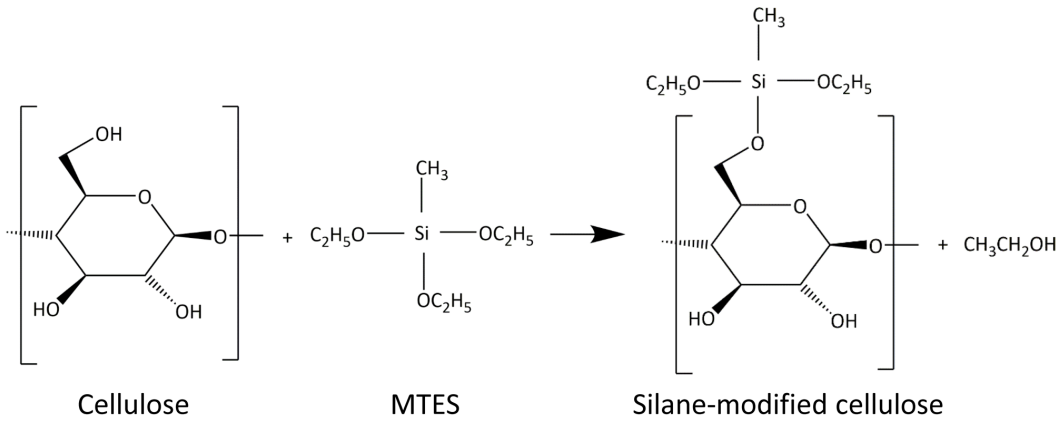

Figure 24 – Modification mechanism of cellulose by means of MTES coupling agent.

The presence of the methyl group in the silane molecule modifies the surface chemistry of cellulose, making it more hydrophobic, and so promoting the compatibility with PHBH matrix. Figure 25 shows the two powders of pristine fibers and silanized ones, dispersed in water. It is easy to qualitatively evaluate the treatment effect onto OHF; in fact, before silanization, neat OHF are easily wettable, while after silanization (Silanized OHF) they stay afloat and do not even get wet, showing an explicitly hydrophobic behavior.

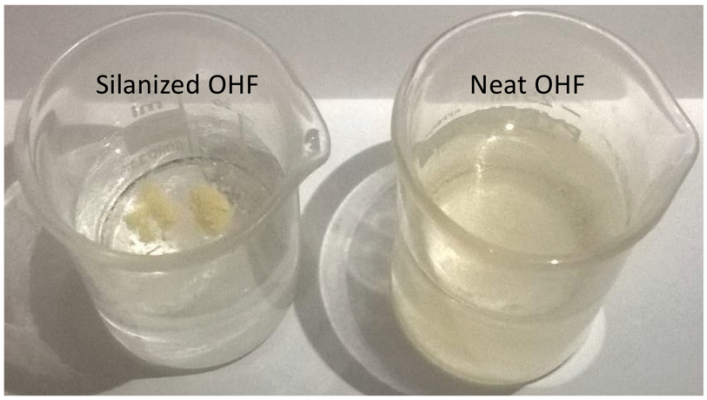

Figure 25 - OHF dispersibility in water before and after the silanization process.

The silanization was pursued following some procedures already tested in previous research; and it was carried out on both OHF and MFC, which below will both be called fibers, for clarity. The procedure consists in mixing the fibers with an hydroalcoholic solution in a basic environment. [165,166] Firstly, a suspension was prepared adding 2.5 g of fibers in 48 mL of water and 74 mL of pure ethanol. Then, 3.6 mL of ammonium hydroxide solution (conc. 30 wt% in water) were added to the previous suspension under magnetic stirring. The obtained suspension was placed into a constant-temperature oil bath at 50 °C and equilibrated for 30 min. After the dispersion reached uniform temperature, 1 mL of MTES was added, drop by drop, and stirring continued at 50 °C for 20 hours. The resulting suspension was then washed from the excess of MTES by two subsequent centrifugations and redispersions in ethanol, and the obtained precipitate was vacuum dried at 35 °C overnight and then milled by an A 10 basic mill (IKA). The same procedure was followed without fibers to obtain a reference sample of sol–gel reaction of MTES, which is referred as hydrolyzed MTES.

2.2.2.2. Acetylation

A second cellulose modification route was investigated to enhance the PHBH-cellulose affinity. This second method was an acetylation process, aimed to bond acetyl groups ($-CO-CH_3$) onto the cellulose surface. This functionalization was chosen because of the expected chemical affinity between the C=O group of PHBH and the $-CO-CH_3$ group of acetylated

cellulose. This procedure was carried out only on CNCs. The acetylation process was run following the precedent research of Olaru et al. without use of any solvent. First, 75 mL of acetic anhydride were mixed with 150 μL of sulfuric acid, used as a catalyst, and then 15 g of CNCs were added to this solution under mechanical stirring at 250 rpm. The acetylation reaction was performed in a round-bottom flask immersed in an oil bath at 30 °C for different reaction times: 1, 2, 8, or 20 hours. A schematic representation is shown in Figure 26. When the desired reaction time expired, each sample was washed by four subsequent centrifugations and redispersions. The precipitated modified CNCs were subsequently redispersed and solvent-exchanged first with ethanol, then with acetone, and finally with chloroform. All centrifugation operations were conducted at 5000 rpm for 10 min. Each redispersion step was carried out using an Ultra-Turrax T25 mixer. Samples were never dried, except for the samples used for Fourier transform infrared spectroscopy (FT-IR) analysis, which were air-dried for 24 hours and then dried for 8 hours in an oven at 45 °C.

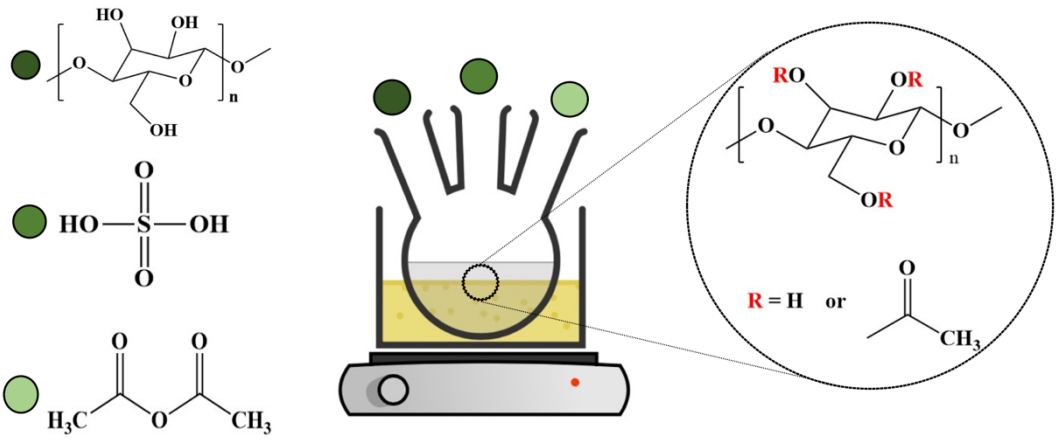

Figure 26 - Schematic of the acetylation process of CNC particles.

2.2.3. Melt compounding

In this research project, a melt compounding technique was adopted to pursue an approach that avoids the use of environmentally harmful solvents, as in the case of solution casting, and that can be an easily scaled-up for industrial applications. Two different melt compounding method were

tried, respectively a continuous compounding with a twin-screw extruder for PHBH and MFC or OHF, and a discontinuous compounding with an internal mixer for PHBH and CNC.

Before any processing, PHBH pellets were oven-dried at 85 °C overnight.

2.2.3.1. Twin-screw extruder

In the beginning, the PHBH pellets and the filler powder, i.e. MFC or OHF, were mechanically mixed; and, in order to obtain a better adhesion of the filler upon the pellets, some drops of paraffin oil (VESTLAN) were used. Thereafter, the mixtures were melt compounded using a corotating twin-screw extruder (Haake Extruder Rheomex CTW100p) operating at a rotational speed of 15 rpm and with a temperature profile varying from 145 °C at the feed zone to 160 °C at the metering zone. After extrusion, the obtained filament was granulated by a pelletizer (Scheer SGS 25-E4).

2.2.3.2. Internal mixer

In this case, the melt-compounding process was preceded by a solvent premixing step, to obtain a higher dispersion of the CNCs in the final biocomposite. This procedure combines the environmental and industrial advantages of melt-compounding with the ones of solvent premixing, thus avoiding CNC aggregation during the drying process and obtaining a good dispersion of CNCs in PHBH compared to direct melt- compounding of the biopolymer pellets with the dry powder of acetylated CNC.

First, to obtain master batches of PHBH matrix filled with modified cellulose nanocrystals, some acetylated CNCs dispersed in chloroform were added to a solution of PHBH dissolved in chloroform, and the mixture was stirred for further 4 hours at room temperature. The composite dispersion was subsequently poured into a Petri dish and the drying process was performed first overnight at room temperature and finished in an oven at 45 °C for 5 hours. The obtained films, used as master batches, were cut into smaller pieces and used for further compounding with neat PHBH pellets in order to obtain composites at different final filler contents: 5, 10, 15, and 20 wt%.

The second compounding was obtained by using a high-shear mixing Rheomix 300 (PolyLab OS, Thermo Electron Corporation, Germany) with roller rotors at a processing temperature of 145 °C, a mixing speed of 10 rpm, and a mixing time of 20 min.

2.2.4. Injection molding

After melt compounding via twin screw-extruder, the biocomposite materials were molded to obtain standard tensile test specimens (UNI EN ISO 527-2, type 1 BA) by injection molding (Tecnicaduebi MegaTech H7/18–1). For an optimized process, these conditions were used:

- hopper temperature = 120 °C;
- screw-barrel temperature = 135 °C;
- die temperature = 130 °C;
- injection pressure = 120 bar;
- holding pressure = 20 bar;
- holding time = 3 s;
- cooling time = 7.5 s.

2.2.5. Filament production

After melt-compounding via internal mixer, the biocomposite materials were filled in a capillary rheometer (Rosand RH7, Netzsch GmbH, Germany) to produce polymer filaments with a diameter of 1.75 ± 0.05 mm to be further used with FDM 3D printer. The filaments were obtained using a capillary die with an orifice of 1.8 mm, a temperature of 145 °C, and an extrusion speed of 8.5 mm min^{-1}. The filaments were then stored in a desiccator to prevent them from absorbing environmental moisture, which would affect the 3D printing process.

2.2.6. 3D printing – Fused Deposition Modeling (FDM)

For the fabrication of 3D printed samples, three different FDM 3D printer were used in this research project, and specifically they were:

1. K8200 3D printer (Velleman NV, Belgium);
2. PRUSA I3 MK3S (Prusa research, Poland);
3. TREA Stilla3D FDM (Stilla 3D, Italy).

All FDM printers, shown in Figure 27, were fed with the same extruded filaments of neat PHBH and biocomposites, with a diameter of 1.75 mm. Also, the printing parameters were almost the same. The bed temperature of the printer was 50 °C, the nozzle temperature was 170 °C, the printing speed was 5 mm s^{-1}, and a linear infill type with a fill percentage of 100% was used. Nozzles of 0.6 and 0.4 mm were used to print layer heights of 0.45 and 0.3 mm, respectively.

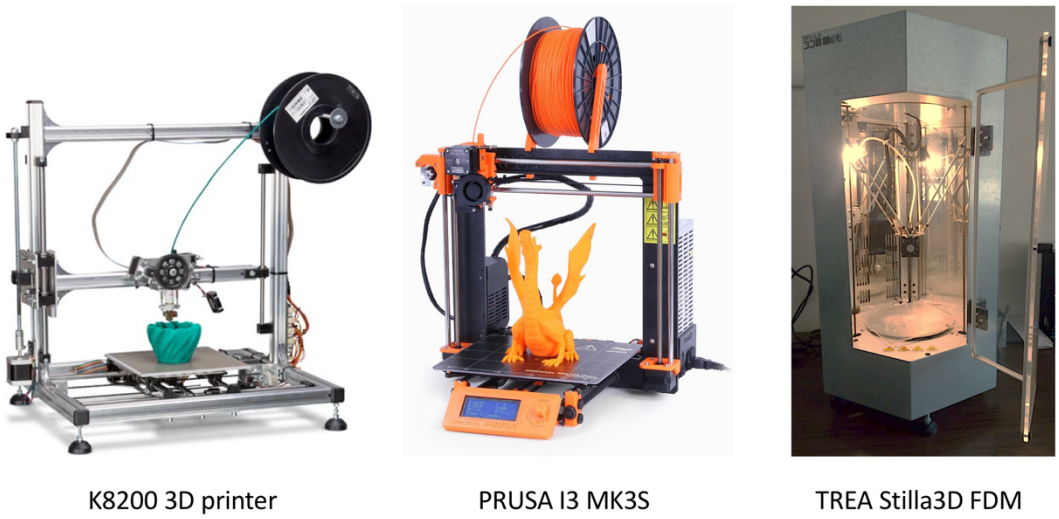

Figure 27 – Images of the FDM 3D printer used in this research project.

The 3D model, exported in a stl format, were then uploaded in a 3D slicing software, for example Slic3r and PrusaSlicer were both used. Here, the files were sliced to generate a G-code file that contains all the instructions to build layer-by-layer the designed architecture.

2.3. Sample preparation and coding

To enhance the clarity of this thesis, in the next sections a schematization of the followed experimental approaches is presented. According to the nature of the cellulose component, and hence to the final application of the composites, two main distinctions can be made:

- in the first case study, a by-product of the agri-food industry (i.e. oat hull fibers) was used as cheap, inert and non-toxic filler for a PHBH matrix;
- in the second case, commercially available CNCs were chemically modified via acetylation and compounded with a PHBH matrix, to investigate the reinforcing effect of this nanoparticles on the biopolymer matrix.

2.3.1. Experimental section: Poly(3-hydroxybutyrate-*co*-3-hydroxyhexanoate) filled with oat hull fiber and microfibrillated cellulose

The overall aim of this research case was to fabricate and characterize a bio-based composite by valorizing a waste of the agro-industry (i.e. oat hull fibers), which was used as filler for a PHBH matrix, in order to reduce the volume of PHA required, without affecting the thermo-mechanical properties of the biopolymer, but decreasing the final cost of the composite.

During this investigation, high-pressure homogenization and chemical silanization were evaluated as process variables affecting the final results. Apart from the PHBH reference matrix, other six biocomposites were produced, and their fabrication processes are schematized and coded in Figure 28.

First, high-pressure homogenization was used to produce MFC, which was further chemically modified by silanization (MFC_silanized) and then melt-compounded with PHBH by a twin-screw extruder at 3 wt% (PHBH_MFC_Sil_3) and 10 wt% (PHBH_MFC_Sil_10) MFC content. To

evaluate the effect of the functionalization procedure, the sample with the higher amount of MFC was also prepared with the unmodified MFC (PHBH_MFC_10).

Afterwards, the use of the as-received OHF was explored, and two different biocomposites were prepared directly melt-compounding the OHF with PHBH in a twin-screw extruder at 3 wt% (PHBH_OHF_3) and 10 wt% (PHBH_OHF_10) OHF content. To appraise the effect of the silanization procedure, also in this case, the sample with the higher amount of cellulose was also prepared with the silanized fiber (PHBH_OHF_Sil_10).

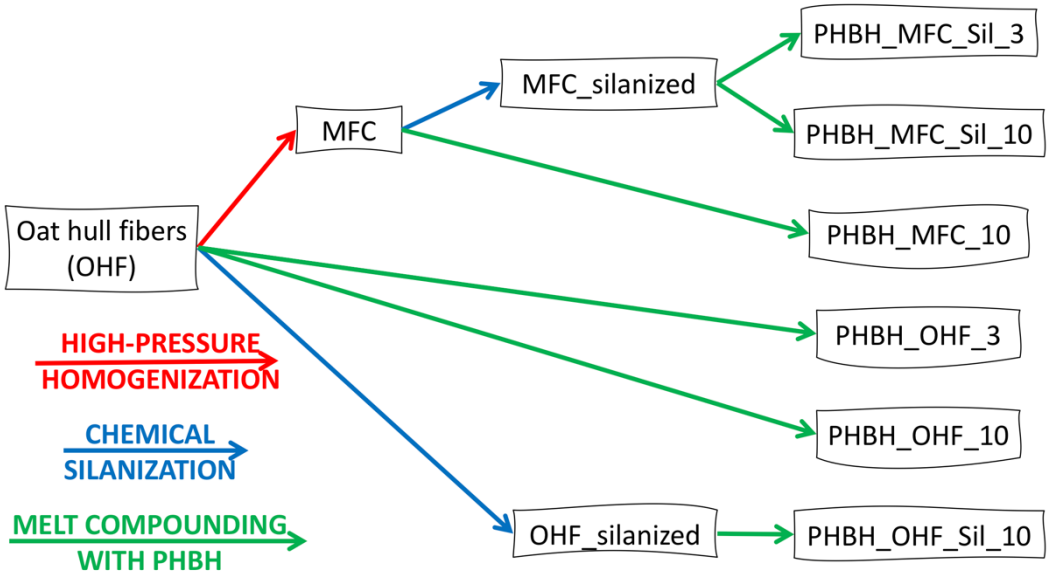

Figure 28 – Schematic representation and coding of the fabrication process of biocomposites with PHBH matrix and MFC or OHF fillers.

2.3.2. Experimental section: Poly(3-hydroxybutyrate-*co*-3-hydroxyhexanoate) reinforced with cellulose nanocrystals and 3D printed by Fused Deposition Modeling

This second research case was aimed to fabricate and characterize a bio-based and biodegradable composite, consisting of a PHBH matrix reinforced with acetylated CNCs. Hence, it was investigated the tailoring

effect of CNCs over thermal and mechanical properties of the composites. The research continued by studying their 3D printability with FDM, and an application in biomedical field was examined. Apart from the PHBH reference matrix, other four biocomposites were produced, varying the acetylated CNC content. Their fabrication process is schematized and coded in Figure 29.

Starting with a chemical acetylation of CNCs, the modified nanocrystals were then melt compounded with PHBH in an internal mixer at four acetylated CNC content: 5, 10, 15, 20 wt%, coded as PHBH+CNC_AC_XX, where XX represents the reinforcing agent content. The composites were further processed into filament, with a capillary rheometer, and used to feed a FDM 3D printer, which manufactured the characterization samples and examples of biomedical devices.

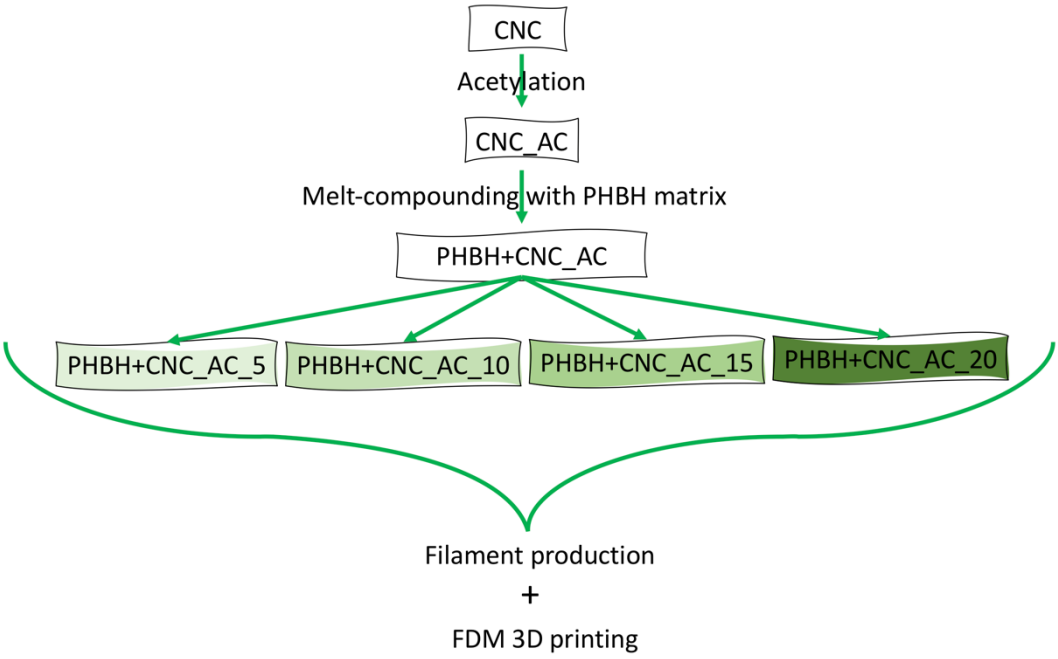

Figure 29 – Schematic representation and coding of the fabrication process of biocomposites with PHBH matrix and CNCs.

2.4. Characterization

2.4.1. Morphological characterization

2.4.1.1. Field Emission Gun-Scanning Electron Microscopy (FEG-SEM)

To obtain a good knowledge of the MFC and OHF microstructure and of the interaction between these fillers and the PHBH matrix, the fracture surface of injection-molded specimens and the filler morphologies were investigated using a Nova NanoSEM 450 Field Emission Gun-Scanning Electron Microscopy (FEG-SEM) (FEI Company). In order to obtain a fragile facture surface, which could be indicative of the fracture morphology surface, the samples were immersed in liquid nitrogen. Each specimen was then mounted on carbon tape and sputter-coated with gold.

2.4.1.2. Environmental Scanning Electron Microscopy (ESEM)

During the simulated composting condition, the PHBH/CNC samples were microscopically characterized to evaluate the different microstructure variation over time. Sample microscopies were acquired by means of the environmental scanning electron microscope ESEM Quanta-200 (Fei Company, U.S.A.). The samples were analyzed in low-vacuum conditions, using the solid-state detector for the backscattered electron imaging signal collection. An accelerating voltage of 15 kV, a spot size of 5, and a working distance of 11 mm were used in the acquisition of all images.

2.4.1.3. Transmission Electron Microscopy (TEM)

CNC morphology was investigated by transmission electron microscopy (TEM) (JEOL JEM-2200FS, JEOL USA, Inc.) using an acceleration voltage of 200 kV. Two plasma-activated carbon-coated grids were used as supports, onto which 0.01 wt/v% suspensions of CNCs in water were deposited before and after the acetylation. The average diameter and length of CNCs were then measured using the measuring tool in ImageJ software.

2.4.1.4. Atomic Force Microscopy (AFM)

The surface roughness of PHBH/CNC samples, and particularly the effect on this one of the CNC content, was evaluated by Atomic Force Microscopy (AFM), using an ICON3 AFM from Bruker. The measurements were carried out with silicon tips (RTESPA 150, Bruker) of 22 nm of curvature, and 10 N/m was used to scan the specimens in semi-contact mode at a scan rate of 0.5 Hz. The samples were obtained cutting out a portion of 3D printed samples, cleaned from dust with pressurized air and then stored in a desiccator under vacuum to avoid contamination prior to measurements. Images were processed with the software NanoScope Analysis from Bruker.

2.4.2. Thermal characterization

2.4.2.1. Differential Scanning Calorimetry (DSC)

The thermal properties, such as the crystallinity degree (X_c), the glass transition temperature (T_g) and the melting temperature (T_m) of the obtained MFC/PHBH and OHF/PHBH composites were measured with a Differential Scanning Calorimeter (DSC 2010, TA Instruments), under N_2 atmosphere. The crystallinity degree (X_c) of PHBH matrix and compounds was calculated by the following equation:

$$X_c = \frac{\Delta H_m}{\Delta H_m^0 (1 - w_f)} \times 100 \qquad \text{(Eq.1)}$$

where ΔH_m^0 (115 J/g) is the enthalpy of 100% crystalline PHBH, [144] w_f is the mass fraction of filler and ΔH_m is the enthalpy of melting measured by DSC.

2.4.2.2. Thermogravimetric Analysis (TGA)

The thermal stability and thermal degradation process of CNC/PHBH composites were investigated by thermogravimetric analysis (TGA) with a

STA 449 F3 Jupiter (Netzsch GmbH, Germany). Each sample was heated from 50 to 600 °C at a ramp rate of 5 °C min^{-1} in air. Specimens of about 20 mg were tested.

2.4.3. Mechanical characterization

2.4.3.1. Tensile test

The tensile tests on MFC/PHBH and OHF/PHBH composites were carried out on injection molded type 1BA specimens, with a tensile testing machine (Universal Testing Machine, TesT GmbH) at a crosshead speed of 2 mm min^{-1} and with a 2 kN load cell. According to UNI EN ISO 527-1 standard, for each sample, five different specimens were tested. The tensile stress and the deformation at break were directly determined by the machine, whilst the Young's modulus (E) was measured, according to the abovementioned standard, as the incremental ratio of stress variation in a strain range, which varies from 0.05% and 0.25%.

2.4.3.2. Dynamic Mechanical Analysis (DMA)

Dynamic mechanical analysis on MFC/PHBH composites were performed with a single cantilever clamp, in temperature ramp/frequency sweep mode using a DMA Q800 (TA Instruments) with heating rate of 3 °C min^{-1}. All the samples were obtained cutting out a portion of the injection molded 1BA tensile specimens, and the final sizes were 40 × 5 × 2 mm^3 (length × width × thickness). The samples were scanned over a temperature range from −20 to 120 °C, applying a strain of 0.1%, under frequency of 1 Hz. All samples were equilibrated for 10 minutes at −20 °C before starting the analysis, in order to homogenize the temperature in the measuring head.

The same instrument, equipped with a film tension clamp, was used to measure the Young's modulus, the ultimate tensile stress and the elongation at break of the CNC/PHBH composites. To do this, hot-pressed films with dimension of 40 x 3 x 0.3 mm^3 (length × width × thickness) were

analyzed with a stress/strain test in controlled force mode. A preload force of 0.5 N along with a ramp force of 0.1 N min^{-1} were chosen.

Differently, the storage modulus (E'), the loss modulus (E") and the loss tangent (tan δ) of CNC/PHBH composites were calculated with a three-point bending clamp in temperature ramp/frequency sweep mode using an RSA III from TA Instruments (Delaware, U.S.A.) with a heating rate of 3 °C min^{-1}. All samples were 3D printed by FDM with dimensions of 45 × 5 × 1.5 mm^3 (length × width × thickness), a linear infill type, a fill percentage of 100% and a fill angle of 0° were used. Samples were scanned over a temperature range from −50 to 110 °C, applying a strain of 0.1% under a frequency of 1 Hz. To homogenize the temperature in the measuring chamber, before starting acquiring the analysis values, all samples were equilibrated for 10 minutes at −50 °C.

2.4.4. Rheological characterization

To estimate the flow behavior of the CNC/PHBH composites during the 3D printing process, rheological measurements were carried out using a rotational rheometer, Anton Paar MCR 502, with a 15 mm parallel plate geometry and a gap of 0.5 mm, at a constant temperature of 170 °C. Flow curves under shear rates ranging from 0.001 to 10 s^{-1} were obtained through time-controlled measurements. Above 10 s^{-1}, the sample was leaving the gap. Therefore, to estimate the viscosity for higher shear rates, the experimental data were successively implemented with the empirical Bird−Carreau−Yasuda model: [167]

$$\eta = \eta_\infty + (\eta_0 - \eta_\infty)[1 + (\lambda\dot{\gamma})^2]^{\frac{n-1}{2}} \qquad \text{(Eq.2)}$$

where η_0 represents the zero-shear-rate viscosity; η_∞ represents the infinite-shear-rate viscosity, which can be assumed to be 0; λ is the relaxation time that reflects the onset shear rate of shear thinning; and n is the power law index that affects the slope of the shear-thinning region.

2.4.5. Chemical characterization

2.4.5.1. Infrared spectroscopy

Fourier Trasform-Infrared (FT-IR) spectroscopy was adopted to validate the chemical modification of cellulose. For MFC and OHF silanization, a FT-IR Vertex 70 spectrometer (Bruker Corporation, U.S.A.) was used; alternately, for CNC acetylation was used a Tensor 27 FT-IR spectrometer (Bruker Corporation, U.S.A.) in attenuated total reflectance mode.

In all cases, the infrared spectra were acquired on unmodified and functionalized powders, previously air-dried for 24 hours and then oven-dried for 8 hours at 45 °C. The spectra were recorded between 4000 and 500 cm^{-1}, with a resolution of 4 cm^{-1} and 32 scans.

2.4.5.2. Energy Dispersive X-ray Spectrometry (EDS)

To highlight the presence of silicon on the surface of silanized MFC and OHF, an X-EDS Oxford INCA-350 microanalysis system (Oxford Instruments) was used as energy dispersive X-ray spectrometer.

2.4.5.3. ^{13}C CP-MAS Nuclear Magnetic Resonance Spectroscopy

Solid state ^{13}C CP-MAS (cross-polarization-magic angle spinning) NMR spectra of unmodified and acetylated CNC were acquired at 300 K using a an AVANCE III HD600 Bruker spectrometer equipped with a 2.5 mm H/X CP-MAS probe operating at 150.90 MHz. Cross-polarization-MAS (CP-MAS) ^{13}C NMR spectra were obtained at 16 kHz MAS rate, using the standard Bruker CP sequence. The parameters used were: 125 kHz spectral width, 10 s relaxation delay, 2.4 μs 90° pulse, 4,000 data points and 32 or 64 scans.

All chemical shifts were referenced by adjusting the spectrometer field to the value corresponding to 38.48 ppm chemical shift for the deshielded line of the adamantane^{13}C NMR signal.

2.4.6. Disintegration under composting condition

The biodegradability of CNC/PHBH composites was first investigated analyzing the disintegration processes of neat PHBH, PHBH biocomposites, along with LDPE, used as reference of traditional petroleum-based plastic. The disintegration process was studied following the EN ISO 20200 standard, simulating the composting conditions in a laboratory-scale test. A solid synthetic waste was prepared mixing all the components listed in Table 5, to mimic the medium of composting degradation.

Table 5 – Composition of synthetic solid waste.

Component	Dry mass [wt%]	Component	Dry mass [wt%]
Sawdust	40	**Sugar**	5
Rabbit food	30	**Corn seed oil**	4
Ripe compost	10	**Urea**	1
Corn starch	10		

After mixing, distilled water was added to the obtained synthetic solid waste to adjust its final water content to 55 wt%.

All the samples were hot-pressed at 120 °C for 30 s to produce squared films (25 × 25 × 0.5 mm^3), which were weighed and buried in composting reactors at 5 cm depth, filled with wet synthetic solid waste. The samples were put inside iron mesh bags to simplify their handling and to allow the contact of the compost with the specimens. Three replicates of each sample were buried and analyzed.

In order to maintain a sufficient and constant relative humidity in the compost medium, water was added, according to the procedure described

in the abovementioned standard, by adjusting periodically the weight of the containers. In Table 6 it is reported the composting procedure.

Table 6 – Composting procedure.

Days from start	Operation
0	Record initial mass of reactors
1; 2; 3; 4; 7; 9; 11; 14	Weigh reactor and add water to restore the initial mass, if needed. Mix the composting matter.
8; 10; 16; 18; 21; 23; 25; 28	Weigh reactor and add water to restore the initial mass, if needed. Do not mix the composting matter.
30; 45	Weigh reactor and add water to restore the mass to 80% of the initial mass, if needed. Mix the composting matter.
From 30 till 60, twice a week	Weigh reactor and add water to restore the mass to 80% of the initial mass, if needed. Mix the composting matter.
From 60 onwards, twice a week	Weigh reactor and add water to restore the mass to 70% of the initial mass, if needed. Mix the composting matter.

Containers were incubated at 58 °C for 90 days in an oven (ISCO NSV 9090 model). Gas exchange between the inner atmosphere and the outside environment was guaranteed by making a hole of 5 mm diameter on the side of each composting reactors.

Films were recovered from the containers every week, washed with distilled water, dried overnight at 85 °C, and reweighed. The degree of disintegration (D) of the samples was calculated by normalizing the sample weights at different composting times to the initial weight using the following equation:

$$D = \frac{m_i - m_f}{m_i} \times 100 \qquad \text{(Eq.3)}$$

where m_i is the initial dry mass of the test material and m_f is the dry mass of the test material recovered at different incubation stages.

2.4.7. Biocompatibility characterization

2.4.7.1. *In vitro* degradation test

To have a first approximation of the *in vivo* degradation rate of an absorbable surgical implant of CNC/PHBH composites, an *in vitro* degradation test was carried out. The ASTM F-1635-16 standard was followed, and it consists in conditioning a sample, 3D printed scaffold in this case, at 37 °C in a phosphate-buffered saline (PBS) solution with constant pH of 7.4 ± 0.2, which can simulate the body fluids. First, the samples were sterilized:

1) washing with distilled water;
2) immersing in ethanol (70%) for 30 minutes;
3) washing with sterile PBS for three times and
4) exposing to UV light (250 nm) for 45 minutes.

Then, test samples were dried to a constant mass before be weighed and placed in the physiological solution. Every week, for six weeks, each sample was removed, rinsed with distilled water and dried to a constant mass, which was further noted. For each composition, three different samples were measured and the average mass loss was calculated according to the following formula:

$$Mass\ loss = \frac{M_t - M_0}{M_0} \times 100 \qquad \text{(Eq.4)}$$

2.4.7.2. *In vitro* cell attachment

CNC/PHBH composites were 3D printed with a grid-infill to fabricate scaffolds used for in vitro cell attachment evaluation. First, the samples were sterilized according to the following protocol: 1) three washing with 1 mL of distilled water; 2) immersion into 1 mL of ethanol 70% solution (v/v) for 16 hours; 3) exposition to UV radiation 16 hours on each side. Afterwards, two different cell lines were seeded on the sterilized scaffolds.

Human Osteoblastic cells (HOB) was cultured in complete medium with a composition of Alpha Minimum Essential Medium (L0476-500, Biowest) supplemented with 10% Fetal Bovine Serum (ECS0170DI, Euroclone), 2 mM L-glutamine (AU-X0550-100, Aurogene) and 1% penicillin/streptomycin (AU-L0022-100, Aurogene). 50,000 cells were seeded on each scaffold and grown until confluence was reached. When the confluence of cells was reached, in order to analyze the images by SEM microscopy, they were fixed in 4% paraformaldehyde for 20 minutes at room temperature, and then, fixed cells were washed in Phosphate Buffered Saline (PBS) solution and dehydrated in graded ethanol and dried at critical point.

2.4.8. Water affinity

2.4.8.1. Water uptake

Water uptake of CNC/PHBH composite scaffolds was determined by soaking FDM 3D printed discs (9 mm of diameter) in deionized water and evaluating the mass increase over time. The dried samples were initially weighed (W_0) and then immersed. After selected times, the samples were extracted, slightly dried with filter paper to remove water from the disc surface and then reweighed (W_t). Measurements were taken after 5 minutes, after 15 minutes, after 30 minutes, and then every 30 minutes until 4 hours. For each composition, three different samples were measured and the average water uptake was calculated according to the following formula:

$$Water\ uptake = \frac{W_t - W_0}{W_0} \times 100 \qquad \text{(Eq.5)}$$

2.4.8.2. Static water contact angle

Surface wettability of CNC/PHBH composite scaffolds, 3D printed via FDM, was investigated by determining the water contact angle with an OCA20 contact angle system (DataPhysics, Germany) at 25 °C. About 6 μL was used as volume for the water drop; and four different points of each sample were measured, and then the average value and the standard deviation were calculated.

3. Results and discussion

3.1. Poly(3-hydroxybutyrate-*co*-3-hydroxyhexanoate) filled with microfibrillated cellulose and oat hull fibers

3.1.1. Morphological analysis

The OHF morphology is composed of long fibrils with a length (L) of several hundreds of microns, a width (d) of some tens of microns, and an aspect ratio (L/d) close to 20 (Figure 30 (a)). However, the sample shape is quite heterogeneous, and some particles have different geometry and smaller aspect ratio. From Figure 30 (b), it is clear to evaluate the effect that a high-pressure homogenization process causes to OHF. In fact, homogenized MFC have a length of some tens of microns and a width of approximately 10 μm. The mean aspect ratio (L/d) of the micro-fibrils is about 100.

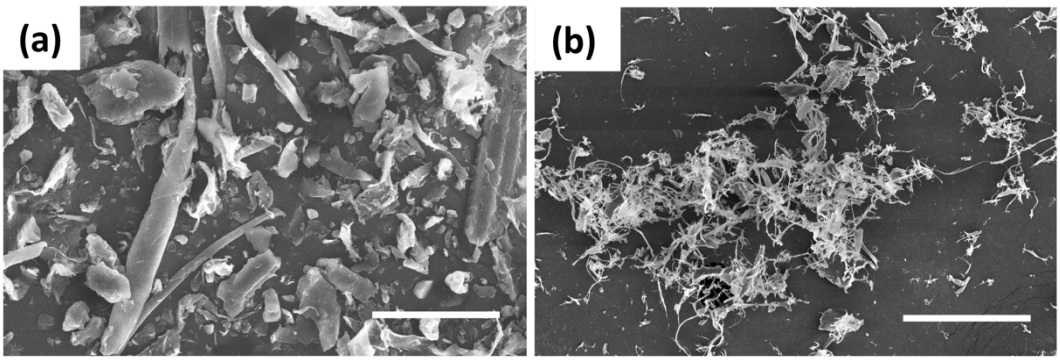

Figure 30 - SEM micrographs before (a) and after (b) high-pressure homogenization process (700 bar for 15 steps) of oat hull fiber (scale bar = 100 μm).

The presence of OHF or MFC in the composites is detected by fibrils that extend out of the cryofractured surface of injection molded samples, as can be seen in Figure 31 (b, c and d). These structures are not observed in the neat sample, Figure 31 (a). Besides, it is interesting to note that the silanization does not affect neither the dimension nor the morphology of the

OHF or MFC samples; although, it visibly affects the interaction between the matrix and the filler. In fact, comparing the micrographs of silanized, Figure 31 (b and d), and untreated fibers, Figure 31 (c), there is a clear indication of a better interfacial compatibility between the PHBH matrix and the silanized cellulose fibers. This enhanced interaction can be ascribed to the presence of apolar condensed Si-CH_3 groups onto fibers surface, rather than the pristine hydroxyl groups. The effect of silanization is highlighted by the absence of empty spaces between the matrix and the silanized OHF, Figure 31 (b), or MFC, Figure 31 (d), which are instead observed in the untreated samples, Figure 31 (a). This condition could imply a better stress transfer between the two phases and therefore an increase in mechanical properties of the composite materials, obtained with silanized OHF or MFC.

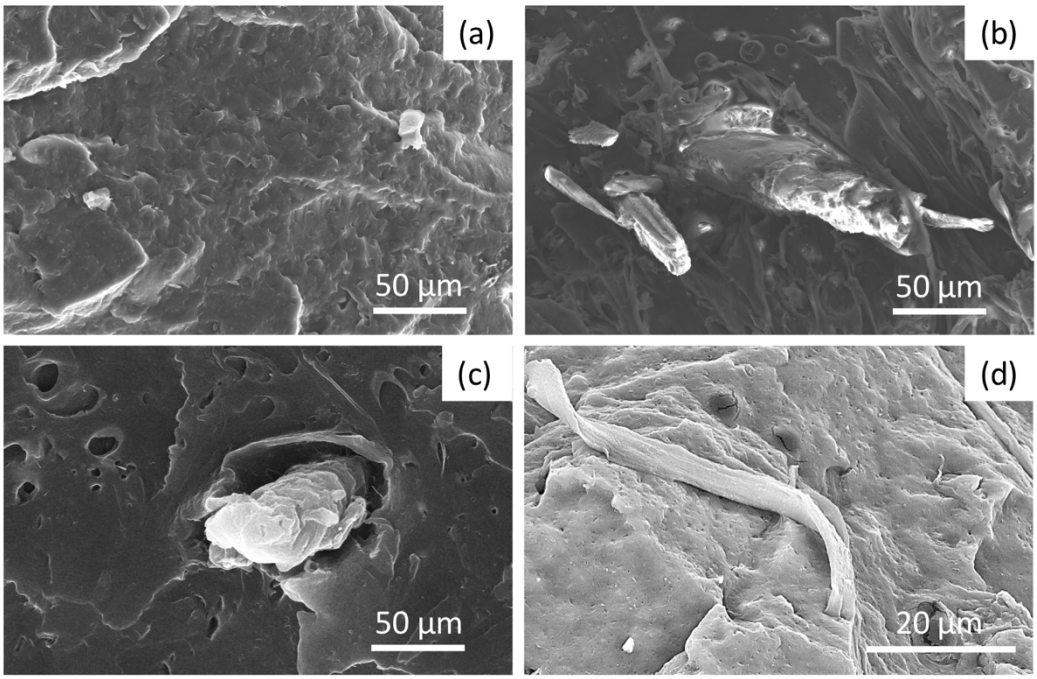

Figure 31 - SEM images of cryofractured surface of PHBH/OHF and PHBH/MFC composites: (a) neat PHBH; (b) PHBH_OHF_Sil_10; (c) PHBH_OHF_10; (d) PHBH_MFC_Sil_10.

3.1.2. Chemical analysis

Two distinct techniques, i.e. FT-IR and EDS, were used to evaluate the occurrence of the silanization procedure of OHF and MFC. Since

homogenization process is only a mechanical disintegration of the fibrils, it does not alter the chemical structure of OHF, and hence, only the results for OHF are reported below. But it has to be considered that MFC analysis are exactly overlapping with the following presented, and therefore, where it is indicated OHF, it could be properly read also MFC.

Firstly, FT-IR spectroscopy was used to follow and evaluate the MTES hydrolysis and subsequently the condensation on OHF. Figure 32 shows the FT-IR spectra of OHF, MTES coupling agent, hydrolyzed MTES coupling agent and silanized OHF.

The spectroscopic variations in the silane after hydrolysis and poly-condensation reactions can be observed, comparing the FT-IR spectrum of pure MTES and the one obtained after the sol–gel reaction. The characteristic IR band at 2971 cm^{-1} is attributed to the asymmetric stretching of CH_3, deriving from ethoxy ($-OCH_2CH_3$) and methyl-silyl ($-Si-CH_3$) groups of MTES, and it is present on both spectra. In the MTES spectrum, there are other two different peaks at 2923 and 2881 cm^{-1}, corresponding, respectively, to the asymmetric and symmetric stretching of CH_2, from ethoxy group. [168] These last two peaks are no more visible in the condensed MTES, since after sol–gel reaction, methylene groups in the ethoxy functionalities are removed as ethanol. In the MTES_hydrolyzed spectrum, the peak at 2971 cm^{-1} is still evident, due to the silyl group, and the weak peak at 2911 cm^{-1} appears, corresponding to the symmetric stretching of CH_3. Moreover the characteristic bending vibration of the methyl group was identified at 1267 cm^{-1}. [169,170] The bands at 1167, 955, 818, and 777 cm^{-1} were attributed to the absorption of $Si–O–CH_2CH_3$ in MTES, whose intensities decrease considerably after sol–gel reaction. [170] Additionally, another proof of the successful silanization is the presence of the characteristic peaks of Si-O-Si with a broad signal at 1100 cm^{-1} and a sharp signal at 766 cm^{-1}. [168,169]

Comparing the FTIR spectrum of OHF_silanized with the spectrum of pristine OHF, three typical peaks can be noticed and they are present only on the OHF_silanized spectrum, denoting the actual condensation of the

coupling agent on the OHF surface. These peaks are at 2971, at 1271 and at 766 cm^{-1}, corresponding respectively to the asymmetric stretching of -CH_3, the bending of -CH_3 and the stretching of Si-O-Si. [168,169] It is clear from these peaks, which are not evident in the pristine OHF spectrum, that the silanization process occurred positively. In the OHF_silanized spectrum, the superimposition of the peaks, due to the aliphatic silane functionalization (Si-CH_3), on the OHF spectrum can be observed. Beside these peaks, other typical absorptions of cellulose can be observed in both spectra: the broad band at 3350 cm^{-1} due to the ─OH stretching and the peaks at 1031 and 895 cm^{-1}, corresponding to the C─O stretching and the CH bending. [171]

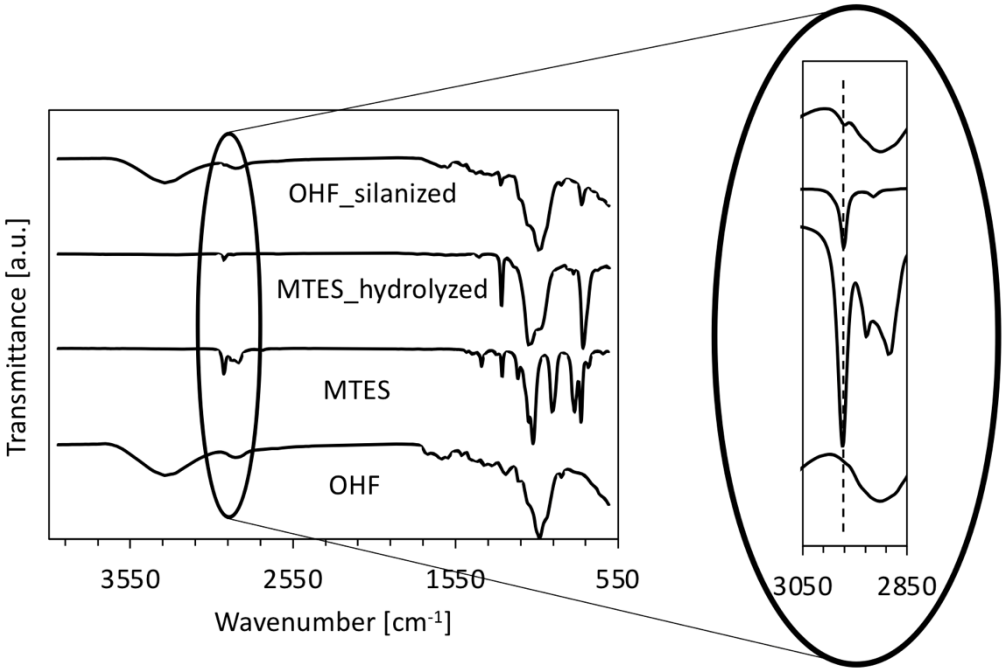

Figure 32 - FT-IR spectra of OHF, MTES, MTES_hydrolzyed, and OHF_silanized.

Assuming the -OH groups as the anchor points for the alkoxysilanes, during the silanization process, the OHF degree of silanization was calculated by the decrease in -OH peak areas, in the range 3700–3000 cm^{-1}, before and after the functionalization. Spectra were normalized to the peak intensity at 1032 cm^{-1}, referred to C–O–C stretching mode of skeletal vibration of pyranose ring. [172,173] The results showed that in OHF_silanized spectrum the –OH peak area decreased of about 33%, indicating that about

one third of the –OH groups were replaced by –O–Si–CH_3 groups during the silanization process.

The second investigation technique that was used to confirm the efficiency of the silanization procedure is EDS, aimed to qualitatively evaluate the surface compositions of modified and untreated OHF/MFC. Figure 33 illustrates their elemental compositions. The unmodified OHF and MFC spectra, Figure 33 (a and b), only show peaks corresponding to photon energies of $K_{\alpha 1}$ emission lines of C and O, near 0.277 and 0.525 keV, respectively. In the spectrum of the silanized OHF and MFC samples, Figure 33 (b and d), an additional peak near 1.74 keV was observed, corresponding to photon energies of silicon emission lines $K_{\alpha 1}$ and $K_{\alpha 2}$, confirming the condensation of silicate groups on the OHF and MFC surfaces.

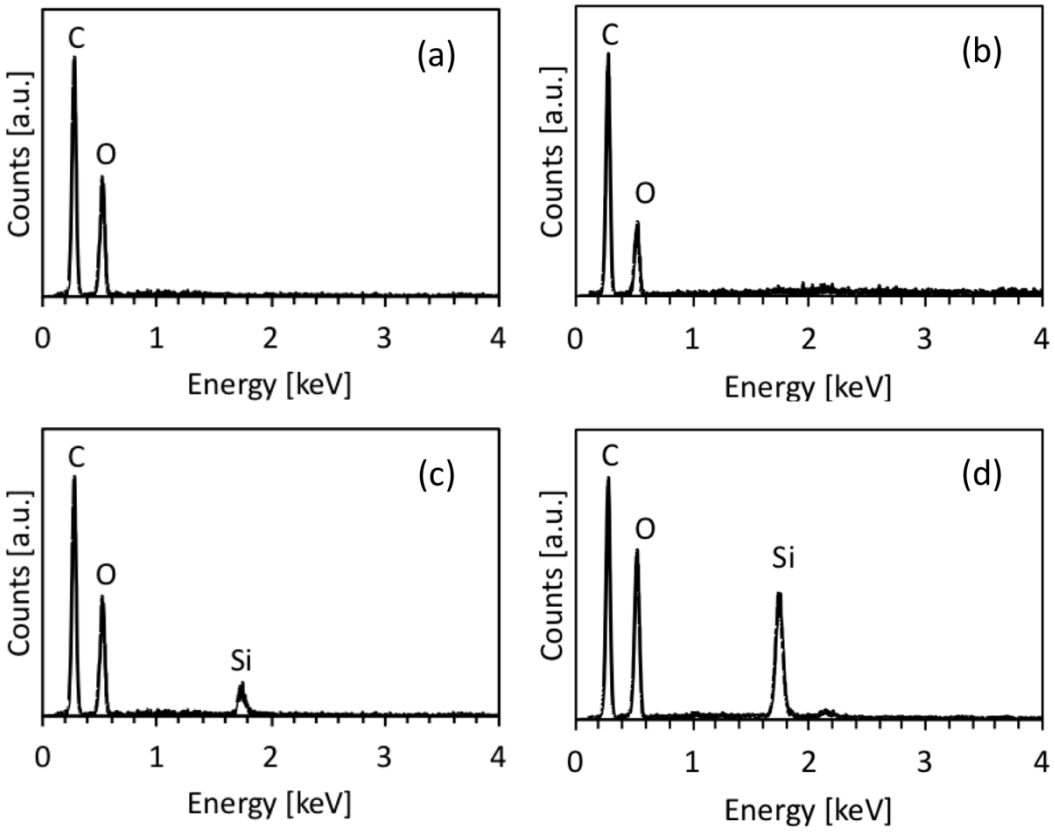

Figure 33 - EDX measurements: (a) OHF; (b) MFC; (c) OHF_silanized; (d) MFC_silanized.

3.1.3. Thermal properties

The effect over thermal properties of compounding MFC and OHF to the PHBH matrix was investigated by DSC, for all the samples produced. The findings of the research illustrate that, independently from the nature of the natural fibers (i.e. OHF or MFC), the thermal properties are only slightly affected, or in some case not influenced, neither by the addition of the filler to PHBH matrix, nor by the silanization process. Even if a clear correlation between thermal properties and filler content cannot be identified, however, we can state that these natural fibers can positively replace part of the biopolymer, without altering the thermal properties of the final composites. Hereafter, the main results are presented more precisely, and they are discussed according to the kind of starting fiber, i.e. OHF or MFC.

For PHBH/OHF composites, neither the compounding with the filler component nor the silanization process do not introduce any significant variation in thermal properties and in crystallization processes. All thermal properties of neat PHBH and PHBH/OHF composites are summarized in Table 7.

Table 7 - Thermal properties of OHF/PHBH composites. T_g: glass transition temperature; T_m: melting temperature; ΔH_m: enthalpy of melting; X_c: degree of crystallinity.

Sample	T_g [°C]	T_m [°C]	ΔH_m [J/g]	X_c [%]
PHBH	6	141	44	38
PHBH_OHF_3	6	148	42	38
PHBH_OHF_10	7	141	38	37
PHBH_OHF_Sil_10	8	146	37	36

These results are in line with the ones showed in previous researches, where no significant variations of thermal behavior of PHBH can be observed as a function of cellulose based filler content. [145,174]

For PHBH/MFC composites, the melting temperature, T_m, is slightly higher for the composites compared to the neat polymer. These results are consistent with already published data and can be ascribed to the reduced flexibility of the PHBH chains, due to the filler presence. [145,174] Differently, the glass transition temperature, T_g, of the polymer can be considered not influenced by the filler addition. Finally, also the crystallization degree is only slightly affected by the MCF presence indicating that the filler does not significantly influence the crystallization process. All thermal properties of neat PHBH and PHBH/MFC composites are summarized in Table 8.

Table 8 - Thermal properties of MFC/PHBH composites. T_g: glass transition temperature; T_m: melting temperature; ΔH_m: enthalpy of melting; X_c: degree of crystallinity.

Sample	T_g [°C]	T_m [°C]	ΔH_m [J/g]	X_c [%]
PHBH	6	141	44	38
PHBH_MFC_Sil_3	7	147	50	44
PHBH_MFC_Sil_10	7	145	41	40
PHBH_MFC_10	7	144	42	41

3.1.4. Mechanical properties

Mechanical properties of the PHBH/OHF and PHBH/MFC composites were investigated to evaluate if these natural fibers could be positively used as filler, without affecting the mechanical resistance of the final material. The

results evinced not only the possibility to replace part of the biopolymer without weakening the resistance of the matrix but also a slight improvement of Young's modulus against a decrease of elongation at break and a maintenance of ultimate tensile strength. For this reason, the findings suggest that OHF and MFC can be used as natural and bio-based filler for PHBH matrix.

Mechanical properties of neat PHBH and PHBH/OHF composites are shown in Table 9. With increasing OHF content, the Young's modulus of PHBH composites gradually increased from 1715 ± 71 MPa to 1912 ± 52 MPa, with a growth of 11.5%. Comparing the values of the samples with and without silanization, we can comment that silanization enhances the Young's modulus values of almost 3%. The better surface interaction between matrix and filler, due to improved chemical compatibility, confirms the remarks emerged from SEM analysis and leads to a higher stiffness of the composite. The decrease in tensile elongation at break is a consequence of the higher system stiffness. [137] The obtained ultimate tensile strength values are also similar to those presented in a previous work and do not vary significantly. [133]

Table 9 – Mechanical properties of OHF/PHBH composites. E: Young's modulus; σ_M: tensile strength; ε_B: tensile strain at break.

Sample	E [MPa]	σ_M [MPa]	ε_B [%]
PHBH	1715 ± 71	23.1 ± 1.6	3.7 ± 0.4
PHBH_OHF_3	1724 ± 140	23 ± 1.4	3.5 ± 0.6
PHBH_OHF_10	1864 ± 31	24.2 ± 1.2	4.1 ± 0.4
PHBH_OHF_Sil_10	1912 ± 52	24.2 ± 0.4	3.5 ± 0.4

Also, in the case study of PHBH/MFC composites, due to a higher elastic modulus of MFC respect to PHBH, the addition of MFC to PHBH leads to an increase of the composites Young's modulus, which is more pronounced using silanized fibers. Moreover, increasing silanized MFC content, Young's modulus of PHBH/MFC composites gradually raises up to 1861 ± 77 MPa, with a growth of 8.5% compared to pristine PHBH. This behavior is accompanied by a slight increase of the tensile strength from 23.1 ± 1.6 MPa to 24,5 ± 0,9 MPa, corresponding to an increase of 6%. The strength increment with respect to the pristine matrix can be considered as a further indirect evidence of the good adhesion between silanized MFC and matrix. At higher filler concentration, a small decrease of the elongation at break occurs, from 3.7 ± 0.4% to 3.2 ± 0.3%, as a result of the greater stiffness of the material. All mechanical properties of neat PHBH and PHBH/MFC composites are summarized in Table 10.

Table 10 - Mechanical properties of MFC/PHBH composites. E: Young's modulus; σ_M: tensile strength; ε_B: tensile strain at break.

Sample	E [MPa]	σ_M [MPa]	ε_B [%]
PHBH	1715 ± 71	23.1 ± 1.6	3.7 ± 0.4
PHBH_MFC_Sil_3	1776 ± 132	24.2 ± 1.2	3.8 ± 0.4
PHBH_MFC_Sil_10	1861 ± 77	24.5 ± 0.9	3.2 ± 0.3
PHBH_MFC_10	1813 ± 133	26.1 ± 0.6	2.7 ± 0.4

To have a deeper evaluation of the filler effect of MFC over PHBH matrix, dynamic mechanical analyses were carried out and the obtained results are aligned with the mechanical properties evaluated by tensile testing. Figure 34 (a) illustrates the temperature dependence of the storage modulus, E', of neat PHBH and PHBH/MFC_silanized composites. E' of

neat PHBH at temperature below T_g is essentially constant with a value of about 4 GPa. The incorporation of MFC, at 10 wt%, increased very slightly E' in the rubbery region, which can be related to an improved compatibility between the filler and the polymer matrix, promoted by the surface modification of the MFC. Figure 6 (b) shows the temperature dependence of the loss factor, tan δ, of neat PHBH and PHBH/MFC_silanized composites. The microfibril addition to the polymeric matrix modifies the number of the mobile chains during the glass transition and the effect depends on the interfacial area and the strength of polymer-filler interactions. Thus, the change in tan δ peak height indicates the variations in the volume of constrained chains. [175,176] Therefore, the introduction of MFC increased the volume of constrained chains and restricted the PHBH chain mobility due to effective interfacial interactions.

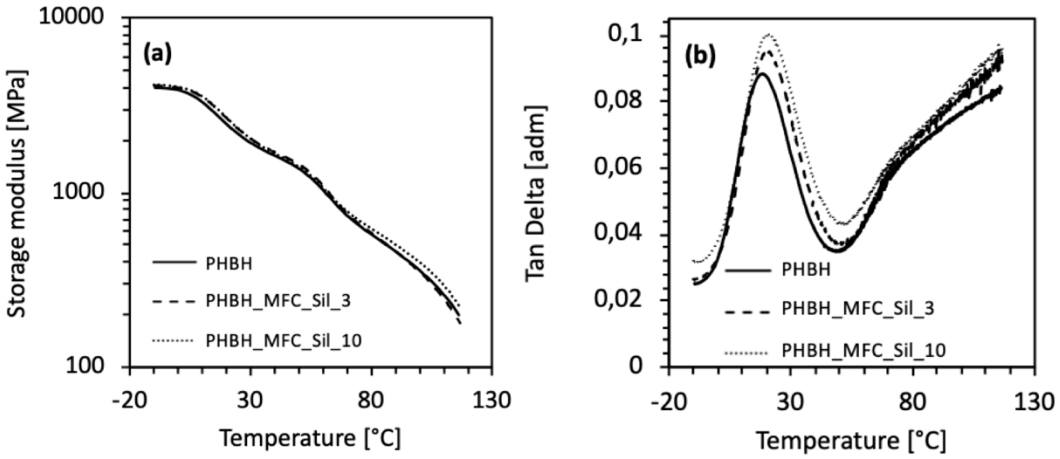

Figure 34 - DMA analysis of neat PHBH and PHBH/MFC_silanized composites. (a) Storage modulus (E') and (b) loss factor (tan δ).

3.2. Poly(3-hydroxybutyrate-*co*-3-hydroxyhexanoate) reinforced with cellulose nanocrystals and 3D printed by Fused Deposition Modeling

3.2.1. Chemical analysis

To enhance the affinity and the compatibility between the hydrophilic CNCs and the hydrophobic PHBH matrix, a surface modification of CNCs was performed. In this case study, an acetylation process was carried out to replace part of the hydroxyl groups (−OH) of cellulose with acetyl groups ($-CO-CH_3$), which are expected to have a relevant chemical affinity with the C=O groups of PHBH, due to the strong dipole−dipole interactions established between the two chemical groups. [177] Differently from previous research, which has extensively used ecologically harmful solvent, e.g. dimethylformamide (DMF) or pyridine, [178,179] this procedure was chosen for its greener chemical route of grafting acetyl groups on the CNC surface. In fact, none other chemical was used other than the acetic anhydride and the sulfuric acid, used as catalyst.

The functionalization was allowed to continue for four different reaction times (i.e. 1, 2, 8 and 20 hours) in order to parametrically evaluate the chemical modification of CNC over time and the relative kinetics of the reaction. Figure 35 shows the FT-IR spectra of the acetylated CNC at different reaction times. A clear indication that the modification occurred positively was given by the FT-IR characterization. In fact, in all spectra, three new characteristic peaks of acetyl group vibration are evident at 1745 cm^{-1}, carbonyl stretching C=O, at 1370 cm^{-1}, methyl in-plane bending in $-O(C=O)-CH_3$, and at 1230 cm^{-1}, C−O stretching of acetyl group. [180,181] Moreover, the decrease of intensity of the broad band with a maximum around 3340 cm^{-1}, which is typical of the −OH stretching, is consistent with a partial substitution of hydroxyl groups with acetyl groups.

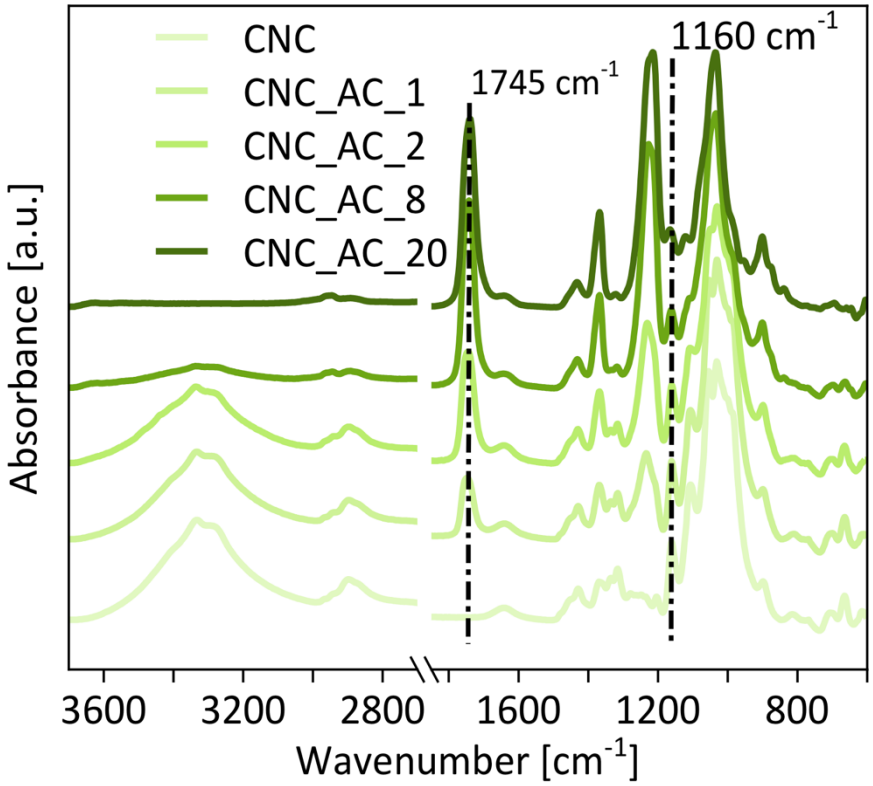

Figure 35 - Chemical characterization by FT-IR analysis of the acetylated CNCs at different reaction times (CNC_AC_XX) where XX corresponds to the reaction times expressed in hours.

Besides, there is a significant correlation between the increase in reaction time and the intensity of the new peaks that appear, as well as with the decrease in the broad band of the hydroxyl group. The chemical acetylation of CNCs over time was evaluated by calculating the absorption ratio (A_r)

$$A_r = \frac{I_{1745}}{I_{1160}} \qquad \text{(Eq.6)}$$

where I_{1745} is the intensity of the C=O stretching band at 1745 cm^{-1}, used to quantify the grafted acetyl group onto a cellulose structure, [178] and I_{1160} is the intensity of the antisymmetric bridge oxygen stretching band of the cellulose molecular skeleton, used to characterize cellulose because it does not change during acetylation. [182] A_r can be considered a suitable qualitative indicator of the acetylation process over time because it is

proportional to the degree of acetylation (DS) according to the following relation,

$$A_r = \varepsilon \cdot DS \qquad \text{(Eq.7)}$$

where ε is a constant, defined as the absorptivity ratios of the bands at 1745 and 1160 cm^{-1}. [182] The absorbance dependence over time reaction is represented in Figure 36.

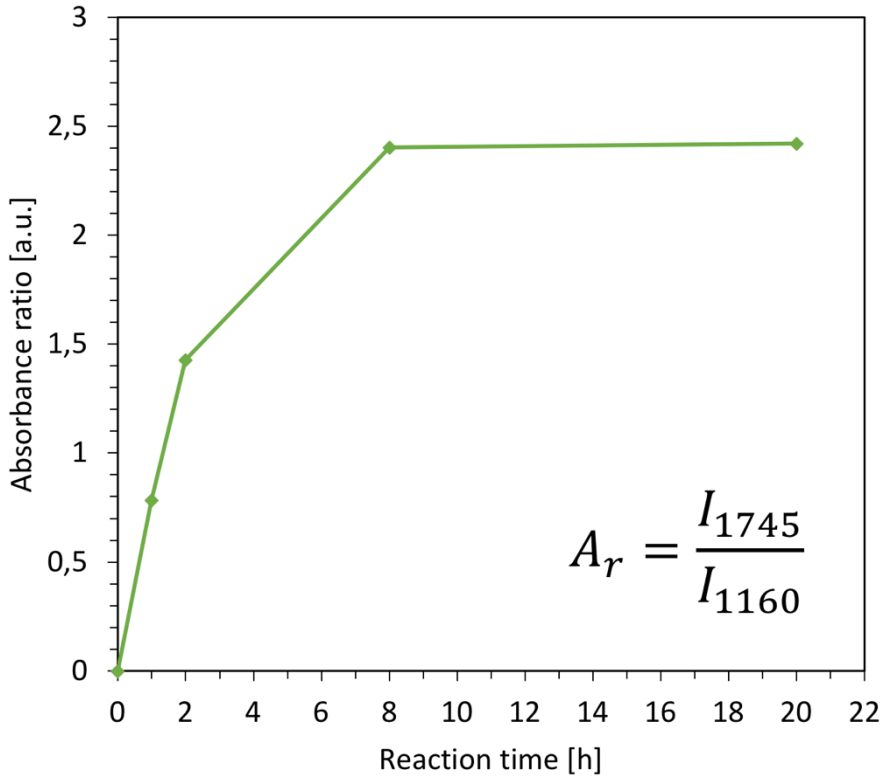

Figure 36 - Absorbance ratio dependence over reaction time, as an indication of the degree of acetylation.

The accurate control of the acetylation degree is a relevant variable for the production of nanocomposites with specific properties. It has been proved that, for longer acetylation times, and thereby for a higher degree of acetylation, significant changes in the cellulose crystalline structure can be promoted and, therefore, also variations of macroscopic properties, such as a decrease in crystallinity degree and an increase in thermal stability and degree of dispersion in organic solvents. [178] The effect of the degree of

acetylation of CNCs over thermal stability was investigated by TGA, and 5% weight loss temperature ($T_{5wt\%}$) was chosen as an indicative factor (Figure 37). All curves show an initial decrease of weight due to the loss of moisture, but this is more evident in untreated CNCs because of the higher amount of free hydroxyl groups compared to the acetylated samples. At 5% weight loss, a $T_{5wt\%}$ of 259 °C was measured for CNCs, and this value shifts to higher values except in the case with 2 hours of acetylation, where it decreases to 233 °C. The maximum $T_{5wt\%}$ of 278 °C is reached for 20 hours of acetylation. These results are useful to fully understand the thermal stabilization effect of acetylated CNCs on the thermal behavior of the final PHBH+CNC_AC_8 composites.

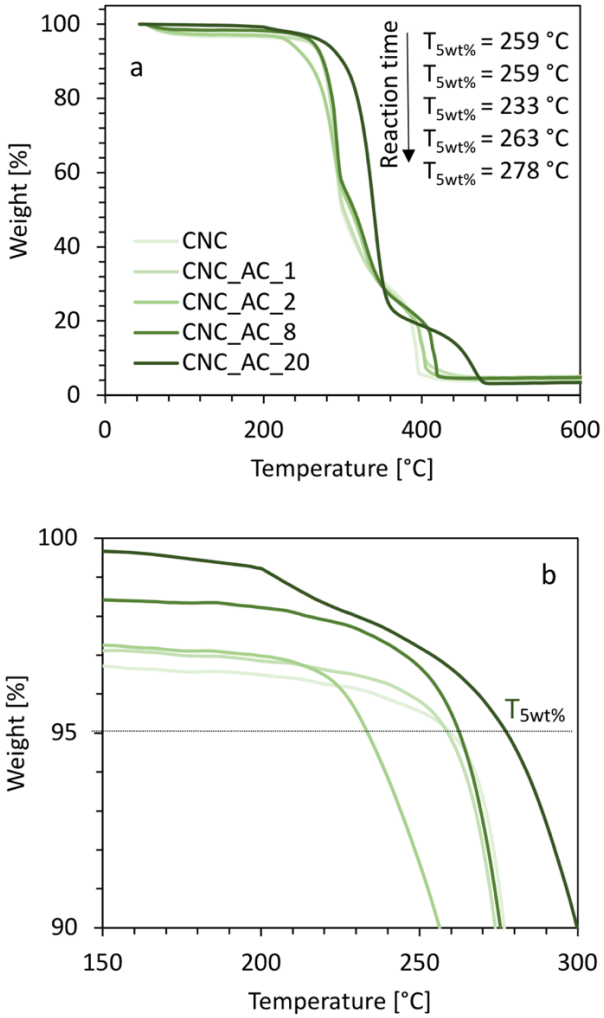

Figure 37 - (a) TGA analysis of pristine CNCs and acetylated CNCs at different reaction times (CNC_AC_X), where X corresponds to the hours of reaction time. (b) Zoom-in of the diagram and indication of the 5% weight loss temperature (T5wt%).

For the development of the compounding steps, only CNCs acetylated for 8 hours (CNC_AC_8) were taken into consideration because they showed a good balance among a high degree of acetylation, a good thermal stability without compromising either the nanostructure or the morphology of the nanocrystals, as proved by TEM images (Figure 38).

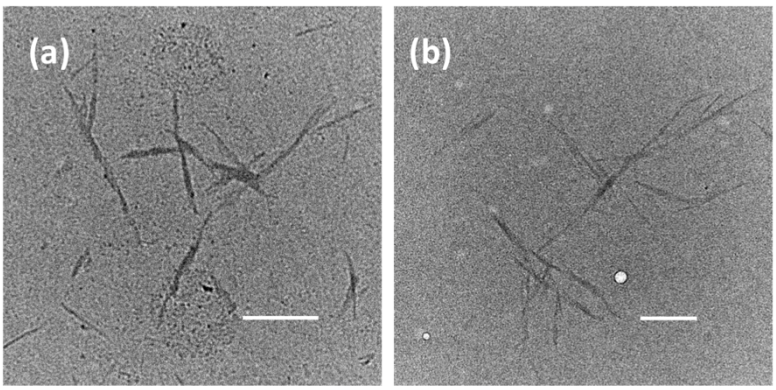

Figure 38 – TEM images showing unmodified CNCs (a) and acetylated CNCs after 8 hours of acetylation (b) (scale bars = 150 nm).

The acetylation of CNC was also confirmed with ^{13}C cross-polarization magic-angle spinning nuclear magnetic resonance spectroscopy (^{13}C CP-MAS NMR). The spectra of untreated CNC and after 8 hours of acetylation are shown in Figure 39. The former spectrum displays typical signals from cellulose that were so assigned:

- C_1 (105 ppm);
- C_4 crystalline (89 ppm), and C_4 amorphous (84 ppm);
- $C_2/C_3/C_5$ (72 and 75 ppm);
- C_6 crystalline (65 ppm), and C_6 amorphous (63 ppm).

After acetylation, the characteristic signals of the acetyl group emerged at 172 and 21 ppm, corresponding, respectively, to the carbons of the carbonyl (C=O) and methyl (CH_3) groups of the grafted moiety.

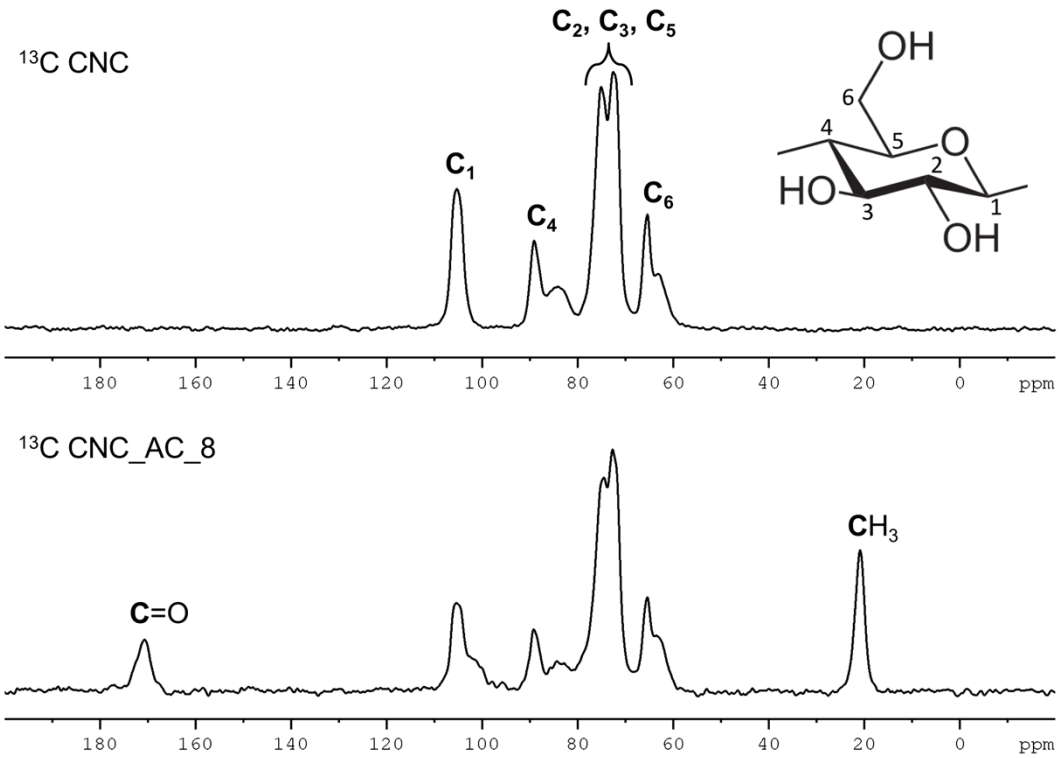

Figure 39 - 13C CP-MAS NMR spectra of pristine CNC and 8 hours acetylated CNC (CNC_AC_8).

Moreover, after acetylation, additional decrease in the C_1 intensity at 105 ppm was observed together with the progressive appearance of a shoulder at 102 ppm. In the literature, it was reported that the acetylation of sugars results in a downfield shift of the peak corresponding to the O-acetylated carbon and a concomitant upfield shift of the carbon corresponding to the adjacent carbon. [178,183] Therefore, the shoulder at 102 ppm was associated with the upfield shift of the C_1 after acetylation of the OH at the C_2 position.

3.2.2. Thermal properties

To experimentally investigate the effect of the acetylated CNCs on thermal properties of the PHBH/CNC composites, all compounded materials were tested with TGA, and Figure 40 highlights the main results.

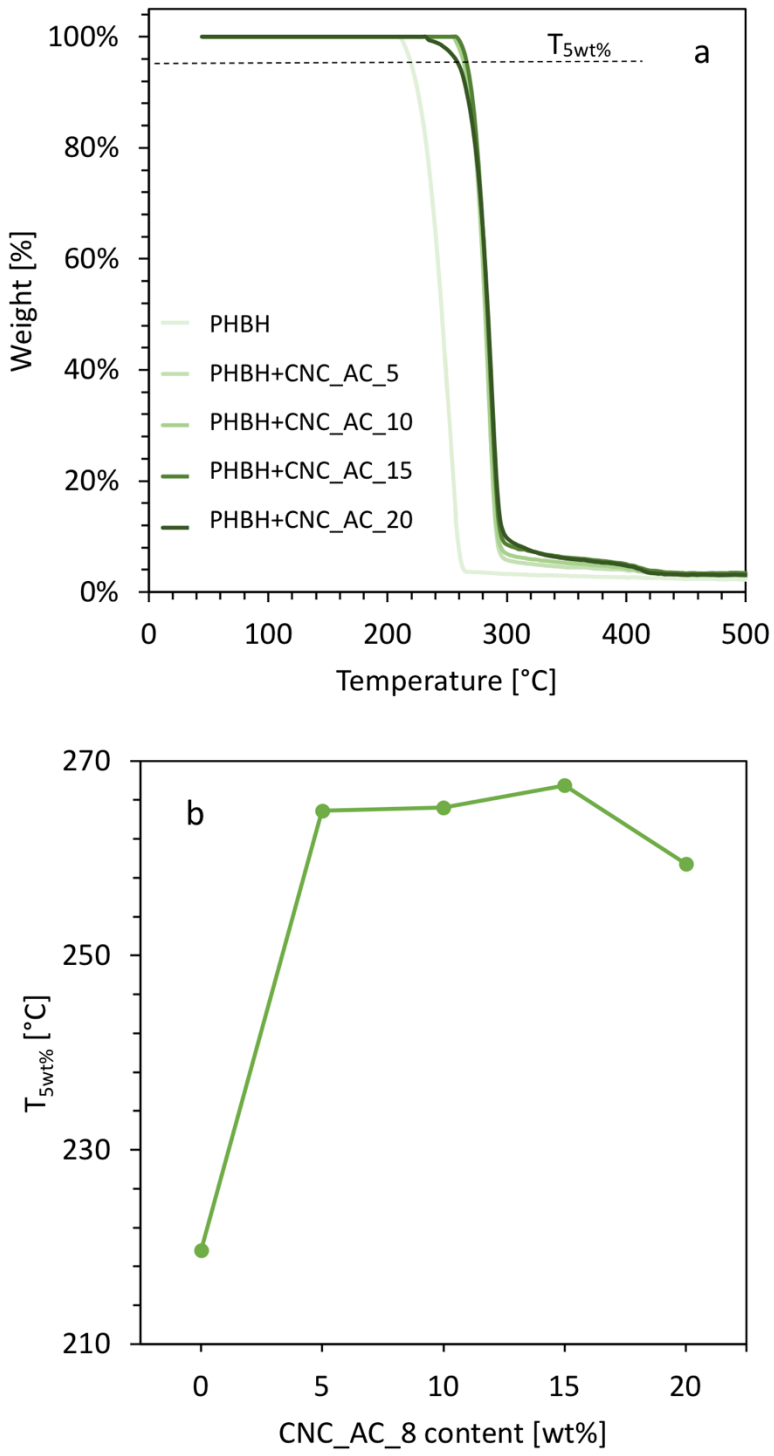

Figure 40 – Thermal properties of PHBH and PHBH/CNC composites as a function of CNC content: 5, 10, 15, and 20 wt%. (a) TGA analysis in air atmosphere. (b) Thermal stability of composites evaluated at a temperature of 5% of mass loss ($T_{5wt\%}$).

When evaluating the temperature associated with a mass loss of 5 wt % ($T_{5wt\%}$), the effect of acetylated CNC addition on the thermal stability of neat

PHBH is clearly observed. In fact, the $T_{5wt\%}$ for composites are systematically all shifted toward higher values, with respect to neat polymer. The increase in thermal stability can be quantified in about 45 °C, regardless of the filler content, starting from a temperature of 220 °C for neat PHBH and arriving to an average value of 265 °C for CNC_AC-based composites.

Derivative thermogravimetry (DTG) measurements evaluated three important temperatures of the degradation process (Table 11), respectively:

- T_{on} – the temperature associated to the onset of the degradation;
- T_{end} – the temperature associated to the end of the degradation;
- T_{max} – the temperature associated to the maximum mass loss rate.

All PHBH/CNC composites samples were characterized by a single step degradation, and all related temperatures were shifted towards higher values, with respect to neat PHBH. Hence, demonstrating consistent results with the previous presented and, overall, a thermal stabilization effect of the acetylated CNC over PHBH matrix.

Table 11 - Derivative thermogravimetry (DTG) data of PHBH and PHBH/CNC composites, at different acetylated CNC content: 5, 10, 15 and 20 wt%.

Sample	T_{on} [°C]	T_{max} [°C]	T_{end} [°C]
PHBH	212	252	272
PHBH+CNC_AC_5	257	285	305
PHBH+CNC_AC_10	258	285	305
PHBH+CNC_AC_15	260	287	312
PHBH+CNC_AC_20	237	289	324

The practical implication of the thermal stabilization effect of acetylated CNC is clear and evident, since it allows to widen the range of use of PHBH, considering also applications with higher working temperature conditions. The thermogravimetric measurements demonstrate that acetylated CNCs improve the thermal stability of the neat PHBH matrix. The same trend has already been individuated in previous research; [144] however, here a 4-fold improvement compared to the cited study was reached. To better understand the enhancing effect of CNCs on the thermal properties of the PHBH matrix, it is important to consider the thermal degradation process of this biopolymer. Previous research indicates that this happens by a random chain scission reaction with a six-membered ring ester intermediate, transforming eventually the ester groups into olefinic and carboxylic acid groups. [184,185] The chain scission rate increases according to the increase in temperature; therefore, at higher operating temperatures this degradation is faster. The formation of a six-membered ring ester during the early stage of the PHBH-degradation process is hindered by the intermolecular hydrogen-bonding interactions that occur between the oxygen of the ester groups of the PHBH matrix and the unreacted hydroxyl groups of acetylated CNCs or the acetyl group bonded to the CNC surface. [186]

3.2.3. Rheological properties

Prior pursuing the effective 3D printing, it was evaluated the flow behavior of the PHBH/CNC composite filaments during the FDM processing. In order to do this, the shear rate was associated with that of a capillary system, and therefore expressed as

$$\dot{\gamma} = \frac{4Q}{\pi r^3} \qquad \text{(Eq.8)}$$

where Q is the flow rate and r is the radius of the nozzle of the printer. Moreover, by considering the flow rate as

$$Q = \pi r^2 v \quad \text{(Eq.9)}$$

where v is the printing speed. Hence, combining the two previous equations, the shear rate was expressed as a function of printing speed and nozzle radius, and precisely as

$$\dot{\gamma} = \frac{4v}{r} \quad \text{(Eq.10)}$$

Assuming a printing speed of 5 mm s^{-1} and a nozzle diameter of 0.4 mm, a typical shear rate of 100 s^{-1} can be assumed as experienced value by the melt polymer during the extrusion through the 3D printer nozzle.

To characterize the rheological behavior of the biocomposites, rheological measurements were carried out with a parallel plate rheometer with a shear rate up to 10 s^{-1}. For higher shear rate, the data were implemented according to the empirical Bird−Carreau−Yasuda (BCY) equation (Eq.2), where the model parameters (n, λ, and η_0), which are listed in Table 12, were determined starting from experimental data.

Table 12 - Experimental parameters for Bird-Carreau-Yasuda model.

Sample	n	λ [s]	η_0 [Pa s]
PHBH	0.29	0.6	4,690
PHBH+CNC_AC_5	0.22	1	12,800
PHBH+CNC_AC_10	0.2	0.75	15,400
PHBH+CNC_AC_15	0.14	1.5	18,500
PHBH+CNC_AC_20	0.1	1.7	26,700

According to the BCY model, the melt bio-composites at low shear rate ($\dot{\gamma} \ll 1/\lambda$) behave as a Newtonian fluid with viscosity η_0 and at intermediate shear

($\dot{\gamma} \geq 1/\lambda$) they behave as a power-law fluid. For this reason, the relaxation time (λ) and the power law index (n) are the most important parameters of this model. The former reflects the onset of shear thinning behavior, and we can notice that by increasing the acetylated CNC content, the relaxation time increases and therefore the starting of the shear thinning behavior shifts toward minor shear rate. The latter parameter affects the slope of the shear thinning region ($n-1$) and it can be observed that the power law index (n) decreases with the increase of CNC content, and hence the overall effect is an increase in the slope of viscosity curves, in the shear thinning region ($\dot{\gamma} \geq 1/\lambda$).

The rheological measurements are presented for composites at 5 and 10 wt% in Figure 41, and for composites at 15 and 20 wt% in Figure 42. For a shear rate below 1 s^{-1}, a plateau can be observed for all curves. As expected, by increasing the CNC content, the viscosity increases because of the interactions between nanocrystals and matrix and between nanocrystals themselves that restrain chain movements and hinder chain relaxation. [187] For a shear rate above 1 s^{-1}, shear-thinning behavior can be observed in all samples. However, the effect of the CNC content can be determined by the change of the exponent n of the Bird−Carreau−Yasuda model. A lower power law index n results in a higher shear-thinning effect of the material. Therefore, the increase of viscosity associated with the filling content is reduced, and hence, the differences between curves obtained at different CNC contents are smaller. It is relevant to note that the shear thinning behavior is a relevant effect that can influence print quality for overhang details, where it is important to avoid polymer drops.

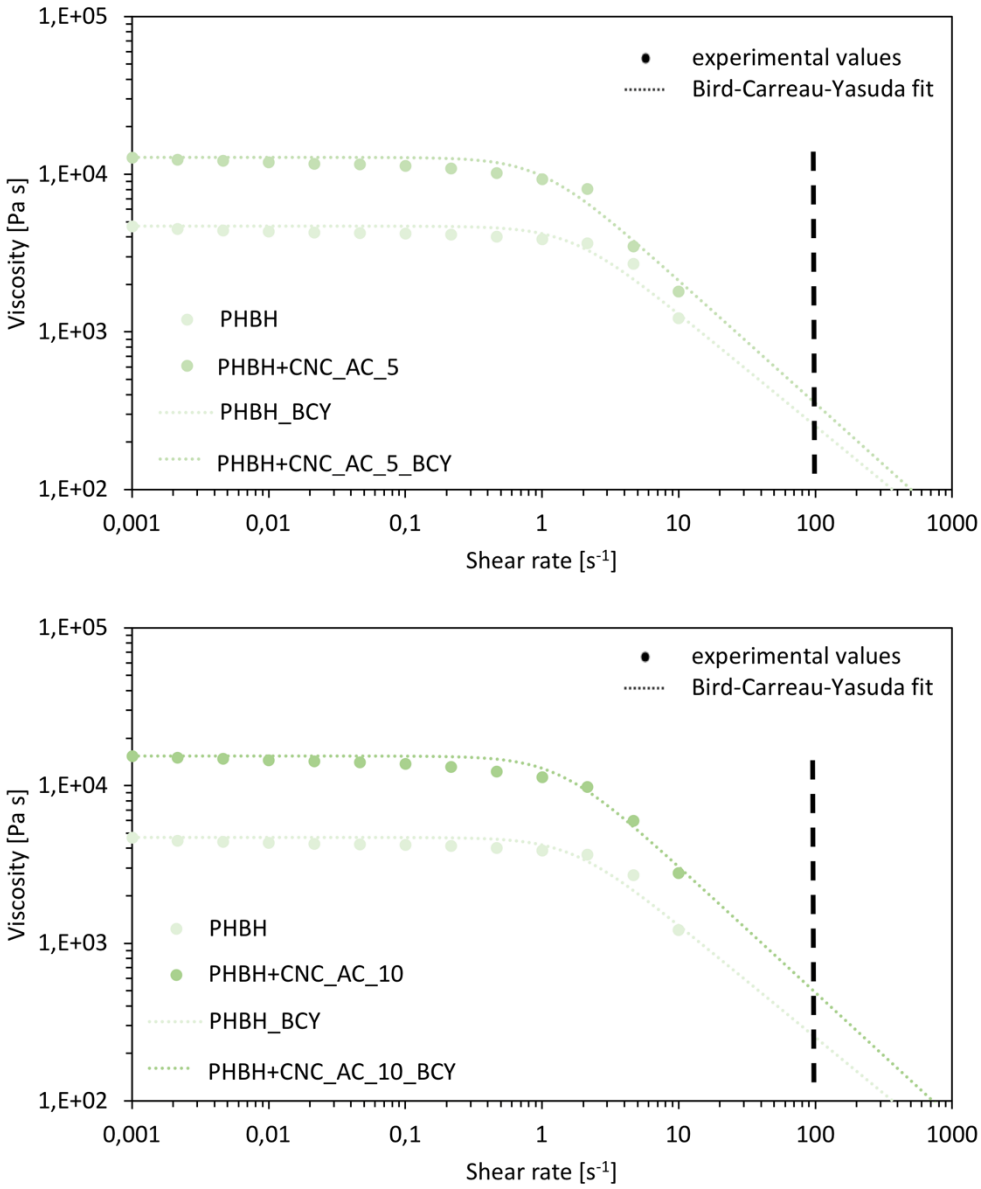

Figure 41 - Experimental shear viscosity values (filled circles) and the Bird-Carreau-Yasuda (BCY) fit model (dotted line) of neat PHBH and PHBH/CNC composites at different CNC content: (a) 5 wt% (b) 10 wt%.

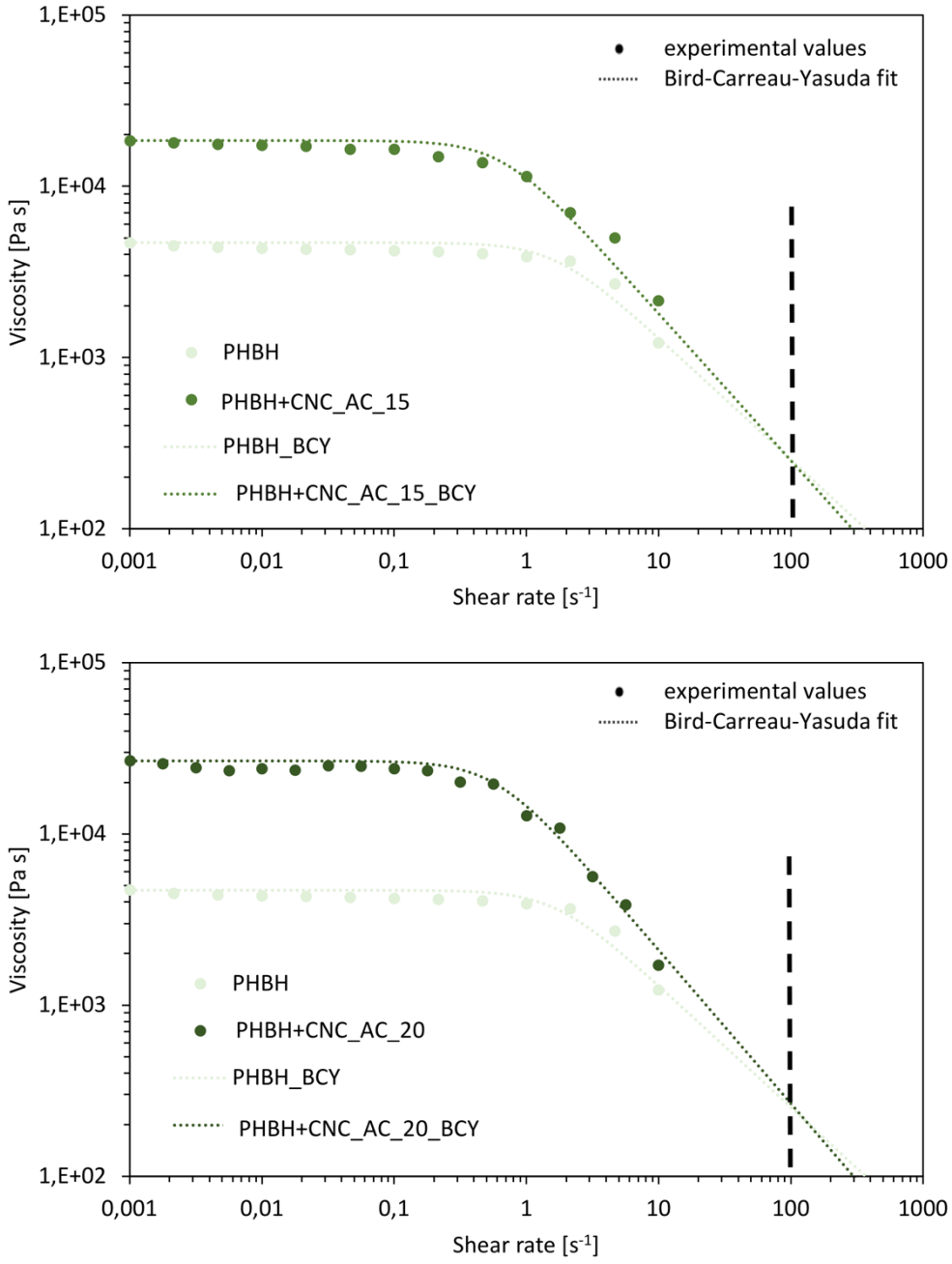

Figure 42 - Experimental shear viscosity values (filled circles) and the Bird-Carreau-Yasuda (BCY) fit model (dotted line) of neat PHBH and PHBH/CNC composites at different CNC content: (a) 15 wt% (b) 20 wt%.

Considering the previously estimated shear rate for the FDM 3D printing process (100 s^{-1}), the viscosities of the biocomposites are 253 Pa·s for neat PHBH and 353, 487, 250, and 266 Pa·s for 5, 10, 15, and 20 wt% of acetylated CNC content, respectively. By comparing the measurements with reference viscosity values for FDM 3D printability, [188,189] and also

considering the shear thinning behavior of the melt biocomposites, it can be concluded that all compounds are 3D printable.

3.2.4. Mechanical properties

Mechanical properties of PHBH/CNC biocomposites were investigated via tensile testing of hot-pressed films. The results for the different compositions are graphically illustrated in Figure 43.

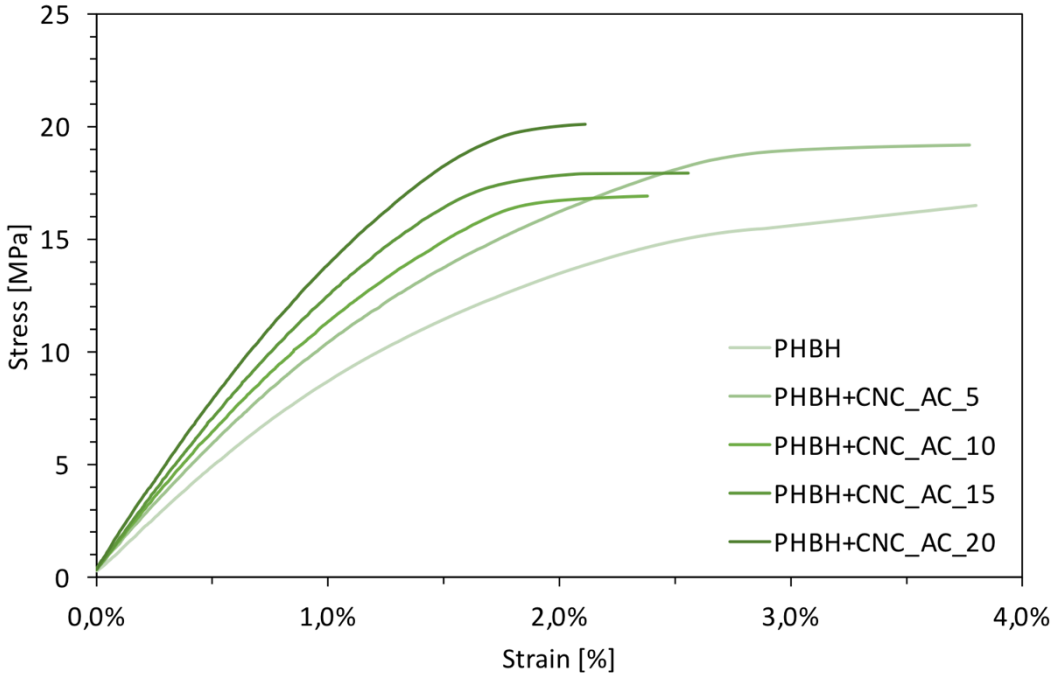

Figure 43 - Stress-strain curves of PHBH and PHBH/CNC composites at different CNC content: 5, 10, 15 and 20 wt%.

It is evident to recognize the reinforcing effect of CNCs over the biopolymer matrix. In fact, at the increasing acetylated CNC content, it corresponds an increase in the initial slope of the stress-strain curves, which implies a higher Young's modulus for the composites, Figure 44 (a). Reasonably, this stiffer behavior occurs with a decrease in flexibility, and hence a reduction of elongation at break, Figure 44 (c). Another important property to consider is the tensile stress at break, which almost corresponds to the ultimate tensile strength, and in these cases, even if not as significantly as for the elastic modulus, with the increase of CNC content, an increase in the maximum stress resistance can be observed, Figure 44 (b).

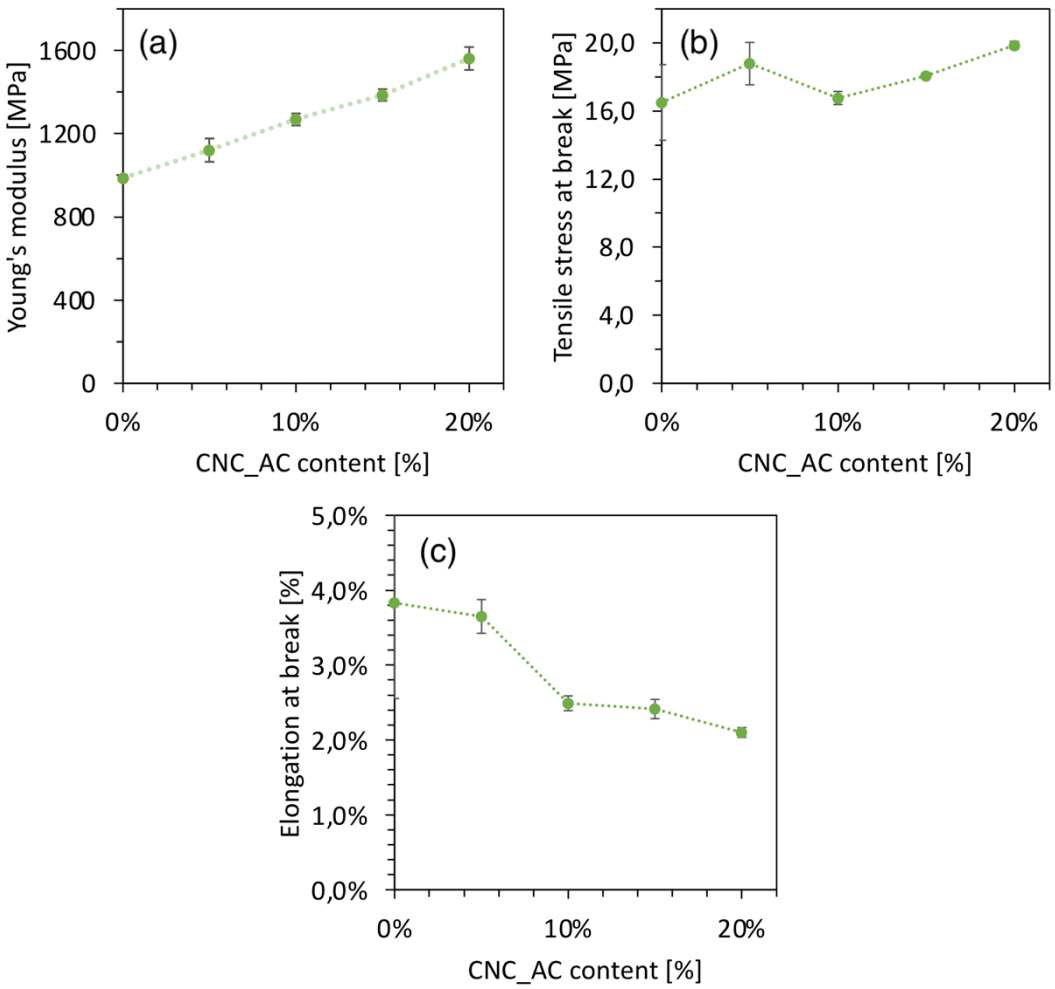

Figure 44 – Mechanical properties of PHBH and PHBH/CNC composites with increasing amount of acetylated CNC content (5, 10, 15 and 20 wt%): (a) Young's modulus, (b) stress at break and (c) elongation at break.

The stiffening effect of the acetylated CNCs could be influenced not only by the higher rigidity of CNCs with respect to neat PHBH, but also by the cellulose acetylation, which improves the adhesion, and hence the stress transmission, between the cellulose nanocrystals and the biopolymer matrix.

Further investigations over the reinforcing effect of acetylated CNCs on viscoelastic properties of PHBH were carried out with dynamic mechanical analysis (DMA) on 3D printed samples, and in Figure 45 the effects on the storage modulus (E') over all range of temperatures are shown.

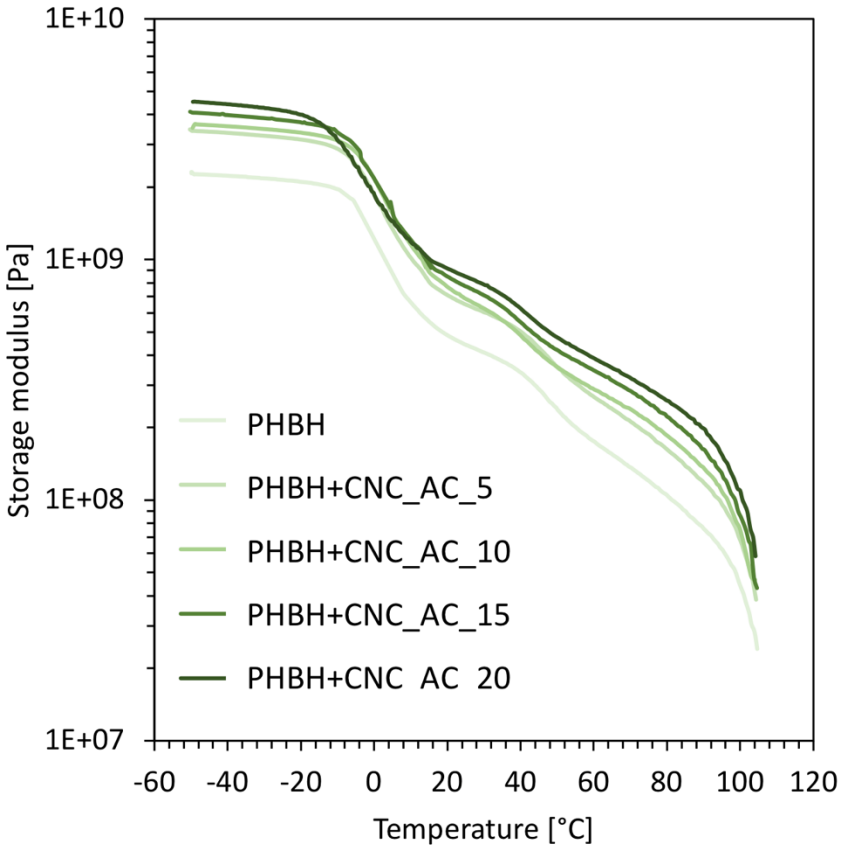

Figure 45 – Storage modulus (E') behavior over temperature range evaluated at different PHBH/CNC contents: 5, 10, 15, and 20 wt%.

The increase of storage modulus follows a typical trend observed for several cellulose-based composites, being directly proportional to the addition of acetylated CNCs. The most noteworthy mechanical reinforcing effect is observed for composites with 20 wt% of acetylated CNCs. It is important to note that the increase in storage modulus is approximately constant both before and after the glass transition. Three temperature conditions were considered for comparison: −20 °C as an indication of the glassy behavior, 25 °C as an indication of the room-temperature behavior, and 80 °C as an indication of a high-temperature application of this material. The corresponding storage modulus values, for each different sample composition, are shown in Table 13.

Table 13 - Results of dynamic mechanical analysis (DMA) on PHBH and PHBH/CNC biocomposites, at different acetylated CNC content: 5, 10, 15 and 20 wt%.

Sample	E' [GPa] at -20 °C	E' [GPa] at 25 °C	E' [GPa] at 80 °C
PHBH	2.10 ± 0.26	0.44 ± 0.05	0.10 ± 0.01
PHBH+CNC_AC_5	3.16 ± 0.51	0.65 ± 0.04	0.16 ± 0.02
PHBH+CNC_AC_10	3.43 ± 0.23	0.69 ± 0.07	0.18 ± 0.01
PHBH+CNC_AC_15	3.72 ± 0.29	0.78 ± 0.05	0.22 ± 0.02
PHBH+CNC_AC_20	4.00 ± 0.10	0.85 ± 0.03	0.26 ± 0.01

The maximum relative increments of storage modulus, assuming the neat PHBH as the reference, were obtained at 80 °C, and they correspond to 58%, 78%, 115%, and 150% respectively for 5, 10, 15, and 20 wt% acetylated CNC contents. Moreover, it is important to note that, for the same value of storage modulus, acetylated CNC widens the range of temperatures of applications by a value of about 20 °C. These results are consistent with the ones obtained via tensile testing, and therefore the hypothesis of mechanical reinforcement effect, attributed mainly to good affinity and adhesion of the CNCs to the biopolymer matrix, is once again supported. Besides, it should be considered that DMA data are referred to FDM printed samples, where also the printing deposition pattern is a relevant parameter, which can cause a filler orientation during FDM printing, and hence an improvement on mechanical resistance. As an indication, in Figure 46, a DMA analysis run over two distinct PHBH+CNC_AC_5 samples is shown. The storage modulus, evaluated at 80 °C, of the 3D printed sample with a fill angle of 0° (PHBH+CNC_AC_5_0°) is 25% higher than that of the sample with a fill angle of ±45° (PHBH+CNC_AC_5_45°).

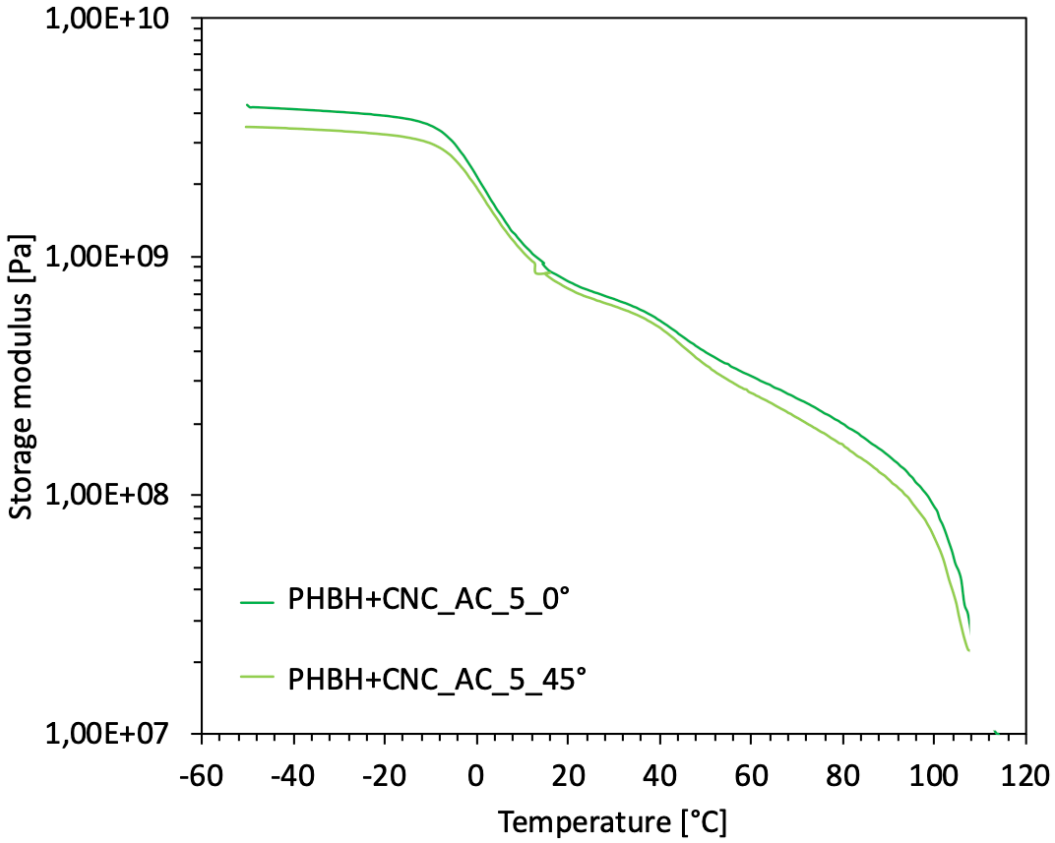

Figure 46 – Influence of 3D printing fill angle on storage modulus for PHBH+CNC_AC_5 samples with 0° (PHBH+CNC_AC_5_0°) and ±45° (PHBH+CNC_AC_5_45°) fill angle.

It is interesting to compare these results, with the only previous study, [145] where a successful melt compounding of CNF and PHBH was obtained and used to 3D print via FDM some test samples, which, however, demonstrated a drop in mechanical performance, probably due to the absence of chemical modification of cellulose.

In Figure 47 are shown the curves of tan δ and loss modulus (E") for all fabricated PHBH/CNC composites. It is possible to state that acetylated CNCs do not affect significantly these properties. Glass-transition temperatures (T_g), evaluated at the maximum peak of the tan δ, reflect the results already presented for OHF and MFC, namely that a cellulose phase, dispersed in PHA matrix, does not have significant influence over the T_g of the final composite.

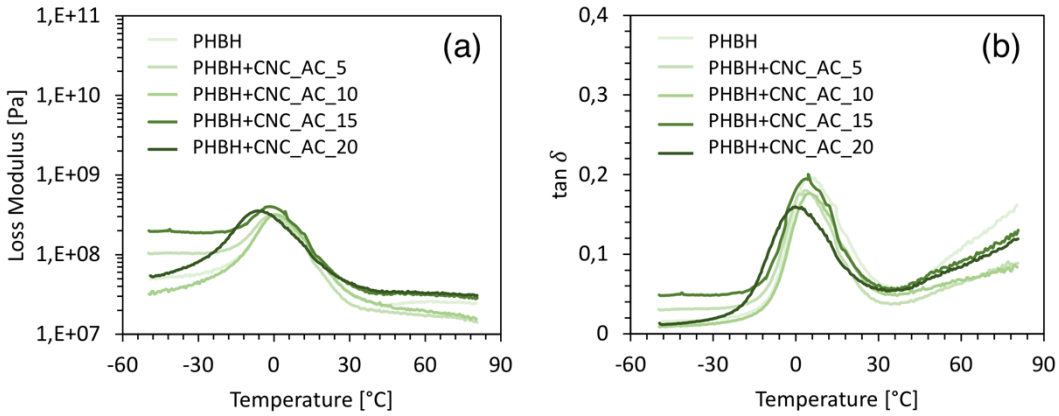

Figure 47 – (a) loss modulus and (b) tan δ variations over temperature range evaluated at different PHBH/CNC contents: 5, 10, 15, and 20 wt%.

3.2.5. Disintegration under composting condition

Biodegradability in composting conditions was tested to study the degree of disintegration of the composites. To this end, the tests were performed according to the ISO 20200 standard and the weight losses of all hot-pressed samples were monitored and registered over a period of time of almost three months. To have a comparison with the behavior of petroleum-based polymers, in the same conditions, the tests were carried out also with low-density polyethylene (LDPE). The evaluation of the obtained results allows to appreciate the effective biodegradation of these innovative composites as compared to a traditional thermoplastic polymer. The degrees of disintegration of the neat polymers and composites were plotted as a function of time and composition in Figure 48.

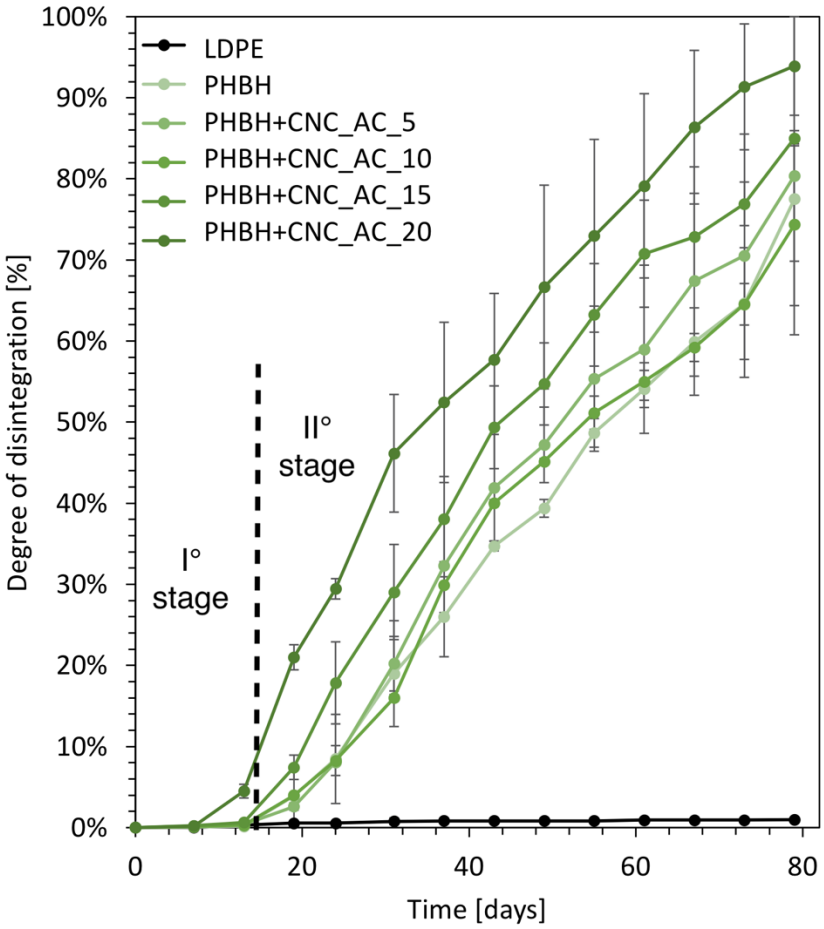

Figure 48 - Plot of the degree of disintegration as a function of the time and acetylated CNC content of PHBH biocomposites and of a traditional petroleum-based LDPE, under composting conditions in a laboratory-scale test.

As expected, LDPE was not morphologically affected by the composting conditions, showing almost perfect mass conservation even after 78 days. On the contrary, neat PHBH and PHBH/CNC composites denote an evident trend of an increased degree of disintegration over the composting time. In the first 2 weeks, the weight loss remained practically unchanged, because in this first step of biodegradation, only small molecules are degraded, and this is indicated by a roughening of the surface. In fact, PHA disintegration is primarily caused by microorganisms that erode the polymer surface and gradually spread into the bulk. [190] After 15 days, the maturation stage starts and a rapid increase in the degree of disintegration is observed, with no tendency to plateau. This second stage is characterized by the biodegradation of high-molecular-weight materials such as PHBH, CNC,

and biomass present in the compost. Within the first three months of the composting process, all biobased samples reached a degree of disintegration higher than 75%. The weight loss rate increased with the increase of acetylated CNC content; in fact, the highest degree of disintegration was measured for PHBH+CNC_AC_20, with a weight loss of 94% after 78 days. Hence, it seems that cellulose nanocrystals also affect the disintegration process of the biopolymer, thereby increasing the biodegradability of the composites, according to the CNC content. Puglia *et al.* observed that montmorillonite favors the presence of residual water and the hydrolysis of polymer chains into smaller molecules digestible by microorganisms. [191] Similarly, the same hypothesis might be extended also for CNCs. The morphological changes of the samples were investigated at different composting times, first to assess the macroscopic impact of degradation over time. The visual appearance of the samples is shown in Figure 49.

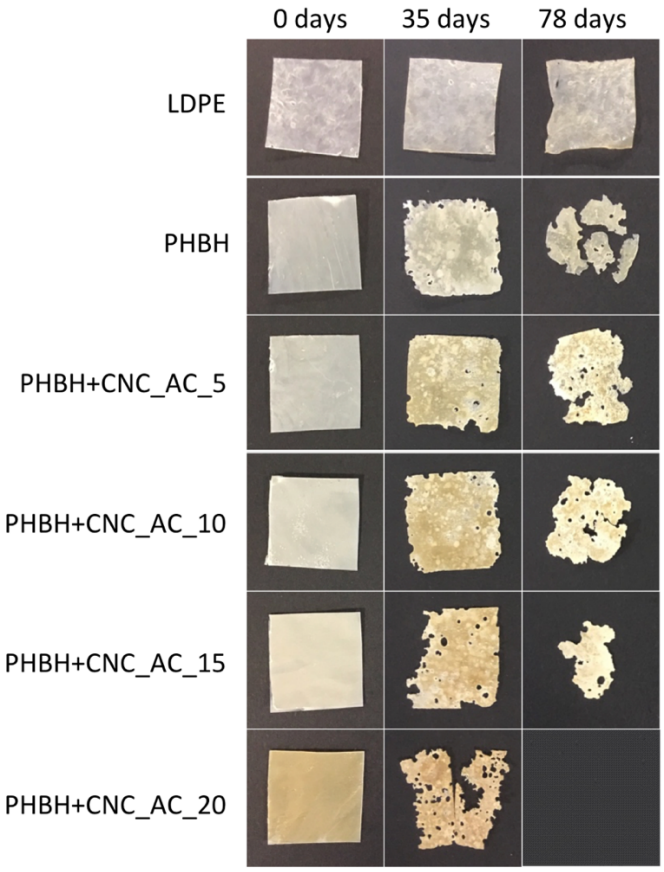

Figure 49 - Visual appearance of the tested films at the starting moment, after 35 and 78 days during the composting process.

To evaluate also at a microscopic level, ESEM observations were carried out to show the heterogeneity and roughness of the surface of the biobased and biodegradable samples, characterized by the presence of holes, cavities, and cracks, as it can be seen in Figure 50 (d, e and f). Differently, LDPE did not denote a significant alteration of the mass nor of the surface morphology, as shown in Figure 50 (a, b and c).

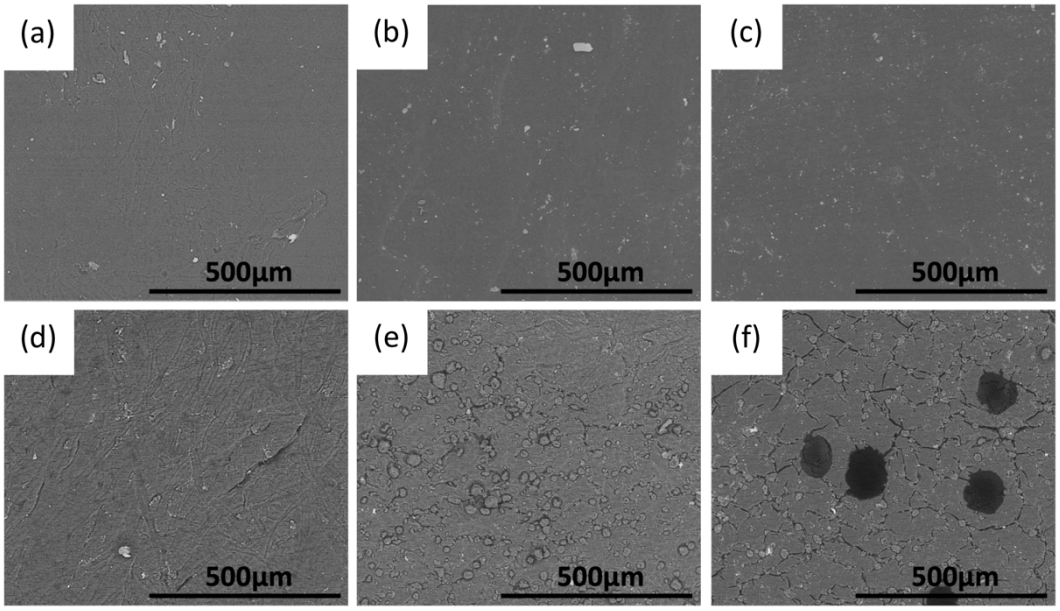

Figure 50 - ESEM micrographs of the LDPE samples at different degradation times: (a) starting moment, (b) after 35 days and (c) after 78 days. ESEM micrographs of the PHBH+CNC_AC_15 samples, chosen as a representative of the behavior of the biobased composites, at different degradation times: (d) starting moment, (e) after 35 days and (f) after 78 days.

The presented results support the great advantage of the sustainable end-of-life of the biobased PHBH/CNC composites over a traditional petroleum-based plastic, such as LDPE, which is completely resistant to a composting process even for long periods.

3.2.6. Biocompatibility analysis

The *in vitro* biocompatibility of 3D printed scaffolds was investigated for three different compositions: PHBH, PHBH+CNC_AC_10 and PHBH+CNC_AC_20. After cell seeding and cell confluence was reached,

the attached Human Osteoblastic cells (HOB) were fixed to be analyzed by SEM imaging. The results are shown in Figure 51, where it is possible to appreciate the HOB cells adhesion and colonization, orienting themselves preferentially along the 3D printed filaments of the scaffolds.

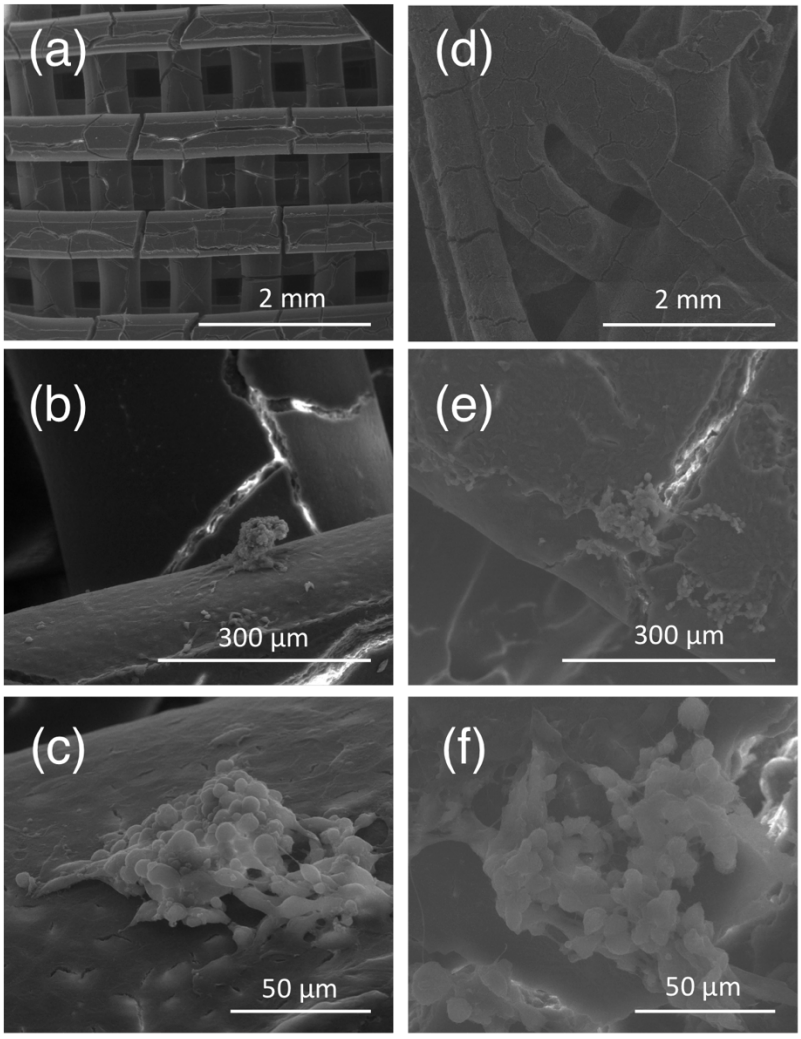

Figure 51 – SEM images of PHBH scaffolds: (a) without cells and (b and c) two different magnifications of seeded scaffolds with HOB cells. SEM images of PHBH+CNC_AC_20 scaffolds: (d) without cells and (e and f) two different magnification of seeded scaffolds with HOB cells.

Although cells colonized all samples, there is a noteworthy consideration to be made, which is that in PHBH, OHB cells tend to aggregate, whilst in PHBH/CNC composites, the OHB cells are more distributed on the surface, and this is probably due to the presence of CNCs.

One important aspect of medical resorbable devices, it is the time of degradation inside the human body, and the correlated time of mechanical stability. In fact, a rapid degradation of the scaffold leads to a poor mechanical resistance and it can hinder the healing process. For example, in hard tissue regeneration, a slow degradation is highly preferable, since the scaffold maintains the mechanical properties, balancing the degradation and the regeneration processes. [192]

In order to evaluate this property, an *in vitro* degradation test was carried out on all PHBH/CNC sample compositions, and in Figure 52 are shown the results of the test for the first 6 weeks.

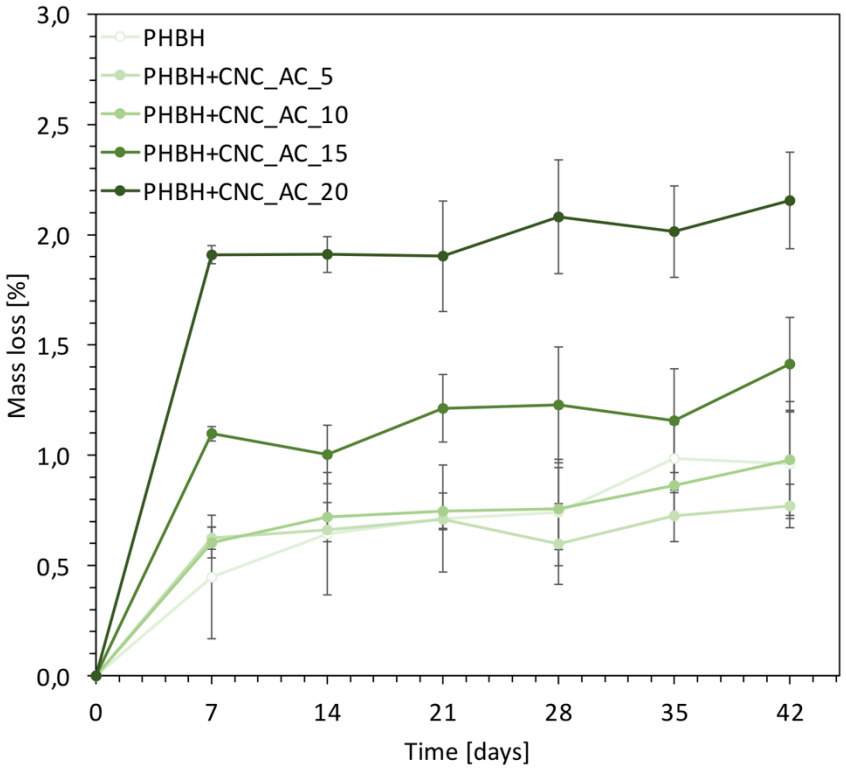

Figure 52 - *In vitro* degradation for PHBH/CNC in PBS at 37 °C.

The degradation of 3D printed scaffolds displayed a low rate, but slowly growing with time. After degradation for six weeks, the weight loss for scaffolds of pure PHBH was almost 1 wt%, and it was doubled for PHBH+CNC_AC_20, therefore it can be appreciated a tunable degradation behavior according to the acetylated CNC content. Since PHAs have a water diffusion-controlled hydrolysis degradation, [192] the possible reason

for the tuned degradation behavior is that CNCs enhance the permeability of the water molecules into the polymer matrix, resulting in water diffusion from the surface to the bulk polymer.

The obtained results are consistent with the previous presented in literature, where it was demonstrated that the degradation in buffer solution without enzymes, such as in this study case, was slower than into a lipase solution. [193] However, it was chosen to follow a testing procedure that is more precautionary, e.g. without mechanical agitation and without enzymatic addition, to demonstrate that, even at less aggressive conditions, these materials could undergo a biological degradation.

Considering that, depending on the species, it usually takes from a few months to a few years, for complete bone regeneration, [194] the above presented results are promising values for a biomedical application in bone tissue engineering, where these composites could be 3D printed as scaffolds for sustaining the regeneration process, throughout the healing period.

3.2.7. Water affinity

Wettable scaffolds were demonstrated to be conducive to better cellular adhesion, growth and proliferation. In fact, a scaffold should have the ability to maintain a humid environment to promote proper fluid exchange between the designed part and the surrounding environment *in vivo*. [195] Therefore, the PHBH/CNC biocomposites were tested to evaluate water affinity and overall, the effect of CNCs on this property, which is expected to increase with respect to the CNCs content.

PHBH is a hydrophobic matrix and it is predictable that this effect is preponderant on the final behavior of the composites, but it was carried out a water uptake measurement on 3D printed scaffolds to evaluate if the compounding of CNC could slightly improve the wettability of the biopolymer. The results are shown in Figure 53.

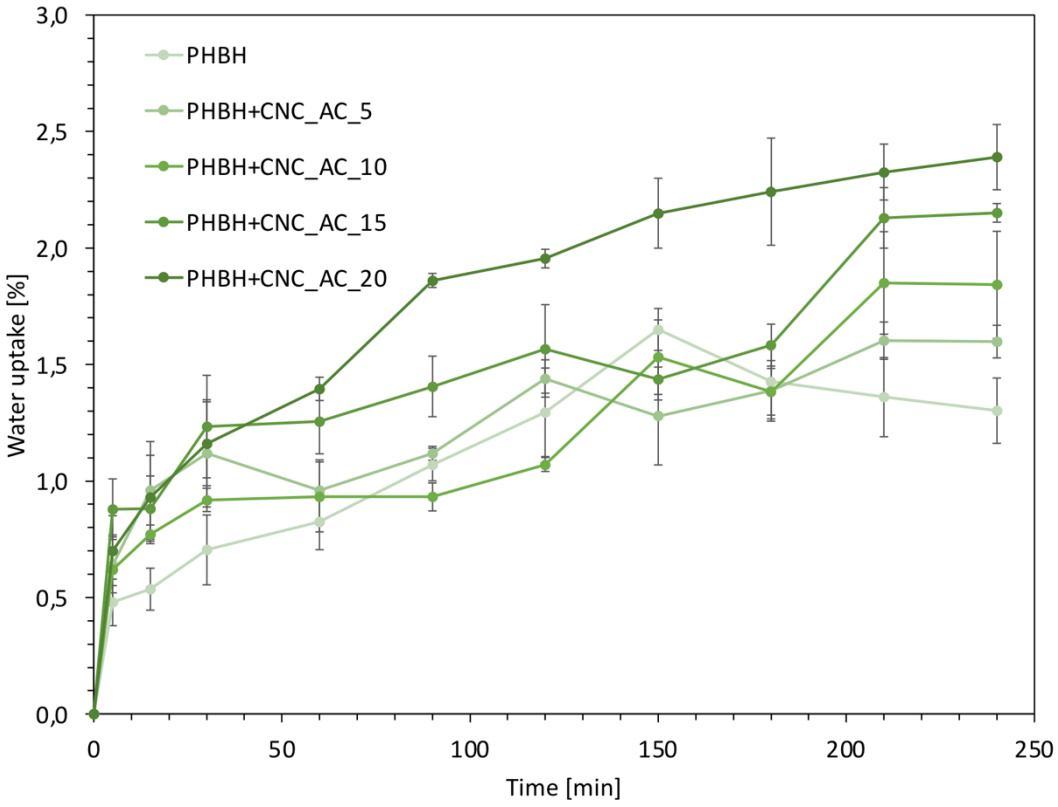

Figure 53 – Water uptake measurements for PHBH and PHBH/CNC composites at different acetylated CNC content.

The water uptake rate increased faster in the first hour, and then it started reaching a saturation state, where, after 4 hours, the maximum water uptake of PHBH and PHBH+CNC_AC composites (5, 10, 15 and 20 wt%) were respectively: $1.3 \pm 0.2\%$, $1.6 \pm 0.1\%$, $1.9 \pm 0.2\%$, $2.2 \pm 0.1\%$ and $2.4 \pm 0.1\%$. Even if the final values do not denote a highly wettable behavior of the scaffolds, it is interesting to note that it was proved the enhancing effect of the introduction of cellulose nanocrystals in improving wettability and water retention of the scaffold.

In order to have further support, also contact angle measurements were carried out on the same 3D printed scaffolds, and the results are schematized in Figure 54.

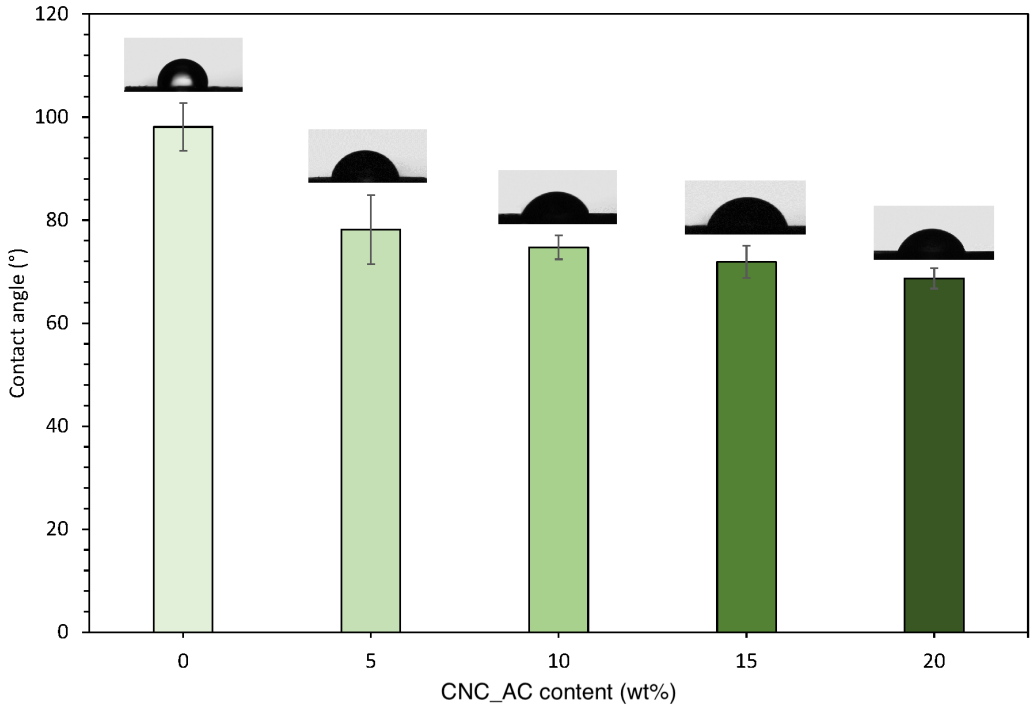

Figure 54 - Contact angle measurements for PHBH and PHBH/CNC composites at different acetylated CNC content.

In this case, the findings indicated even a higher hydrophilicity behavior of the composites; in fact, the contact angles of PHBH and PHBH+CNC_AC composites (5, 10, 15 and 20 wt%) were respectively: 98.1 ± 4.6°, 78.2 ± 6.7°, 74.7 ± 2.3°, 71.9 ± 3.1° and 68.7 ± 2°. Hence, increasing the content of acetylated CNC, the water contact angle decreased in the biocomposites, denoting a more hydrophilic behavior. These experimental results confirmed and strengthened those of water uptake, and therefore, it can be considered that the improved surface hydrophilicity of nanocomposite scaffolds, by incorporation of CNC, is advantageous to provide a suitable environment for cell growth and proliferation in tissue regeneration.

3.2.8. 3D printing medical devices with FDM

After a theoretical validation of 3D printability by rheological measurements, the PHBH/CNC composites were actually 3D printed with FDM to fabricate

different shapes and objects. This section is aimed to illustrate the printability of these biocomposites in 3D (x, y, and z).

First, simple grids with a filling pattern alternating from 0 to 90° were printed with a nozzle diameter of 0.6 mm, a printing speed of 5 mm s^{-1}, and an extrusion temperature of 170 °C. Both by visual and microscopy inspection, it was possible to investigate the internal porous structure, the definition of each extruded filament, and the pore sizes of the printed samples. They denote a good maintenance of the filamentary shape with a circular cross section of 600 ± 15 µm, without collapsing of parts or layer delamination. Besides that, also the internal porous structure follows the original filling pattern, alternating each layer of 0-90°; this can be evaluated in Figure 55, considering the effective angle between each layer.

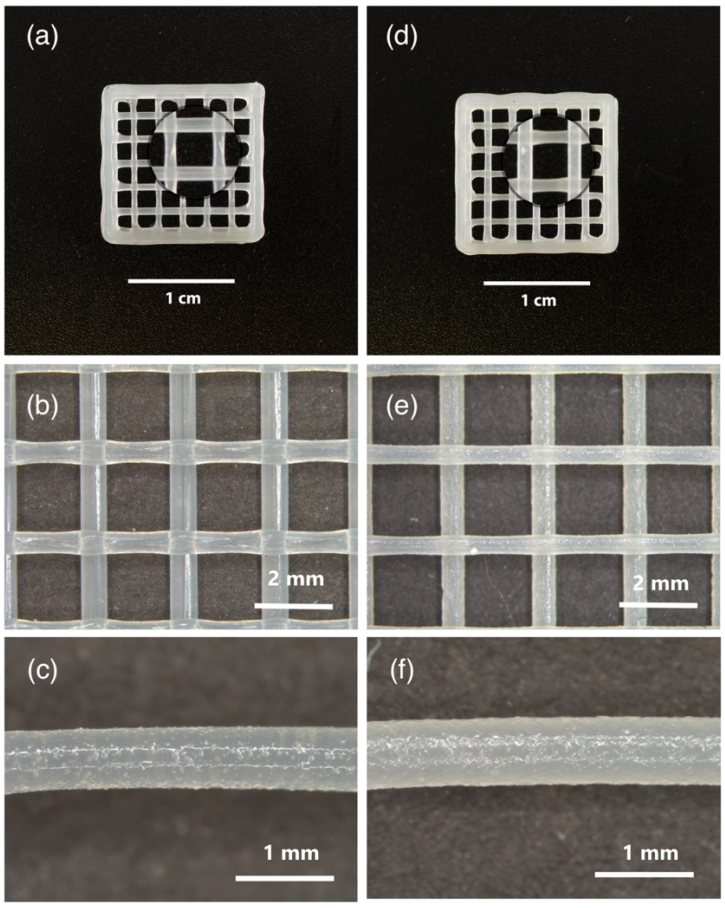

Figure 55 - Representative top view of a grid FDM 3D printed by a filament of (a) neat PHBH and (d) PHBH+CNC_AC_10, with an alternation of 0−90° for directions of layers. Optical microscopy images of composites 3D printed filaments and grids of different compositions: (b and c) PHBH and (e and f) PHBH+CNC_AC_10.

It is well-known that the surface roughness of a medical implant is of great importance since it is in direct contact with the host tissue, whether it is bone or fibrous one. Therefore, it was investigated the effect of acetylated CNC over the superficial roughness of the 3D printed scaffolds, and some AFM measurements were carried out to evaluate this parameter on PHBH and PHBH+CNC_AC composites at 10 and 20 wt%. The results are graphically represented in Figure 56.

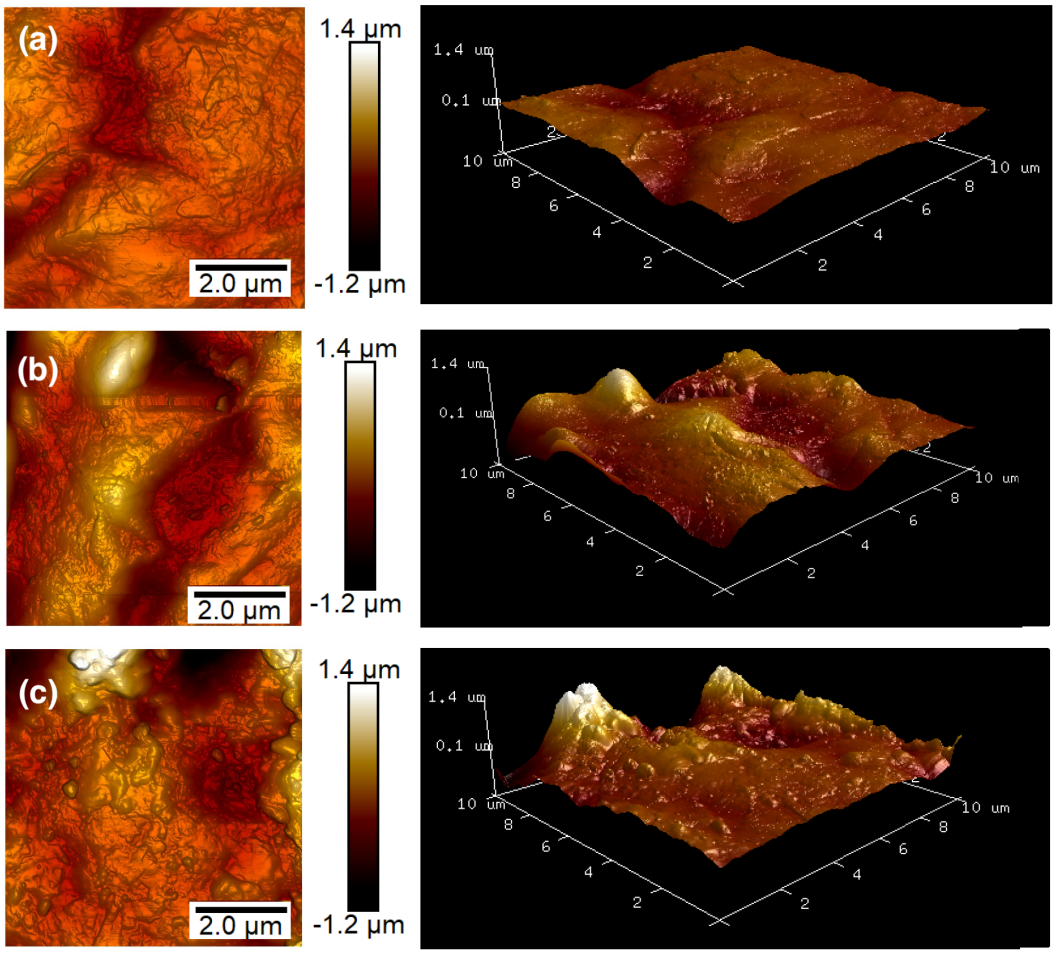

Figure 56 - AFM measurements over superficial roughness for 3D printed scaffolds of: (a) PHBH, (b) PHBH+CNC_AC_10 and (c) PHBH+CNC_AC_20.

It is possible to recognize the increasing superficial roughness of scaffolds, at increasing acetylated CNC content. The average roughness (R_a), for every sample, is synthetized in Table 14.

Table 14 – Average roughness (R_a) of 3D printed scaffolds with PHBH, PHBH+CNC_AC at 10 and 20 wt% content.

Sample	R_a [nm]
PHBH	79 ± 3
PHBH+CNC_AC_10	223 ± 32
PHBH+CNC_AC_20	411 ± 44

It was demonstrated that the response of cells to roughness is different depending on the cell type, for example osteoblasts show a significantly increased proliferation rate with increasing surface roughness, while fibroblasts showed the opposite proliferation behavior. [196] Hence, it is an interesting discovery that the roughening morphology of the PHBH/CNC biocomposites can be tuned by the regulation of CNC content, in order to optimize the interaction between cells and scaffold, according to the final application of the medical device.

The quality and the accuracy of the printing were also examined for more complex and dense geometries of scaffolds. For example, in Figure 57 is shown an example of a PHBH+CNC_AC_15 scaffold 3D printed with an infill density of 60% and an alternation of ±45° for layer directions. In this case, the pore size is 300 μm, which is an accurate dimension for biological scaffold, where cells can proliferate. From the top view and the cross-section view it is possible to appreciate the fidelity of the printing and the self-supporting structure, which has 20 layers.

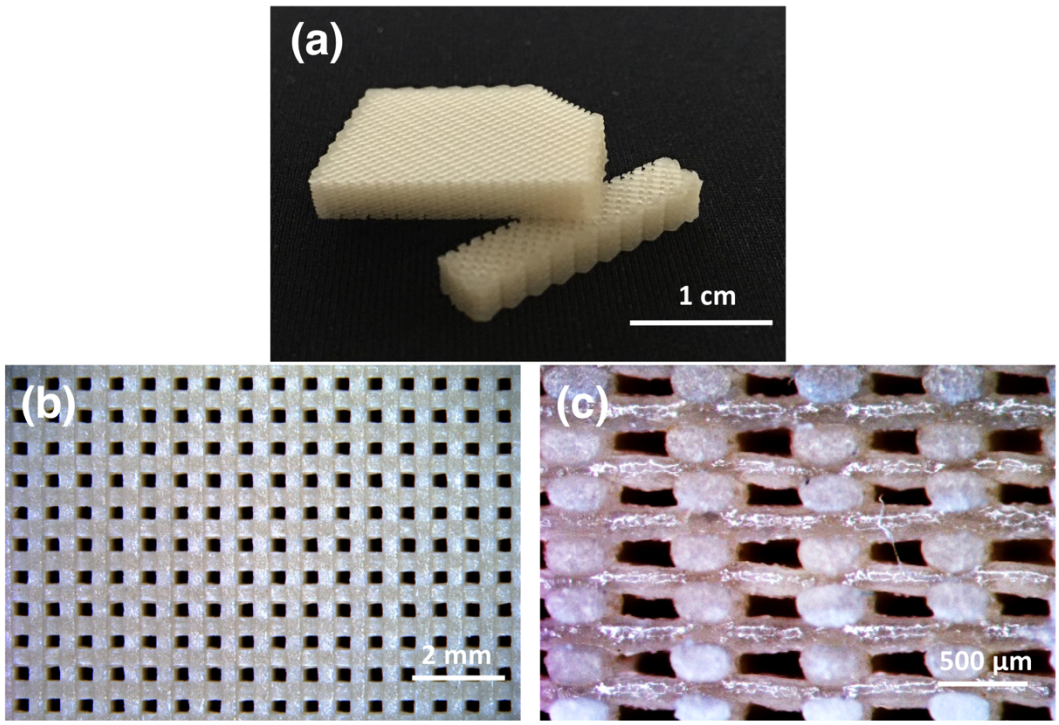

Figure 57 – (a) Representative view, (b) top view and (c) cross-section view of a FDM 3D printed scaffold of PHBH+CNC_AC_15, with an alternation of ±45° for layer directions, and an infill density of 60%.

Subsequently, even more complex-shaped and fully customized objects were 3D printed with FDM, such as a wearable finger cast shown in Figure 58. This medical device was printed with a similar speed and temperature to those of the grid like scaffolds but with a nozzle diameter of 0.4 mm. The wearable finger cast counts 170 layers and an inclination of the axis of 20° in the upper part, in order to best fit to the natural conformation of the finger. It should be highlighted that the complexity of the object rises not only because of its vertical development in the z-direction or to the inclination of the axis but also to the close alternation of full and empty spaces and the circular shapes of the holes.

Figure 58 - Complex shaped object as a finger cast 3D printed by a filament of PHBH+CNC_AC_10, used as personalized medical device in case of finger dislocation.

The above presented medical application could be successfully used by substituting a rigid plaster in the case of dislocation, resulting in being recyclable and custom-fitted, with the advantage that it could be taken off to wash and ventilate the injured area. Nevertheless, not only could external medical devices be 3D-printed with these innovative composites but another possible application could be the fabrication of scaffolds that could serve as biomedical templates for cell culturing or biodegradable and bioresorbable implants for tissue engineering, which could eventually be used as unique, patient-customized surgical implants. As an indication, it was 3D printed

with FDM a PHBH clavicle plate, which could be used to treat a broken fracture, and in Figure 59 is represented its final application.

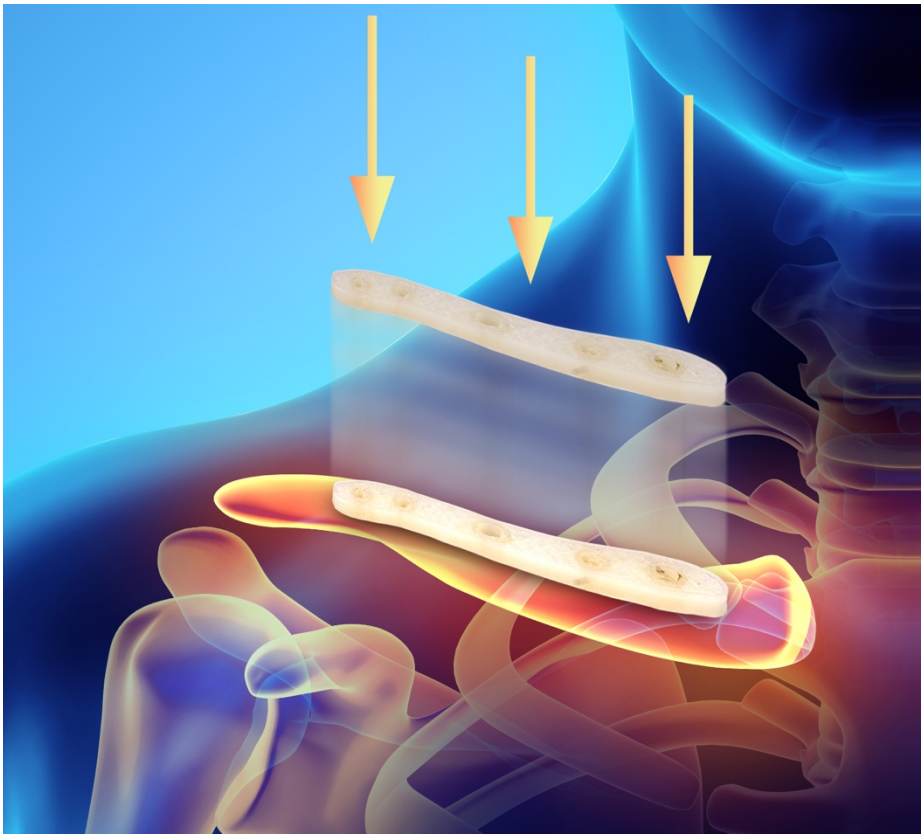

Figure 59 - Graphical representation of a PHBH clavicle plate 3D printed by FDM and its final surgical application for bone regeneration.

Especially due to the resorbability, to the biocompatibility and to the osteogenesis induction of PHBH, this biocomposites allow to think of a future in medicine, where all components are bio-based, perfectly compatible with human body and devices can be harmlessly reabsorbed by our organism, when are no more needed.

4. Conclusions

This PhD thesis was aimed to present the most important results obtained during the author's doctorate studies. More specifically, the purpose of the research was the investigation over the design, fabrication and characterization of bio-based and biodegradable composites, starting from a polyhydroxyalkanoate matrix and different cellulose sources, meant to explore the petroleum-based plastic replacement.

According to the kind of cellulose that was used, versatile results were obtained which could be favorable for applications ranging from household or agricultural items manufacturing, packaging, electronics or automotive sectors and biomedicine.

In this work, one distinction has to be made according to the purpose of the cellulose phase: used as a filler or as a reinforcing agent. In the former use, cellulose-based inert filler is aimed to replace the biopolymer matrix without affecting the general properties. Differently, nanocellulose could be used as reinforcing agent and therefore giving an added value, introducing new functionalities to the final biocomposite.

Cellulose used as a filler agent

In the first case, a totally bio-based composite material was produced, consisting of a PHBH matrix compounded with natural byproduct-based fillers, i.e. neat oat hull fibers (OHF) and microfibrillated cellulose (MFC), obtained from the same agri-food waste, but undergone a chemical-free process of high-pressure homogenization.

The findings demonstrated that OHF and MFC can be positively used as filler for biopolymer matrix without affecting negatively neither the thermal nor the mechanical properties. On the contrary, the results evidenced a slightly improvement of the latter ones, proportional to the amount of filler. The highest increase was obtained for 10 wt% of biopolymer replaced by OHF, and it consists in a Young's modulus increase up to 12%, without a loss in tensile elongation at break.

The effect of homogenization over OHF did not introduce particular enhancement of the mechanical properties nor thermal ones. Besides, a silanization procedure was followed to enhance the fiber adhesion with the matrix. However, despite indications that the chemical modification occurred positively were found, the effect of functionalization upon mechanical properties is not so pronounced. In fact, at the same filler content, and both for OHF and MFC, there is only a 2.6% increase of Young's modulus against a decrease of elongation at break and a maintenance of ultimate tensile strength.

As a consequence, with a view to rationalizing technological and production processes for a lower energy, time and cost impact, it is possible to conclude that OHF is a proper filler that can be used as received, without further mechanical nor chemical modifications. And despite no major improvements in composite properties were observed, the proposed approach is equally a worthy valorization of an agri-food industrial waste, for the production of environmentally friendly durable and semi durable goods devices, supporting the replacement of conventional plastics.

Nanocellulose used as a reinforcing agent

In this case, cellulose nanocrystals (CNCs) were melt-compounded with a PHBH matrix to fabricate biocomposites with tunable final properties, according to the CNC content. Nanocellulose was demonstrated to have different tailoring effect over different characteristics, for example: stiffening effect, higher thermal stability, superficial roughening, increasing the hydrophilicity and the disintegration rate.

A solvent-free cellulose acetylation was followed to enhance the affinity between the biodegradable PHBH matrix and the cellulose nanocrystals. The compounding procedure adopted was a melt-compounding approach that enabled high reinforcing content from 5 up to 20 wt% of acetylated CNCs. Considerable reinforcement effects caused a shift toward higher thermal stability temperatures, which vary from 220 °C for neat PHBH to 265 °C for composites. Storage modulus has shown a 150% increase in

values for 20 wt% acetylated CNC composites. Furthermore, the findings of this research show that CNC, in addition to enhancing the thermal and mechanical properties of the biocomposites, also offers a way to tune the water affinity, the *in vitro* degradation of the composite materials and the degree of disintegration, in line with the nanocellulose content. The biodegradation test showed an expected difference between a traditional thermoplastic, with no degradation during the composting process, and the PHBH/CNC biocomposites, whose degree of disintegration increased with respect to the acetylated CNC content, up to a maximum weight loss of 94% after 78 days.

After fundamental examination of the composite's constituents and of the optimization of the technological processes, constant size filaments were experimentally obtained and used to FDM 3D print different architectures, also with complex and extended shapes. This investigation turned on the lights to different possible applications in biomedical field, due to the high design customization in additive manufacturing (AM).

The introduction of PHA and additive manufacturing in biomedicine boosted the advancements of innovative solutions for problems that were totally or partially unresolved. Apart from the high level of customization of AM, the main reasons for this success was certainly due to the interesting properties of PHA like a wide processing and application versatility, biological origin, biocompatibility and biodegradability. Among additive manufacturing techniques, FDM owns some well-known advantages: its simplicity, rapidity and ecological sustainability, in fact, any organic solvent is required. However, FDM use with PHA for biomedical application is still limited; but, according to the above-mentioned properties and advantages of PHA and FDM, it is reasonable to believe that its use will be increasingly investigated and the number of 3D printed devices by FDM will grow significantly in the next years.

Therefore, since a quick and important development in this research field can be expected, the innovative PHBH/CNC composite material, explored in this research thesis, and its adaptable approach open promising

opportunities for the development of a novel grade of printable customized materials with tunable mechanical properties and different possible applications for biobased, sustainable, and biodegradable designs with improved properties.

References

1. ASTM D6866 - 20 Standard Test Methods for Determining the Biobased Content of Solid, Liquid, and Gaseous Samples Using Radiocarbon Analysis. *ASTM Stand.* **2020**.

2. ISO 14855-1:2012 Determination of the ultimate aerobic biodegradability of plastic materials under controlled composting conditions — Method by analysis of evolved carbon dioxide — Part 1: General method. *ISO Stand.* **2012**.

3. EN 13432:2000 Packaging - Requirements for packaging recoverable through composting and biodegradation - Test scheme and evaluation criteria for the final acceptance of packaging. *EN Stand.* **2000**.

4. European Bioplastics Available online: https://www.european-bioplastics.org/bioplastics/materials/.

5. Li, P.; Wang, X.; Su, M.; Zou, X.; Duan, L.; Zhang, H. Characteristics of Plastic Pollution in the Environment: A Review. *Bull. Environ. Contam. Toxicol.* **2020**, doi:10.1007/s00128-020-02820-1.

6. George, A.; Sanjay, M.R.; Srisuk, R.; Parameswaranpillai, J.; Siengchin, S. A comprehensive review on chemical properties and applications of biopolymers and their composites. *Int. J. Biol. Macromol.* **2020**, *154*, 329–338, doi:10.1016/j.ijbiomac.2020.03.120.

7. Lemoigne, M. Produit de deshydratation et de polymerisation de l'acide β=oxybutyrique. *Bull. Soc. Chim. Biol. (Paris).* **1926**, *8*, 770–782.

8. Kumar, M.; Rathour, R.; Singh, R.; Sun, Y.; Pandey, A.; Gnansounou, E.; Andrew Lin, K.Y.; Tsang, D.C.W.; Thakur, I.S. Bacterial polyhydroxyalkanoates: Opportunities, challenges, and prospects. *J.*

Clean. Prod. **2020**, *263*, 121500, doi:10.1016/j.jclepro.2020.121500.

9. Snell, K.D.; Singh, V.; Brumbley, S.M. Production of novel biopolymers in plants: Recent technological advances and future prospects. *Curr. Opin. Biotechnol.* **2015**, *32*, 68–75, doi:10.1016/j.copbio.2014.11.005.

10. Muneer, F.; Rasul, I.; Azeem, F.; Siddique, M.H.; Zubair, M.; Nadeem, H. Microbial Polyhydroxyalkanoates (PHAs): Efficient Replacement of Synthetic Polymers. *J. Polym. Environ.* **2020**, *28*, 2301–2323, doi:10.1007/s10924-020-01772-1.

11. Aljuraifani, A.A.; Berekaa, M.M.; Ghazwani, A.A. Bacterial biopolymer (polyhydroxyalkanoate) production from low-cost sustainable sources. *Microbiologyopen* **2019**, *8*, 1–7, doi:10.1002/mbo3.755.

12. Kunasundari, B.; Sudesh, K. Isolation and recovery of microbial polyhydroxyalkanoates. *Express Polym. Lett.* **2011**, *5*, 620–634, doi:10.3144/expresspolymlett.2011.60.

13. Lee, S.Y. Review Bacterial Polyb ydroxyalkanoates. *Biotechnol. Bioeng.* **1996**, *49*, 1–14.

14. Reddy, C.S.K.; Ghai, R.; Kalia, V.C. Polyhydroxyalkanoates : an overview. **2003**, *87*, 137–146.

15. Winnacker, M. Polyhydroxyalkanoates: Recent Advances in Their Synthesis and Applications. *Eur. J. Lipid Sci. Technol.* **2019**, *121*, 1–9, doi:10.1002/ejlt.201900101.

16. Obruca, S.; Benesova, P.; Marsalek, L.; Marova, I. Use of lignocellulosic materials for PHA production. *Chem. Biochem. Eng. Q.* **2015**, *29*, 135–144, doi:10.15255/CABEQ.2014.2253.

17. Aneesh, B.P.; Arjun, J.K.; Kavitha, T.; Harikrishnan, K. Production of Short Chain Length Polyhydroxyalkanoates by Bacillus megaterium PHB29 from Starch Feed Stock. *Int. J. Curr. Microbiol. Appl. Sci.*

2016, *5*, 816–823, doi:10.20546/ijcmas.2016.507.094.

18. Arikawa, H.; Matsumoto, K.; Fujiki, T. Polyhydroxyalkanoate production from sucrose by Cupriavidus necator strains harboring csc genes from Escherichia coli W. *Appl. Microbiol. Biotechnol.* **2017**, *101*, 7497–7507, doi:10.1007/s00253-017-8470-7.

19. Povolo, S.; Romanelli, M.G.; Fontana, F.; Basaglia, M.; Casella, S. Production of Polyhydroxyalkanoates from Fatty Wastes. *J. Polym. Environ.* **2012**, *20*, 944–949, doi:10.1007/s10924-012-0485-7.

20. Walsh, M.; O'Connor, K.; Babu, R.; Woods, T.; Kenny, S. Plant oils and products of their hydrolysis as substrates for polyhydroxyalkanoate synthesis. *Chem. Biochem. Eng. Q.* **2015**, *29*, 123–133, doi:10.15255/CABEQ.2014.2252.

21. Jiang, G.; Hill, D.J.; Kowalczuk, M.; Johnston, B.; Adamus, G.; Irorere, V.; Radecka, I. Carbon sources for polyhydroxyalkanoates and an integrated biorefinery. *Int. J. Mol. Sci.* **2016**, *17*, doi:10.3390/ijms17071157.

22. Cui, Y.W.; Shi, Y.P.; Gong, X.Y. Effects of C/N in the substrate on the simultaneous production of polyhydroxyalkanoates and extracellular polymeric substances by Haloferax mediterranei via kinetic model analysis. *RSC Adv.* **2017**, *7*, 18953–18961, doi:10.1039/c7ra02131c.

23. Raza, Z.A.; Tariq, M.R.; Majeed, M.I.; Banat, I.M. Recent developments in bioreactor scale production of bacterial polyhydroxyalkanoates. *Bioprocess Biosyst. Eng.* **2019**, *42*, 901–919, doi:10.1007/s00449-019-02093-x.

24. Sreekanth, M.S.; Vijayendra, S.V.N.; Joshi, G.J.; Shamala, T.R. Effect of carbon and nitrogen sources on simultaneous production of α-amylase and green food packaging polymer by Bacillus sp. CFR 67. *J. Food Sci. Technol.* **2013**, *50*, 404–408, doi:10.1007/s13197-012-0639-6.

25. de Souza Reis, G.A.; Michels, M.H.A.; Fajardo, G.L.; Lamot, I.; de Best, J.H. Optimization of green extraction and purification of PHA produced by mixed microbial cultures from sludge. *Water (Switzerland)* **2020**, *12*, doi:10.3390/W12041185.

26. Aramvash, A.; Moazzeni Zavareh, F.; Gholami Banadkuki, N. Comparison of different solvents for extraction of polyhydroxybutyrate from Cupriavidus necator. *Eng. Life Sci.* **2018**, *18*, 20–28, doi:10.1002/elsc.201700102.

27. J.A. Ramsay, E. Berger, R. Voyer, C.C. and B.A.R. Extraction of PHB using chlorinated solvents. *Biotechnol. Tech.* **1994**, *8*, 589–594, doi:https://doi.org/10.1007/BF00152152.

28. Jiang, G.; Johnston, B.; Townrow, D.E.; Radecka, I.; Koller, M.; Chaber, P.; Adamus, G.; Kowalczuk, M. Biomass extraction using non-chlorinated solvents for biocompatibility improvement of polyhydroxyalkanoates. *Polymers (Basel).* **2018**, *10*, doi:10.3390/polym10070731.

29. Neves, A.; Müller, J. Use of enzymes in extraction of polyhydroxyalkanoates produced by Cupriavidus necator. *Biotechnol. Prog.* **2012**, *28*, 1575–1580, doi:10.1002/btpr.1624.

30. Madkour, M.H.; Heinrich, D.; Alghamdi, M.A.; Shabbaj, I.I.; Steinbüchel, A. PHA recovery from biomass. *Biomacromolecules* **2013**, *14*, 2963–2972, doi:10.1021/bm4010244.

31. Sanhueza, C.; Acevedo, F.; Rocha, S.; Villegas, P.; Seeger, M.; Navia, R. Polyhydroxyalkanoates as biomaterial for electrospun scaffolds. *Int. J. Biol. Macromol.* **2019**, *124*, 102–110, doi:10.1016/j.ijbiomac.2018.11.068.

32. Koller, M.; Niebelschütz, H.; Braunegg, G. Strategies for recovery and purification of poly[(R)-3-hydroxyalkanoates] (PHA) biopolyesters from surrounding biomass. *Eng. Life Sci.* **2013**, *13*, 549–562,

doi:10.1002/elsc.201300021.

33. Haddadi, M.H.; Asadolahi, R.; Negahdari, B. The bioextraction of bioplastics with focus on polyhydroxybutyrate: a review. *Int. J. Environ. Sci. Technol.* **2019**, *16*, 3935–3948, doi:10.1007/s13762-019-02352-0.

34. Chodak, I. Polyhydroxyalkanoates: Origin, Properties and Applications. In *Monomers , Polymers and Composites from Renewable Resources*; Belgacem, M.N., Gandini, A., Eds.; 2008; pp. 451–477 ISBN 9780080453163.

35. Elmowafy, E.; Abdal-Hay, A.; Skouras, A.; Tiboni, M.; Casettari, L.; Guarino, V. Polyhydroxyalkanoate (PHA): Applications in drug delivery and tissue engineering. *Expert Rev. Med. Devices* **2019**, *16*, 467–482, doi:10.1080/17434440.2019.1615439.

36. Luo, Z.; Wu, Y.L.; Li, Z.; Loh, X.J. Recent Progress in Polyhydroxyalkanoates-Based Copolymers for Biomedical Applications. *Biotechnol. J.* **2019**, *14*, 1–16, doi:10.1002/biot.201900283.

37. Licciardello, G.; Catara, A.F.; Catara, V. Production of polyhydroxyalkanoates and extracellular products using Pseudomonas corrugata and P. mediterranea: A review. *Bioengineering* **2019**, *6*, doi:10.3390/bioengineering6040105.

38. Nomura, C.T.; Tanaka, T.; Gan, Z.; Kuwabara, K.; Abe, H.; Takase, K.; Taguchi, K.; Doi, Y. Effective enhancement of short-chain-length - Medium-chain-length polyhydroxyalkanoate copolymer production by coexpression of genetically engineered 3-ketoacyl-acyl-carrier-protein synthase III (fabH) and polyhydroxyalkanoate synthesis genes. *Biomacromolecules* **2004**, *5*, 1457–1464, doi:10.1021/bm049959v.

39. Koller, M. Chemical and biochemical engineering approaches in

manufacturing polyhydroxyalkanoate (PHA) biopolyesters of tailored structure with focus on the diversity of building blocks. *Chem. Biochem. Eng. Q.* **2018**, *32*, 413–438, doi:10.15255/CABEQ.2018.1385.

40. Puppi, D.; Pecorini, G.; Chiellini, F. Biomedical processing of polyhydroxyalkanoates. *Bioengineering* **2019**, *6*, doi:10.3390/bioengineering6040108.

41. Luzi, F.; Torre, L.; Kenny, J.M.; Puglia, D. Bio- and fossil-based polymeric blends and nanocomposites for packaging: Structure-property relationship. *Materials (Basel).* **2019**, *12*, doi:10.3390/ma12030471.

42. Urtuvia, V.; Maturana, N.; Peña, C.; Díaz-Barrera, A. Accumulation of poly(3-hydroxybutyrate-co-3-hydroxyvalerate) by Azotobacter vinelandii with different 3HV fraction in shake flasks and bioreactor. *Bioprocess Biosyst. Eng.* **2020**, *43*, 1469–1478, doi:10.1007/s00449-020-02340-6.

43. Willson, A.; Takashi, K. Effects of Glass Fibers on Mechanical and Thermal Properties of Poly(3-hydroxybutyrate-co-3-hydroxyhexanoate). *Polym. Compos.* **2018**, *39*, 491–503.

44. Rastogi, V.K.; Samyn, P. Bio-based coatings for paper applications. *Coatings* **2015**, *5*, 887–930, doi:10.3390/coatings5040887.

45. Anjum, A.; Zuber, M.; Zia, K.M.; Noreen, A.; Anjum, M.N.; Tabasum, S. Microbial production of polyhydroxyalkanoates (PHAs) and its copolymers: A review of recent advancements. *Int. J. Biol. Macromol.* **2016**, *89*, 161–174, doi:10.1016/j.ijbiomac.2016.04.069.

46. Grigore, M.E.; Grigorescu, R.M.; Iancu, L.; Ion, R.M.; Zaharia, C.; Andrei, E.R. Methods of synthesis, properties and biomedical applications of polyhydroxyalkanoates: a review. *J. Biomater. Sci. Polym. Ed.* **2019**, *30*, 695–712,

doi:10.1080/09205063.2019.1605866.

47. Johnston, B.; Radecka, I.; Hill, D.; Chiellini, E.; Ilieva, V.I.; Sikorska, W.; Musioł, M.; Zięba, M.; Marek, A.A.; Keddie, D.; et al. The microbial production of Polyhydroxyalkanoates from Waste polystyrene fragments attained using oxidative degradation. *Polymers (Basel).* **2018**, *10*, doi:10.3390/polym10090957.

48. Gómez, E.F.; Michel, F.C. Biodegradability of conventional and bio-based plastics and natural fiber composites during composting, anaerobic digestion and long-term soil incubation. *Polym. Degrad. Stab.* **2013**, *98*, 2583–2591, doi:10.1016/j.polymdegradstab.2013.09.018.

49. Emadian, S.M.; Onay, T.T.; Demirel, B. Biodegradation of bioplastics in natural environments. *Waste Manag.* **2017**, *59*, 526–536, doi:10.1016/j.wasman.2016.10.006.

50. Gebauer, B.; Jendrossek, D. Assay of poly(3-hydroxybutyrate) depolymerase activity and product determination. *Appl. Environ. Microbiol.* **2006**, *72*, 6094–6100, doi:10.1128/AEM.01184-06.

51. Boyandin, A.N.; Prudnikova, S. V.; Karpov, V.A.; Ivonin, V.N.; Dỗ, N.L.; Nguyễn, T.H.; Lê, T.M.H.; Filichev, N.L.; Levin, A.L.; Filipenko, M.L.; et al. Microbial degradation of polyhydroxyalkanoates in tropical soils. *Int. Biodeterior. Biodegrad.* **2013**, *83*, 77–84, doi:10.1016/j.ibiod.2013.04.014.

52. Ishii-Hyakutake, M.; Mizuno, S.; Tsuge, T. Biosynthesis and characteristics of aromatic polyhydroxyalkanoates. *Polymers (Basel).* **2018**, *10*, 1–24, doi:10.3390/polym10111267.

53. Bátori, V.; Åkesson, D.; Zamani, A.; Taherzadeh, M.J.; Sárvári Horváth, I. Anaerobic degradation of bioplastics: A review. *Waste Manag.* **2018**, *80*, 406–413, doi:10.1016/j.wasman.2018.09.040.

54. Dilkes-Hoffman, L.S.; Lant, P.A.; Laycock, B.; Pratt, S. The rate of

biodegradation of PHA bioplastics in the marine environment: A meta-study. *Mar. Pollut. Bull.* **2019**, *142*, 15–24, doi:10.1016/j.marpolbul.2019.03.020.

55. Kolstad, J.J.; Vink, E.T.H.; De Wilde, B.; Debeer, L. Assessment of anaerobic degradation of Ingeo™ polylactides under accelerated landfill conditions. *Polym. Degrad. Stab.* **2012**, *97*, 1131–1141, doi:10.1016/j.polymdegradstab.2012.04.003.

56. Kanesawa, Y.; Tanahashi, N.; Doi, Y.; Saito, T. Enzymatic degradation of microbial poly(3-hydroxyalkanoates). *Polym. Degrad. Stab.* **1994**, *45*, 179–185, doi:10.1016/0141-3910(94)90135-X.

57. Koller, M. Biodegradable and biocompatible polyhydroxy-alkanoates (PHA): Auspicious microbial macromolecules for pharmaceutical and therapeutic applications. *Molecules* **2018**, *23*, doi:10.3390/molecules23020362.

58. Kalia, V.C. *Biotechnological Applications of Polyhydroxyalkanoates*; 2019; ISBN 9789811337598.

59. Khosravi-Darani, K.; Bucci, D.Z. Application of poly(hydroxyalkanoate) in food packaging: Improvements by nanotechnology. *Chem. Biochem. Eng. Q.* **2015**, *29*, 275–285, doi:10.15255/CABEQ.2014.2260.

60. Mangaraj, S.; Yadav, A.; Bal, L.M.; Dash, S.K.; Mahanti, N.K. Application of Biodegradable Polymers in Food Packaging Industry: A Comprehensive Review. *J. Packag. Technol. Res.* **2019**, *3*, 77–96, doi:10.1007/s41783-018-0049-y.

61. Singh, A.K.; Srivastava, J.K.; Chandel, A.K.; Sharma, L.; Mallick, N.; Singh, S.P. Biomedical applications of microbially engineered polyhydroxyalkanoates: an insight into recent advances, bottlenecks, and solutions. *Appl. Microbiol. Biotechnol.* **2019**, *103*, 2007–2032, doi:10.1007/s00253-018-09604-y.

62. Tarrahi, R.; Fathi, Z.; Seydibeyoğlu, M.Ö.; Doustkhah, E.; Khataee, A. Polyhydroxyalkanoates (PHA): From production to nanoarchitecture. *Int. J. Biol. Macromol.* **2020**, *146*, 596–619, doi:10.1016/j.ijbiomac.2019.12.181.

63. Ang, H.Y.; Huang, Y.Y.; Lim, S.T.; Wong, P.; Joner, M.; Foin, N. Mechanical behavior of polymer-based vs. metallic-based bioresorbable stents. *J. Thorac. Dis.* **2017**, *9*, S923–S934, doi:10.21037/jtd.2017.06.30.

64. Generali, M.; Dijkman, P.E.; Hoerstrup, S.P. Bioresorbable Scaffolds for Cardiovascular Tissue Engineering. *EMJ Interv. Cardiol.* **2014**, *1*, 91–99.

65. Sabapathy, P.C.; Devaraj, S.; Meixner, K.; Anburajan, P.; Kathirvel, P.; Ravikumar, Y.; Zabed, H.M.; Qi, X. Recent developments in Polyhydroxyalkanoates (PHAs) production – A review. *Bioresour. Technol.* **2020**, *306*, 123132, doi:10.1016/j.biortech.2020.123132.

66. Gholami, A.; Mohkam, M.; Rasoul-Amini, S.; Ghasemi, Y. industrial production of polyhydroxyalkanoates by bacteria: opportunities and challenges. *Minerva Biotecnol.* **2016**, *28*, 59–74, doi:10.13140/RG.2.1.5129.4169.

67. Leong, Y.K.; Show, P.L.; Lan, J.C.W.; Loh, H.S.; Lam, H.L.; Ling, T.C. Economic and environmental analysis of PHAs production process. *Clean Technol. Environ. Policy* **2017**, *19*, 1941–1953, doi:10.1007/s10098-017-1377-2.

68. Tan, D.; Wang, Y.; Tong, Y.; Chen, G.Q. Grand Challenges for Industrializing Polyhydroxyalkanoates (PHAs). *Trends Biotechnol.* **2021**, 1–11, doi:10.1016/j.tibtech.2020.11.010.

69. Chen, G.-Q.; Chen, X.-Y.; Wu, F.-Q.; Chen, J.-C. Polyhydroxyalkanoates (PHA) toward cost competitiveness and functionality. *Adv. Ind. Eng. Polym. Res.* **2020**, *3*, 1–7,

doi:10.1016/j.aiepr.2019.11.001.

70. Favaro, L.; Basaglia, M.; Casella, S. Improving polyhydroxyalkanoate production from inexpensive carbon sources by genetic approaches: a review. *Biofuels, Bioprod. Biorefining* **2019**, *13*, 208–227, doi:10.1002/bbb.1944.

71. Ortiz, A.A.; Sucozhañay, D.; Vanegas, P.; Martínez-Moscoso, A. A regional response to a global problem: Single use plastics regulation in the countries of the pacific alliance. *Sustain.* **2020**, *12*, 1–21, doi:10.3390/su12198093.

72. Matthews, C.; Moran, F.; Jaiswal, A.K. A review on European Union's strategy for plastics in a circular economy and its impact on food safety. *J. Clean. Prod.* **2021**, *283*, 125263, doi:10.1016/j.jclepro.2020.125263.

73. Mondal, S. Preparation, properties and applications of nanocellulosic materials. *Carbohydr. Polym.* **2017**, *163*, 301–316, doi:10.1016/j.carbpol.2016.12.050.

74. Endes, C.; Camarero-Espinosa, S.; Mueller, S.; Foster, E.J.; Petri-Fink, A.; Rothen-Rutishauser, B.; Weder, C.; Clift, M.J.D. A critical review of the current knowledge regarding the biological impact of nanocellulose. *J. Nanobiotechnology* **2016**, *14*, 1–14, doi:10.1186/s12951-016-0230-9.

75. Dufresne, A. 1. Cellulose and potential reinforcement. In *Nanocellulose*; 2017; pp. 1–46 ISBN 9783110480412.

76. Dufresne, A. 6. Rheological behavior of nanocellulose suspensions and self-assembly. In *Nanocellulose*; 2017 ISBN 9783110480412.

77. Rol, F.; Belgacem, M.N.; Gandini, A.; Bras, J. Recent advances in surface-modified cellulose nanofibrils. *Prog. Polym. Sci.* **2019**, *88*, 241–264, doi:10.1016/j.progpolymsci.2018.09.002.

78. Pereira Oliveira Moreira, R.L.; Simão, J.A.; Gouveia, R.F.; Strauss, M. Exploring the Hierarchical Structure and Alignment of Wood Cellulose Fibers for Bioinspired Anisotropic Polymeric Composites. *ACS Appl. Bio Mater.* **2020**, *3*, 2193–2200, doi:10.1021/acsabm.0c00038.

79. Dufresne, A. Nanocellulose: A new ageless bionanomaterial. *Mater. Today* **2013**, *16*, 220–227, doi:10.1016/j.mattod.2013.06.004.

80. Dias, O.A.T.; Konar, S.; Leão, A.L.; Yang, W.; Tjong, J.; Sain, M. Current State of Applications of Nanocellulose in Flexible Energy and Electronic Devices. *Front. Chem.* **2020**, *8*, doi:10.3389/fchem.2020.00420.

81. Dufresne, A. 2. Preparation of microfibrillated cellulose. In *Nanocellulose*; 2017 ISBN 9783110480412.

82. Dufresne, A. 3. Preparation of cellulose nanocrystals. In *Nanocellulose*; 2017 ISBN 9783110480412.

83. Brown, J.A. XLIIL-On an Acetic Ferment which forms Cellulose. *J. Chem. Soc.* **1886**, *49*, 432–439.

84. Dufresne, A. 4. Bacterial cellulose. In *Nanocellulose*; 2017 ISBN 9783110480412.

85. Manoukian, O.S.; Sardashti, N.; Stedman, T.; Gailiunas, K.; Ojha, A.; Penalosa, A.; Mancuso, C.; Hobert, M.; Kumbar, S.G. Biomaterials for Tissue Engineering and Regenerative Medicine. *Biomed. Eng.* **2019**, 462–482.

86. Gorgieva, S.; Trček, J. Bacterial cellulose: Production, modification and perspectives in biomedical applications. *Nanomaterials* **2019**, *9*, 1–20, doi:10.3390/nano9101352.

87. Andriani, D.; Apriyana, A.Y.; Karina, M. The optimization of bacterial cellulose production and its applications: a review. *Cellulose* **2020**,

27, 6747–6766, doi:10.1007/s10570-020-03273-9.

88. Mishra, R.K.; Sabu, A.; Tiwari, S.K. Materials chemistry and the futurist eco-friendly applications of nanocellulose: Status and prospect. *J. Saudi Chem. Soc.* **2018**, *22*, 949–978, doi:10.1016/j.jscs.2018.02.005.

89. Lavoine, N.; Desloges, I.; Dufresne, A.; Bras, J. Microfibrillated cellulose - Its barrier properties and applications in cellulosic materials: A review. *Carbohydr. Polym.* **2012**, *90*, 735–764, doi:10.1016/j.carbpol.2012.05.026.

90. Dufresne, A.; CavaiÌlé, J.Y.; Vignon, M.R. Mechanical behavior of sheets prepared from sugar beet cellulose microfibrils. *J. Appl. Polym. Sci.* **1997**, *64*, 1185–1194, doi:10.1002/(sici)1097-4628(19970509)64:6<1185::aid-app19>3.3.co;2-2.

91. Baati, R.; Mabrouk, A. Ben; Magnin, A.; Boufi, S. CNFs from twin screw extrusion and high pressure homogenization: A comparative study. *Carbohydr. Polym.* **2018**, *195*, 321–328, doi:10.1016/j.carbpol.2018.04.104.

92. de Moura, M.R.; Monteiro Cordeiro de Azeredo, F.A.A.H.; Capparelli Mattoso, L.H. Microfluidizer Technique for Improving Microfiber Properties Incorporated Into Edible and Biodegradable Films. In *Advances in Microfluidics*; 2012; pp. 219–240.

93. Chakraborty, A.; Sain, M.; Kortschot, M. Cellulose microfibrils: A novel method of preparation using high shear refining and cryocrushing. *Holzforschung* **2005**, *59*, 102–107.

94. Kondo, T.; Kose, R.; Naito, H.; Kasai, W. Aqueous counter collision using paired water jets as a novel means of preparing bio-nanofibers. *Carbohydr. Polym.* **2014**, *112*, 284–290, doi:10.1016/j.carbpol.2014.05.064.

95. Zhao, H.-P.; Feng, X.-Q. Ultrasonic technique for extracting

nanofibers from nature materials. *Appl. Phys. Lett.* **2007**, *90*.

96. Zeng, J.; Liu, L.; Li, J.; Dong, J.; Cheng, Z. Properties of cellulose nanofibril produced from wet ball milling after enzymatic treatment vs. mechanical grinding of bleached softwood kraft fibers. *BioResources* **2020**, *15*, 3809–3820, doi:10.15376/biores.15.2.3809-3820.

97. Siró, I.; Plackett, D. Microfibrillated cellulose and new nanocomposite materials: A review. *Cellulose* **2010**, *17*, 459–494, doi:10.1007/s10570-010-9405-y.

98. Panaitescu, D.M.; Gabor, R.A.; Frone, A.N.; Vasile, E. Influence of thermal treatment on mechanical and morphological characteristics of polyamide 11/cellulose nanofiber nanocomposites. *J. Nanomater.* **2015**, *2015*, doi:10.1155/2015/136204.

99. Yano, H.; Omura, H.; Honma, Y.; Okumura, H.; Sano, H.; Nakatsubo, F. Designing cellulose nanofiber surface for high density polyethylene reinforcement. *Cellulose* **2018**, *25*, 3351–3362, doi:10.1007/s10570-018-1787-2.

100. Dufresne, A. Cellulose nanomaterials as green nanoreinforcements for polymer nanocomposites. *Philos. Trans. R. Soc. A Math. Phys. Eng. Sci.* **2018**, *376*, doi:10.1098/rsta.2017.0040.

101. Fujisawa, S.; Ikeuchi, T.; Takeuchi, M.; Saito, T.; Isogai, A. Superior reinforcement effect of TEMPO-oxidized cellulose nanofibrils in polystyrene matrix: optical, thermal, and mechanical studies. *Biomacromolecules* **2012**, *13*, 2188–2194, doi:10.1021/bm300609c.

102. Rajala, S.; Siponkoski, T.; Sarlin, E.; Mettänen, M.; Vuoriluoto, M.; Pammo, A.; Juuti, J.; Rojas, O.J.; Franssila, S.; Tuukkanen, S. Cellulose Nanofibril Film as a Piezoelectric Sensor Material. *ACS Appl. Mater. Interfaces* **2016**, *8*, 15607–15614, doi:10.1021/acsami.6b03597.

103. Mapelli, C.; Musatti, A.; Barbiroli, A.; Saini, S.; Bras, J.; Cavicchioli,

D.; Rollini, M. Cellulose nanofiber (CNF)–sakacin-A active material: production, characterization and application in storage trials of smoked salmon. *J. Sci. Food Agric.* **2019**, *99*, 4731–4738, doi:10.1002/jsfa.9715.

104. Halib, N.; Perrone, F.; Cemazar, M.; Dapas, B.; Farra, R.; Abrami, M.; Chiarappa, G.; Forte, G.; Zanconati, F.; Pozzato, G.; et al. Potential applications of nanocellulose-containing materials in the biomedical field. *Materials (Basel).* **2017**, *10*, doi:10.3390/ma10080977.

105. Lin, N.; Dufresne, A. Nanocellulose in biomedicine: Current status and future prospect. *Eur. Polym. J.* **2014**, *59*, 302–325, doi:https://doi.org/10.1016/j.eurpolymj.2014.07.025.

106. Yadav, S.; Illa, M.P.; Rastogi, T.; Sharma, C.S. High absorbency cellulose acetate electrospun nanofibers for feminine hygiene application. *Appl. Mater. Today* **2016**, *4*, 62–70, doi:https://doi.org/10.1016/j.apmt.2016.07.002.

107. Habibi, Y.; Goffin, A.L.; Schiltz, N.; Duquesne, E.; Dubois, P.; Dufresne, A. Bionanocomposites based on poly(ε-caprolactone)-grafted cellulose nanocrystals by ring-opening polymerization. *J. Mater. Chem.* **2008**, *18*, 5002–5010, doi:10.1039/b809212e.

108. Mahfoudhi, N.; Boufi, S. Nanocellulose as a Millennium Material with Enhancing Adsorption Capacities. In *Biodegradable and Biobased Polymers for Environmental and Biomedical Applications*; 2016; pp. 349–383.

109. Wu, X.; Moon, R.J.; Martini, A. Crystalline cellulose elastic modulus predicted by atomistic models of uniform deformation and nanoscale indentation. *Cellulose* **2013**, *20*, 43–55, doi:10.1007/s10570-012-9823-0.

110. Tayeb, A.H.; Amini, E.; Ghasemi, S.; Tajvidi, M. Cellulose nanomaterials-binding properties and applications: A review.

Molecules **2018**, *23*, 1–24, doi:10.3390/molecules23102684.

111. Xu, Q.; Gao, Y.; Qin, M.; Wu, K.; Fu, Y.; Zhao, J. Nanocrystalline cellulose from aspen kraft pulp and its application in deinked pulp. *Int. J. Biol. Macromol.* **2013**, *60*, 241–247, doi:https://doi.org/10.1016/j.ijbiomac.2013.05.038.

112. Cunha, A.G.; Mougel, J.B.; Cathala, B.; Berglund, L.A.; Capron, I. Preparation of double pickering emulsions stabilized by chemically tailored nanocelluloses. *Langmuir* **2014**, *30*, 9327–9335, doi:10.1021/la5017577.

113. Herrera, M.A.; Mathew, A.P.; Oksman, K. Gas permeability and selectivity of cellulose nanocrystals films (layers) deposited by spin coating. *Carbohydr. Polym.* **2014**, *112*, 494–501, doi:https://doi.org/10.1016/j.carbpol.2014.06.036.

114. Gao, W.; Sun, L.; Zhang, Z.; Li, Z. Cellulose nanocrystals reinforced gelatin/bioactive glass nanocomposite scaffolds for potential application in bone regeneration. *J. Biomater. Sci. Polym. Ed.* **2020**, *31*, 984–998, doi:10.1080/09205063.2020.1735607.

115. Osorio, D.A.; Lee, B.E.J.; Kwiecien, J.M.; Wang, X.; Shahid, I.; Hurley, A.L.; Cranston, E.D.; Grandfield, K. Cross-linked cellulose nanocrystal aerogels as viable bone tissue scaffolds. *Acta Biomater.* **2019**, *87*, 152–165, doi:10.1016/j.actbio.2019.01.049.

116. Magnani, C.; Idström, A.; Nordstierna, L.; Müller, A.J.; Dubois, P.; Raquez, J.M.; Lo Re, G. Interphase Design of Cellulose Nanocrystals/Poly(hydroxybutyrate- ran-valerate) Bionanocomposites for Mechanical and Thermal Properties Tuning. *Biomacromolecules* **2020**, *21*, 1892–1901, doi:10.1021/acs.biomac.9b01760.

117. Giubilini, A.; Siqueira, G.; Clemens, F.J.; Sciancalepore, C.; Messori, M.; Nystrom, G.; Bondioli, F. 3D Printing Nanocellulose-Poly(3-

hydroxybutyrate-co-3-hydroxyhexanoate) Biodegradable Composites by Fused Deposition Modeling. *ACS Sustain. Chem. Eng.* **2020**, doi:10.1021/acssuschemeng.0c03385.

118. Cataldi, A.; Rigotti, D.; Nguyen, V.D.H.; Pegoretti, A. Polyvinyl alcohol reinforced with crystalline nanocellulose for 3D printing application. *Mater. Today Commun.* **2018**, *15*, 236–244, doi:10.1016/j.mtcomm.2018.02.007.

119. Espino-Pérez, E.; Bras, J.; Ducruet, V.; Guinault, A.; Dufresne, A.; Domenek, S. Influence of chemical surface modification of cellulose nanowhiskers on thermal, mechanical, and barrier properties of poly(lactide) based bionanocomposites. *Eur. Polym. J.* **2013**, *49*, 3144–3154, doi:10.1016/j.eurpolymj.2013.07.017.

120. Dufresne, A. 5. Chemical modification of nanocellulose. In *Nanocellulose: From Nature to High Performance Tailored Materials*; 2017; pp. 221–286 ISBN 9783110254600.

121. Hebeish, A.; Guthrie, J.T. *The Chemistry and Technology of Cellulosic Copolymers*; Springer-Verlag: Berlin, 1981;

122. Wang, Y.; Wang, X.; Xie, Y.; Zhang, K. Functional nanomaterials through esterification of cellulose: a review of chemistry and application. *Cellulose* **2018**, *25*, 3703–3731, doi:10.1007/s10570-018-1830-3.

123. Barbosa, R.F.S.; Souza, A.G.; Ferreira, F.F.; Rosa, D.S. Isolation and acetylation of cellulose nanostructures with a homogeneous system. *Carbohydr. Polym.* **2019**, *218*, 208–217, doi:10.1016/j.carbpol.2019.04.072.

124. Zimmermann, M.V.G.; da Silva, M.P.; Zattera, A.J.; Campomanes Santana, R.M. Effect of nanocellulose fibers and acetylated nanocellulose fibers on properties of poly(ethylene-co-vinyl acetate) foams. *J. Appl. Polym. Sci.* **2017**, *134*, 1–12, doi:10.1002/app.44760.

125. Frank, B.P.; Durkin, D.P.; Caudill, E.R.; Zhu, L.; White, D.H.; Curry, M.L.; Pedersen, J.A.; Fairbrother, D.H. Impact of Silanization on the Structure, Dispersion Properties, and Biodegradability of Nanocellulose as a Nanocomposite Filler. *ACS Appl. Nano Mater.* **2018**, *1*, 7025–7038, doi:10.1021/acsanm.8b01819.

126. Beaumont, M.; Bacher, M.; Opietnik, M.; Gindl-Altmutter, W.; Potthast, A.; Rosenau, T. A general aqueous silanization protocol to introduce vinyl, mercapto or azido functionalities onto cellulose fibers and nanocelluloses. *Molecules* **2018**, *23*, 1–15, doi:10.3390/molecules23061427.

127. Carlsson, D.O.; Lindh, J.; Nyholm, L.; Strømme, M.; Mihranyan, A. Cooxidant-free TEMPO-mediated oxidation of highly crystalline nanocellulose in water. *RSC Adv.* **2014**, *4*, 52289–52298, doi:10.1039/c4ra11182f.

128. Isogai, A.; Saito, T.; Fukuzumi, H. TEMPO-oxidized cellulose nanofibers. *Nanoscale* **2011**, *3*, 71–85, doi:10.1039/c0nr00583e.

129. Wei, L.; McDonald, A.G.; Stark, N.M. Grafting of Bacterial Polyhydroxybutyrate (PHB) onto Cellulose via In Situ Reactive Extrusion with Dicumyl Peroxide. *Biomacromolecules* **2015**, *16*, 1040–1049, doi:10.1021/acs.biomac.5b00049.

130. Barsbay, M.; Güven, O. Surface modification of cellulose via conventional and controlled radiation-induced grafting. *Radiat. Phys. Chem.* 2019, *160*, 1–8.

131. Mahmood, H.; Pegoretti, A.; Brusa, R.S.; Ceccato, R.; Penasa, L.; Tarter, S.; Checchetto, R. Molecular transport through 3-hydroxybutyrate co-3-hydroxyhexanoate biopolymer films with dispersed graphene oxide nanoparticles: Gas barrier, structural and mechanical properties. *Polym. Test.* **2020**, *81*, 106181, doi:10.1016/j.polymertesting.2019.106181.

132. Melo, J.D.D.; Carvalho, L.F.M.; Medeiros, A.M.; Souto, C.R.O.; Paskocimas, C.A. A biodegradable composite material based on polyhydroxybutyrate (PHB) and carnauba fibers. *Compos. Part B Eng.* **2012**, *43*, 2827–2835, doi:10.1016/j.compositesb.2012.04.046.

133. Srithep, Y.; Ellingham, T.; Peng, J.; Sabo, R.; Clemons, C.; Turng, L.S.; Pilla, S. Melt compounding of poly (3-hydroxybutyrate-co-3-hydroxyvalerate)/ nanofibrillated cellulose nanocomposites. *Polym. Degrad. Stab.* **2013**, *98*, 1439–1449, doi:10.1016/j.polymdegradstab.2013.05.006.

134. Hosoda, N.; Tsujimoto, T.; Uyama, H. Green composite of poly(3-hydroxybutyrate-co-3-hydroxyhexanoate) reinforced with porous cellulose. *ACS Sustain. Chem. Eng.* **2014**, *2*, 248–253, doi:10.1021/sc400290y.

135. Reis, K.C.; Pereira, L.; Melo, I.C.N.A.; Marconcini, J.M.; Trugilho, P.F.; Tonoli, G.H.D. Particles of coffee wastes as reinforcement in polyhydroxybutyrate (PHB) based composites. *Mater. Res.* **2015**, *18*, 546–552, doi:10.1590/1516-1439.318114.

136. Jonnalagadda, D.; Kuboki, T. Effect of natural flours on crystallization behaviors of poly(3-hydroxybutyrate-co-3-hydroxyhexanoate). *J. Appl. Polym. Sci.* **2016**, *133*, 1–11, doi:10.1002/app.43600.

137. Jun, D.; Guomin, Z.; Mingzhu, P.; Leilei, Z.; Dagang, L.; Rui, Z. Crystallization and mechanical properties of reinforced PHBV composites using melt compounding: Effect of CNCs and CNFs. *Carbohydr. Polym.* **2017**, *168*, 255–262, doi:10.1016/j.carbpol.2017.03.076.

138. Malmir, S.; Montero, B.; Rico, M.; Barral, L.; Bouza, R. Morphology, thermal and barrier properties of biodegradable films of poly (3-hydroxybutyrate-co-3-hydroxyvalerate) containing cellulose nanocrystals. *Compos. Part A Appl. Sci. Manuf.* **2017**, *93*, 41–48, doi:10.1016/j.compositesa.2016.11.011.

139. Melendez-Rodriguez, B.; Torres-Giner, S.; Aldureid, A.; Cabedo, L.; Lagaron, J.M. Reactive melt mixing of poly(3-hydroxybutyrate)/rice husk flour composites with purified biosustainably produced poly(3-hydroxybutyrate-co-3-hydroxyvalerate). *Materials (Basel).* **2019**, *12*, doi:10.3390/ma12132152.

140. Panaitescu, D.M.; Ionita, E.R.; Nicolae, C.A.; Gabor, A.R.; Ionita, M.D.; Trusca, R.; Lixandru, B.E.; Codita, I.; Dinescu, G. Poly(3-hydroxybutyrate) modified by nanocellulose and plasma treatment for packaging applications. *Polymers (Basel).* **2018**, *10*, 1–24, doi:10.3390/polym10111249.

141. Cinelli, P.; Seggiani, M.; Mallegni, N.; Gigante, V.; Lazzeri, A. Processability and degradability of PHA-based composites in terrestrial environments. *Int. J. Mol. Sci.* **2019**, *20*, doi:10.3390/ijms20020284.

142. Xu, P.; Cao, Y.; Wu, B.; Ma, P.; Dong, W.; Bai, H.; Zhang, H.; Zhu, H.; Chen, M. the hydrophilicity , crystallization and mechanical. *New J. Chem.* **2018**, *42*, 11972–11978, doi:10.1039/C8NJ02012D.

143. Zhou, J.; Ma, X.; Li, J.; Zhu, L. Preparation and characterization of a bionanocomposite from poly (3-hydroxybutyrate-co-3-hydroxyhexanoate) and cellulose nanocrystals. *Cellulose* **2019**, *26*, 979–990, doi:10.1007/s10570-018-2136-1.

144. Li, D.; Zhou, J.; Ma, X.; Li, J. Synthesis of a novel biocomposite of poly (3-hydroxybutyrate-co-3-hydroxyhexanoate) reinforced with acetylated cellulose nanocrystals. *Cellulose* **2019**, *26*, 8729–8743, doi:10.1007/s10570-019-02708-2.

145. Valentini, F.; Dorigato, A.; Rigotti, D.; Pegoretti, A. Polyhydroxyalkanoates/Fibrillated Nanocellulose Composites for Additive Manufacturing. *J. Polym. Environ.* **2019**, *27*, 1333–1341, doi:10.1007/s10924-019-01429-8.

146. Nanni, A.; Messori, M. Effect of the wine wastes on the thermal stability, mechanical properties, and biodegradation's rate of poly(3-hydroxybutyrate). *J. Appl. Polym. Sci.* **2020**, 1–13, doi:10.1002/app.49713.

147. Reddy, J.P.; Misra, M.; Mohanty, A. Injection moulded biocomposites from oat hull and polypropylene/polylactide blend: Fabrication and performance evaluation. *Adv. Mech. Eng.* **2013**, *2013*, doi:10.1155/2013/761840.

148. Wu, F.; Misra, M.; Mohanty, A.K. Sustainable green composites from biodegradable plastics blend and natural fibre with balanced performance: Synergy of nano-structured blend and reactive extrusion. *Compos. Sci. Technol.* **2020**, 108369, doi:10.1016/j.compscitech.2020.108369.

149. Ngo, T.D.; Kashani, A.; Imbalzano, G.; Nguyen, K.T.Q.; Hui, D. Additive manufacturing (3D printing): A review of materials, methods, applications and challenges. *Compos. Part B Eng.* **2018**, *143*, 172–196, doi:10.1016/j.compositesb.2018.02.012.

150. Coon, C.; Pretzel, B.; Lomax, T.; Strlič, M. Preserving rapid prototypes: A review. *Herit. Sci.* **2016**, *4*, 1–16, doi:10.1186/s40494-016-0097-y.

151. Taormina, G.; Sciancalepore, C.; Messori, M.; Bondioli, F. 3D printing processes for photocurable polymeric materials: technologies, materials, and future trends. *J. Appl. Biomater. Funct. Mater.* **2018**, *16*, 151–160, doi:10.1177/2280800018764770.

152. Vyavahare, S.; Teraiya, S.; Panghal, D.; Kumar, S. Fused deposition modelling: a review. *Rapid Prototyp. J.* **2020**, *26*, 176–201, doi:10.1108/RPJ-04-2019-0106.

153. Boparai, K.S.; Singh, R.; Singh, H. Development of rapid tooling using fused deposition modeling: A review. *Rapid Prototyp. J.* **2019**, *22*,

281–299, doi:10.1108/RPJ-04-2014-0048.

154. Haleem, A.; Javaid, M. Polyether ether ketone (PEEK) and its manufacturing of customised 3D printed dentistry parts using additive manufacturing. *Clin. Epidemiol. Glob. Heal.* **2019**, *7*, 654–660, doi:10.1016/j.cegh.2019.03.001.

155. Sezer, H.K.; Eren, O. FDM 3D printing of MWCNT re-inforced ABS nano-composite parts with enhanced mechanical and electrical properties. *J. Manuf. Process.* **2019**, *37*, 339–347, doi:https://doi.org/10.1016/j.jmapro.2018.12.004.

156. Mazzanti, V.; Malagutti, L.; Mollica, F. FDM 3D printing of polymers containing natural fillers: A review of their mechanical properties. *Polymers (Basel).* **2019**, *11*, doi:10.3390/polym11071094.

157. Yang, L.; Chen, Y.; Wang, M.; Shi, S.; Jing, J. Fused Deposition Modeling 3D Printing of Novel Poly(vinyl alcohol)/Graphene Nanocomposite with Enhanced Mechanical and Electromagnetic Interference Shielding Properties. *Ind. Eng. Chem. Res.* **2020**, *59*, 8066–8077, doi:10.1021/acs.iecr.0c00074.

158. Schmitt, M.; Mehta, R.M.; Kim, I.Y. Additive manufacturing infill optimization for automotive 3D-printed ABS components. *Rapid Prototyp. J.* **2020**, *26*, 89–99, doi:10.1108/RPJ-01-2019-0007.

159. Najmon, J.C.; Raeisi, S.; Tovar, A. 2 - Review of additive manufacturing technologies and applications in the aerospace industry. In; Froes, F., Boyer, R.B.T.-A.M. for the A.I., Eds.; Elsevier, 2019; pp. 7–31 ISBN 978-0-12-814062-8.

160. Guerra, V.; Wan, C.; McNally, T. Fused deposition modelling (FDM) of composites of graphene nanoplatelets and polymers for high thermal conductivity: a mini-review. *Funct. Compos. Mater.* **2020**, *1*, 1–11, doi:10.1186/s42252-020-00005-x.

161. Guo, R.; Ren, Z.; Bi, H.; Xu, M.; Cai, L. Electrical and thermal

conductivity of polylactic Acid (PLA)-based biocomposites by incorporation of nano-graphite fabricated with fused deposition modeling. *Polymers (Basel).* **2019**, *11*, 1–19, doi:10.3390/polym11030549.

162. Dhavalikar, P.; Lan, Z.; Kar, R.; Salhadar, K.; Gaharwar, A.K.; Cosgriff-Hernandez, E. 1.4.8 - Biomedical Applications of Additive Manufacturing. In *Biomaterials Science (Fourth Edition)*; Wagner, W.R., Sakiyama-Elbert, S.E., Zhang, G., Yaszemski, M.J., Eds.; Academic Press, 2020; pp. 623–639 ISBN 978-0-12-816137-1.

163. Liu, J.; Yan, C. 3D Printing of Scaffolds for Tissue Engineering. In; 2018.

164. Wu, C.S.; Liao, H.T. Interface design of environmentally friendly carbon nanotube-filled polyester composites: Fabrication, characterisation, functionality and application. *Express Polym. Lett.* **2017**, *11*, 187–198, doi:10.3144/expresspolymlett.2017.20.

165. Ohmori, M.; Matijević, E. LETTER TO THE EDITOR Preparation and Properties of Uniform Coated Colloidal Particles. VII. Silica on Hematite. *J. Colloid Interface Sci.* **1992**, *150*, 594–598.

166. Hong, C.K.; Hwang, I.; Kim, N.; Park, D.H.; Hwang, B.S.; Nah, C. Mechanical properties of silanized jute-polypropylene composites. *J. Ind. Eng. Chem.* **2008**, *14*, 71–76, doi:10.1016/j.jiec.2007.07.002.

167. Carreau, P.J. Rheological Equations from Molecular Network Theories. *J. Rheol. (N. Y. N. Y).* **1972**, *16*, 99–127.

168. Silverstein, R.M.; Webster, F.X.; Kiemle, D.J. *Spectrometric identification of organic compound*; 7th Editio.; 2005;

169. Zhang, Z.; Sèbe, G.; Rentsch, D.; Zimmermann, T.; Tingaut, P. Ultralightweight and flexible silylated nanocellulose sponges for the selective removal of oil from water. *Chem. Mater.* **2014**, *26*, 2659–2668, doi:10.1021/cm5004164.

170. Jiang, H.; Zheng, Z.; Wang, X. Kinetic study of methyltriethoxysilane (MTES) hydrolysis by FTIR spectroscopy under different temperatures and solvents. *Vib. Spectrosc.* **2008**, *46*, 1–7, doi:10.1016/j.vibspec.2007.07.002.

171. Lee, J.A.; Yoon, M.J.; Lee, E.S.; Lim, D.Y.; Kim, K.Y. Preparation and characterization of cellulose nanofibers (CNFs) from microcrystalline cellulose (MCC) and CNF/polyamide 6 composites. *Macromol. Res.* **2014**, *22*, 738–745, doi:10.1007/s13233-014-2121-y.

172. Yue, Y.; Han, J.; Han, G.; Zhang, Q.; French, A.D.; Wu, Q. Characterization of cellulose I/II hybrid fibers isolated from energycane bagasse during the delignification process: Morphology, crystallinity and percentage estimation. *Carbohydr. Polym.* **2015**, *133*, 438–447, doi:10.1016/j.carbpol.2015.07.058.

173. Tamburini, D.; Łucejko, J.J.; Zborowska, M.; Modugno, F.; Cantisani, E.; Mamoňová, M.; Colombini, M.P. The short-term degradation of cellulosic pulp in lake water and peat soil: A multi-analytical study from the micro to the molecular level. *Int. Biodeterior. Biodegrad.* **2017**, *116*, 243–259, doi:10.1016/j.ibiod.2016.10.055.

174. Zhou, J.; Ma, X. Preparation and characterization of a bionanocomposite from poly (3-hydroxybutyrate-co-3-hydroxyhexanoate) and cellulose nanocrystals. *Cellulose* **2018**, *1*, doi:10.1007/s10570-018-2136-1.

175. Sciancalepore, C.; Bondioli, F.; Messori, M. Non-hydrolytic sol–gel synthesis and reactive suspension method: an innovative approach to obtain magnetite–epoxy nanocomposite materials. *J. Sol-Gel Sci. Technol.* **2017**, *81*, 69–83, doi:10.1007/s10971-016-4095-z.

176. Barrera, G.; Tiberto, P.; Sciancalepore, C.; Messori, M.; Bondioli, F.; Allia, P. Verwey transition temperature distribution in magnetic nanocomposites containing polydisperse magnetite nanoparticles. *J. Mater. Sci.* **2019**, *54*, 8346–8360, doi:10.1007/s10853-019-03510-y.

177. Xu, C.; Chen, J.; Wu, D.; Chen, Y.; Lv, Q.; Wang, M. Polylactide/acetylated nanocrystalline cellulose composites prepared by a continuous route: A phase interface-property relation study. *Carbohydr. Polym.* **2016**, *146*, 58–66, doi:10.1016/j.carbpol.2016.03.058.

178. Tingaut, P.; Zimmermann, T.; Lopez-Suevos, F. Synthesis and characterization of bionanocomposites with tunable properties from poly(lactic acid) and acetylated microfibrillated cellulose. *Biomacromolecules* **2010**, *11*, 454–464, doi:10.1021/bm901186u.

179. Lin, N.; Huang, J.; Chang, P.R.; Feng, J.; Yu, J. Surface acetylation of cellulose nanocrystal and its reinforcing function in poly(lactic acid). *Carbohydr. Polym.* **2011**, *83*, 1834–1842, doi:10.1016/j.carbpol.2010.10.047.

180. Popescu, C.M.; Larsson, P.T.; Olaru, N.; Vasile, C. Spectroscopic study of acetylated kraft pulp fibers. *Carbohydr. Polym.* **2012**, *88*, 530–536, doi:10.1016/j.carbpol.2011.12.046.

181. Olaru, N.; Olaru, L.; Vasile, C.; Ander, P. Surface modified cellulose obtained by acetylation without solvents of bleached and unbleached kraft pulps. *Polimery* **2011**, *56*, 834–840, doi:10.14314/polimery.2011.834.

182. Li, W.; Cai, G.; Zhang, P. A simple and rapid Fourier transform infrared method for the determination of the degree of acetyl substitution of cellulose nanocrystals. *J. Mater. Sci.* **2019**, *54*, 8047–8056, doi:10.1007/s10853-019-03471-2.

183. Jebrane, M.; Sèbe, G. A novel simple route to wood acetylation by transesterification with vinyl acetate. *Holzforschung* **2007**, *61*, 143–147.

184. Li, S.; He, J.; Yu, P.H.; Cheung, M.K. Thermal Degradation of Poly (3-hydroxybutyrate) and Poly (3-hydroxybutyrate- co -3-

hydroxyvalerate) as Studied by TG , TG – FTIR , and Py – GC / MS. *J. Appl. Polym. Sci.* **2003**, *89*, 1530–1536.

185. Erceg, M.; Kovačić, T.; Klarić, I. Dynamic thermogravimetric degradation of poly(3-hydroxybutyrate)/aliphatic- aromatic copolyester blends. *Polym. Degrad. Stab.* **2005**, *90*, 86–94, doi:10.1016/j.polymdegradstab.2005.02.014.

186. Yu, H.Y.; Qin, Z.Y.; Liu, Y.N.; Chen, L.; Liu, N.; Zhou, Z. Simultaneous improvement of mechanical properties and thermal stability of bacterial polyester by cellulose nanocrystals. *Carbohydr. Polym.* **2012**, *89*, 971–978, doi:10.1016/j.carbpol.2012.04.053.

187. Ching, Y.C.; Ershad Ali, M.; Abdullah, L.C.; Choo, K.W.; Kuan, Y.C.; Julaihi, S.J.; Chuah, C.H.; Liou, N.S. Rheological properties of cellulose nanocrystal-embedded polymer composites: a review. *Cellulose* **2016**, *23*, 1011–1030, doi:10.1007/s10570-016-0868-3.

188. Esposito Corcione, C.; Scalera, F.; Gervaso, F.; Montagna, F.; Sannino, A.; Maffezzoli, A. One-step solvent-free process for the fabrication of high loaded PLA/HA composite filament for 3D printing. *J. Therm. Anal. Calorim.* **2018**, *134*, 575–582, doi:10.1007/s10973-018-7155-5.

189. Qahtani, M.; Wu, F.; Misra, M.; Gregori, S.; Mielewski, D.F.; Mohanty, A.K. Experimental Design of Sustainable 3D-Printed Poly(Lactic Acid)/Biobased Poly(Butylene Succinate) Blends via Fused Deposition Modeling. *ACS Sustain. Chem. Eng.* **2019**, *7*, 14460–14470, doi:10.1021/acssuschemeng.9b01830.

190. Iggui, K.; Le Moigne, N.; Kaci, M.; Cambe, S.; Degorce-Dumas, J.R.; Bergeret, A. A biodegradation study of poly(3-hydroxybutyrate-co-3-hydroxyvalerate)/organoclay nanocomposites in various environmental conditions. *Polym. Degrad. Stab.* **2015**, *119*, 77–86, doi:10.1016/j.polymdegradstab.2015.05.002.

191. Puglia, D.; Fortunati, E.; D'Amico, D.A.; Manfredi, L.B.; Cyras, V.P.; Kenny, J.M. Influence of organically modified clays on the properties and disintegrability in compost of solution cast poly(3-hydroxybutyrate) films. *Polym. Degrad. Stab.* **2014**, *99*, 127–135, doi:10.1016/j.polymdegradstab.2013.11.013.

192. Jacob, J.; More, N.; Mounika, C.; Gondaliya, P.; Kalia, K.; Kapusetti, G. Smart Piezoelectric Nanohybrid of Poly(3-hydroxybutyrate-co-3-hydroxyvalerate) and Barium Titanate for Stimulated Cartilage Regeneration. *ACS Appl. Bio Mater.* **2019**, *2*, 4922–4931, doi:10.1021/acsabm.9b00667.

193. Rebia, R.A.; Rozet, S.; Tamada, Y.; Tanaka, T. Biodegradable PHBH/PVA blend nanofibers: Fabrication, characterization, in vitro degradation, and in vitro biocompatibility. *Polym. Degrad. Stab.* **2018**, *154*, 124–136, doi:10.1016/j.polymdegradstab.2018.05.018.

194. Marsell, R.; Einhorn, T.A. The biology of fracture healing. *Injury* **2011**, *42*, 551–555, doi:10.1016/j.injury.2011.03.031.

195. Montalbano, G.; Fiorilli, S.; Caneschi, A.; Vitale-Brovarone, C. Type I Collagen and Strontium-Containing Mesoporous Glass Particles as Hybrid Material for 3D Printing of Bone-Like Materials. *Mater. (Basel, Switzerland)* **2018**, *11*, 700, doi:10.3390/ma11050700.

196. Kunzler, T.P.; Drobek, T.; Schuler, M.; Spencer, N.D. Systematic study of osteoblast and fibroblast response to roughness by means of surface-morphology gradients. *Biomaterials* **2007**, *28*, 2175–2182, doi:10.1016/j.biomaterials.2007.01.019.